From the Department of Cardiac Surgery
Ludwig-Maximilians-Universität München
Head of Department: Prof. Dr. Christian Hagl

The Effect of TAVI-Simulation and Perfusion on the Cell Layer of decellularized and re-seeded Homografts

Doctoral Thesis
submitted for the fulfillment of the requirements
for the degree Doctor of Human Medicine
at the Faculty of Medicine of the
Ludwig-Maximilians-Universität München

submitted by

Stefanie Eilenberger

from
Vienna, Austria

2019

Mit Genehmigung der Medizinischen Fakultät
der Universität München

Berichterstatter:	Prof. Dr. Christian Hagl
Mitberichterstatter:	Prof. Dr. Alexander Bartelt
Mitbetreuung durch den promovierten Mitarbeiter:	Dr. Nikolaus Thierfelder
Dekan:	Prof. Dr. med. dent. Reinhard Hickel
Tag der mündlichen Prüfung:	28.11.2019

Table of content

List of Abbreviations

AV	Aortic valve
AVP	Aortic valve prosthesis
AVS	Aortic valve stenosis
BHV	Biological heart valve
CGM	Cell growth medium
DMSO	Dimethyl sulfoxide
EC	Endothelial cells
ECM	Extracellular matrix
ECGM	Endothelial cell growth medium
FB	Fibroblasts
FBGM	Fibroblast growth medium
GAG	Glycosaminoglycans
HLA	Human leukocyte antibodies
IE	Infectious endocarditis
IHC	Immunohistochemical
LV	Left ventricle
LVAD	Left ventricular assist device
MHV	Mechanical heart valves
MSC	Mesenchymal stem cells
NYHA Stadium	New York Heart Association
PBS	Phosphate buffered saline
PEG	Polyethylene glycol
PEGDA	Poly(ethylene glycol) diacrylate
PGA	Polyglycolic acid
PGS	Polyglycerol sebacate
PHA	Polyhydroxyalcanoate
PHO	Polyhydroxyoctanoate
PVA	Poly(vinyl alcohol)
RPM	Rounds per minute
RT	Room temperature
RV	Right ventricle
SD	Sodium deoxycholate
SDS	Sodium dodecyl sulfate

SEM	Scanning electron microscopy
TAVI	Transcatheter aortic valve implantation
TEHV	Tissue engineered heart valve
VEC	Valvular endothelial cells
VIC	Valvular interstitial cells

List of Figures

	mounting in the bioreactor	
Fig 3-5	*The high flow bioreactor which was used for the perfusion phase of the study*	own
Fig 3-6	*The control unit and the pump*	own
Fig 3-7	*The closure and opening of the aortic valve during perfusion*	own
Chapter 4: Analysis		
Fig 4-1	*FB and EC in culture*	own
Fig 4-2	*Neubauer counting chamber*	(a) Hecht Assitent, Germany http://www.hecht-assistent.de/183/ (b) Microbehunter Austria http://www.microbehunter.com/the-hemocytometer-counting-chamber/ Last checked 2017/12/30, 09:33 AM
Chapter 5: Results		
Fig 5-1	*EC and FB cultures in phase contrast microscopy*	own
Fig 5-2	*Immunocytochemical staining of a representative EC and FB culture*	own
Fig 5-3	*Macroscopic views of the aortic homograft during processing*	own
Fig 5-4	*SEM image of the native homograft surface*	own
Fig 5-5	*SEM image of the homograft surface after decellularization*	own
Fig 5-6	*SEM image of the homograft after recellularization*	own
Fig 5-7	*SEM image of the aortic wall after crimping and perfusion*	own
Fig 5-8	*SEM image of the aortic valve leaflet after crimping and perfusion*	own
Fig 5-9	*IHC staining of a representative native homograft*	own
Fig 5-10	*IHC staining of a representative homograft after decellularization*	own
Fig 5-11	*IHC staining of a representative homograft after recellularization*	own
Fig 5-12	*Cell layer after crimping and perfusion on a representative homograft*	own
Fig 5-13	Intercellular adhesion molecules	own

List of Tables

1. Abstract

Objective

Tissue engineering aspires to create organs and tissue from autologous cells, which mimic the function of native tissue as closely as possible. However, before a tissue engineered valve can be implanted, various experiments on the performance of the valve are necessary. Information regarding the reaction of a cell layer to different stimuli enables the prediction of the reaction *in vivo*. A minimal invasive implantation procedure might have effects on the cell layer. The transcatheter valve implantation (TAVI) is a minimal invasive procedure to implant an aortic valve. Escpecially for older and morbid patients the minimal invasive approach decreases postoperative morbidity and mortality. Currently available valves for TAVI are biologic valves with a limited durability. Younger patients in particular would benefit from a tissue engineered valve with a potentially longer durability and growth potential.

Methods and Material

Aortic homografts (n=4) were first decellularized and then recellularized with fibroblasts (FB) and endothelial cells (EC). The cells were harvested from saphenous veins, which were collected during aortocoronary bypass operations. After valve recellularization, a TAVI simulation was performed. The homografts were crimped for 10 min and then expanded using a catheter balloon. A dynamic bioreactor enabled the simulation of pulsatile flow conditions. The valves were exposed to increasing flow rates over the period of three days (d1 = 1 l/min, d2 = 1.5 l/min, d3 = 2 l/min). After all processing steps, the final testing samples were taken and analyzed. Cell layer topography was evaluated with scanning electron microscopy (SEM). An immunohistochemial (IHC) analysis enabled the assessment of the cell layer, structure of the extracellular matrix (ECM) and inflammation reaction.

Results

SEM evaluation of the samples after perfusion displayed an inhomogeneous cell layer. EC staining demonstrated a damaged cell layer. The IHC analysis of FB presented a similar result, with the exception of the ventricular side of the aortic valve leaflet. This part of the leaflet retained more of the earlier seeded FB.

Conclusion

The cell layers on the homografts, especially the EC layer, took considerable damage during the crimping and perfusion procedure. Interestingly, the ventricular side of the aortic valve leaflet seemed to have sustained less damage compared to the arterial side. A tissue engineered construct for TAVI has to withstand the strains of the implantation and perfusion process. Further studies are necessary to

evaluate the damage and to develop a procedure which enables a safe transportation of the tissue-engineered valve.

Zusammenfassung

Zielsetzung

Das Ziel von Tissue Engineering ist es, aus autologen Zellen Organe und Gewebe zu entwickeln, die die Funktionen von nativem Gewebe exakt nachahmen. Bevor eine so entwickelte Herzklappe implantiert werden kann, müssen Tests zur Evaluation der Leistungsfähigkeit durchgeführt werden. Aussagen zur Reaktion einer Zelle auf verschiedene Stimuli *in vitro* erlauben die Vorhersage einer möglichen Reaktion *in vivo*. Auch eine minimal invasive Implantationsmethode hat eventuell Auswirkungen auf die Zellschicht. Die TAVI (transcatheter valve implantation) ist eine minimal invasive Methode, um eine Aortenklappe zu implantieren. Vor allem bei alten und multimorbiden Patienten reduziert die minimal invasive Implantation die postoperative Morbiditäts- und Mortalitätsrate. Die zurzeit erhältlichen Klappen für die TAVI sind tierischen Ursprungs und deswegen von begrenzter Haltbarkeit. Insbesondere jüngere Patienten würden von einer durch Tissue Engineering entwickelten Klappe profitieren, da diese Wachstumspotential sowie potentiell längere Haltbarkeit besitzt.

Methoden und Material

Aorten-Homografts (n = 4) wurden zuerst dezellularisiert und dann mit Fibroblasten (FB) und Endothelzellen (EC) rezellularisiert. Die Zellen wurden aus Venae saphenae gewonnen, die während aortokoronaren Bypass-Operationen gesammelt wurden. Nach der Klappen-Rezellularisation wurde eine TAVI-Simulation durchgeführt. Die Homografts wurden für 10 min gecrimpt und dann mit einem Katheter-Ballon aufgedehnt. Ein dynamischer Bioreaktor simulierte pulsatile Flussbedingungen. Über einen Zeitraum von drei Tagen wurden die Klappen steigenden Flussraten (d1 = 1 l/min, d2 = 1.5 l/min, d3 = 2 l/min) ausgesetzt. Nachdem alle Schritte abgeschlossen waren, wurden die letzten Proben entnommen und analysiert. Die Topographie der Zellschicht wurde mit Rasterelektronenmikroskopie (REM) evaluiert. Eine abschließende immunhistochemische Analyse ermöglichte die Beurteilung der Zellschicht, der Struktur der extrazellulären Matrix und des Ausmaßes der Entzündungsreaktion.

Resultate

In der REM-Ansicht der Proben nach Perfusion zeigte sich eine inhomogene Zellschicht. Die immunhistochemische Färbung gegen CD 31 ließ eine Beschädigung der EC-Schicht erkennen. Ein ähnliches Resultat ergab die FB-Färbung (TE-7), mit Ausnahme der ventrikulären Seite des Aortenklappensegels. Auf dieser Seite waren die zuvor angesiedelten FB in höherem Maße erhalten geblieben.

Conclusio

Während des Crimpens und der Perfusion nahm die Zellschicht auf den Homografts, besonders die EC-Schicht, deutlich Schaden. Auffällig war, dass die ventrikuläre Seite des Klappensegels verglichen mit der arteriellen Seite weniger beschädigt wurde. Eine mit Hilfe von Tissue Engineering erzeugte Klappe für die TAVI muss dem Stress, der während der Implantation und Perfusion *in vivo* auftritt, widerstehen können. Weitere Studien sind daher notwendig, um den Schaden zu evaluieren und Methoden zu entwickeln, die einen sicheren Transport der Klappe ermöglichen.

2. Introduction

2.1. The Heart – Anatomy and Physiology

On the 23rd day the heart of a human embryo starts to beat. Long before the brain and other organs are functioning, the heart has already begun its work (Sacks et al. 2009). The heart starts out as a contracting tube and develops into a well designed machine, whose beat accompanies the human throughout his life. During a lifespan of 70 years the heart contracts over 3 x 10^9 times.

The contractions of the heart are triggered by specified myocardial cells. The sinus node, which is composed of this specified myocardial cells, is part of the cardiac conduction system. It enables specific expansion of the electric pulses and a guided contraction with maximal ejection fraction, depending on the current necessity. A full cardiac cycle includes the systole (contraction/ejection phase) and diastole (relaxation phase) of the heart ventricles (Aumüller 2007). The right atrium fills with venous blood from the systemic circulation during the systole. Via the tricuspid valve the blood flows into the right ventricle (RV) and is then ejected into the pulmonary circulation, where the blood is oxygenated. After passing the lungs, the blood collects in the left atrium before the left ventricle (LV) fills during diastole. During systole, the oxygenated blood is then ejected into the systemic circulation. Due to the higher resistance in the systemic circulation, the transvalvular pressures on the left side of the heart (atrioventricular and ventriculosystemic pressure) are 5-8 times higher than on the right side (pulmonary valve: 10 mmHg, aortic valve: 80 mmHg) (Sacks et al. 2009). To overcome these pressures the myocard of the LV is thicker than the RV (myocardium LV: 8-12 mm, myocardium RV: 3-5 mm) (Kirsch 2010). During the cardiac cycle the semilunar and atrio-ventricular valves ensure an unidirectional blood flow (Sacks et al. 2009). The mitral and tricuspid valve coordinate the blood flow from the atria into the ventricles, hence atrio-ventricular valves. The aortic valve (AV) and the pulmonary valve direct the blood flow from the ventricles into the systemic and pulmonary circulation, respectively (Fig 2-1) (Aumüller 2007). The four valves compose the valve plane (Schmidt, Thews 1983). The AV forms the centre while the pulmonary valve lies anterior, the mitral valve posteriolateral, and the tricuspid valve posteriomedial (Mackie 2013).

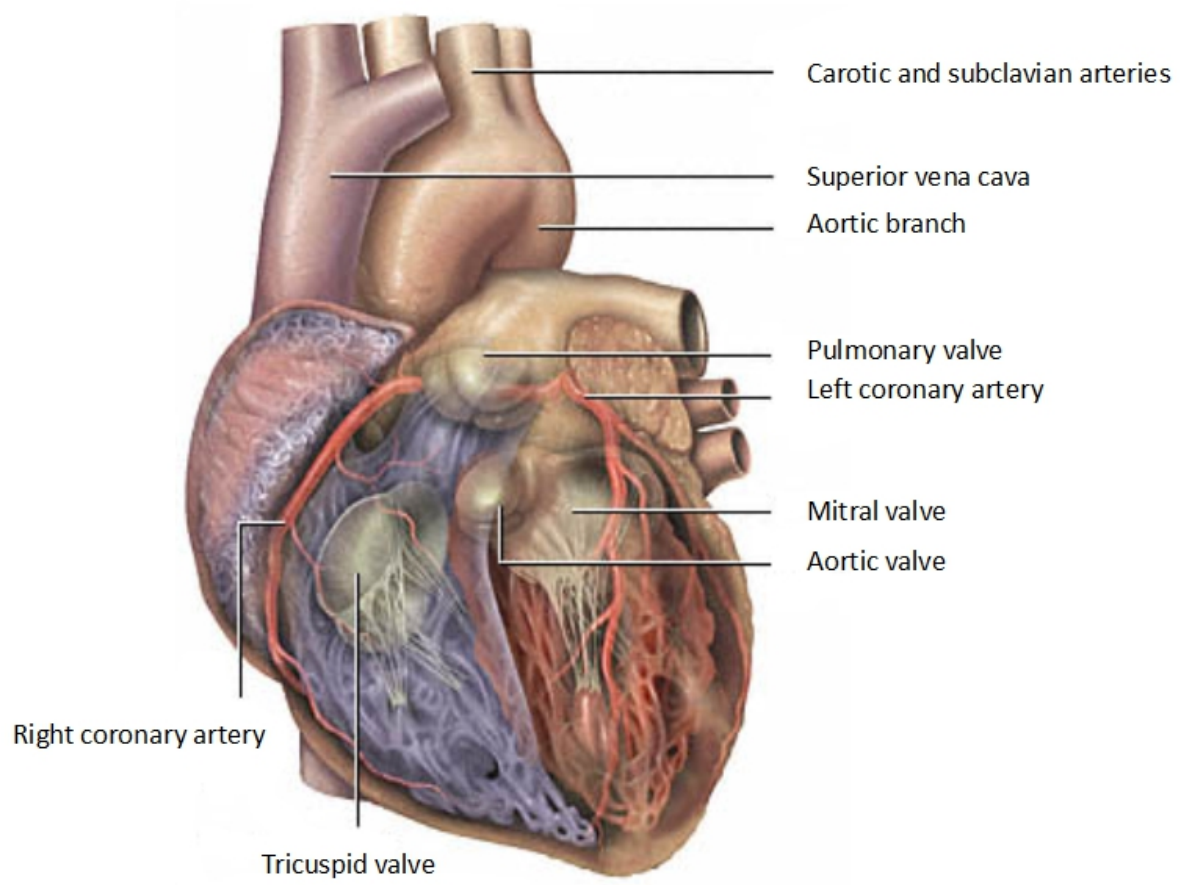

Fig 2-1 The human heart *Through the semi-visible myocardium the four heart valves can be seen. The blue colored myocardium indicates the right ventricular system, including the tricuspid and pulmonary valve. The red colored myocardium demonstrates the left ventricular system, including the mitral and the aortic valve.*

2.2. The Aortic Valve

2.2.1. Macroscopic and Microscopic Structure

The AV is one of two semilunar valves in the human heart. Basically the AV is passive tissue which moves accordingly to the pressure changes caused by the contracting heart. Its main task is to enable an unidirectional blood flow as well as reducing flow resistance and increasing flow rate. (Sacks et al. 2009)
Three central elements shape the AV: the leaflets, the annulus and the commissures (Mackie 2013). The leaflets have a semilunar shape. At the point of contact with the aortic wall they form a crown-like structure, the aortic *annulus*. Although the word "*annulus*" indicates a round shape, there is no specific histological structure or anatomic body, which befits this description. The term "*annulus*" in clinical use often implies the smallest diameter of the outflow tract between the LV and the aorta. The sizing of a

valve prosthesis as well as the positioning of the prosthesis depends on this "*virtual annulus*", which is a circular ring limited by the nadirs of the leaflet attachments. (Charitos, Sievers 2013) In the middle of the free edges of the leaflets the margins thickens and forms the so called "*Noduli Arantii*" (Misfeld, Sievers 2007). During diastole, the *Noduli Arantii* form a coadaptation region. On both sides of the *Noduli* the so called "*lannula*", thin semilunar parts of the valve, extend to the aortic wall where they merge with the commissures. At the commissures the peripheral edges of the leaflets connect and are attached to the aortic wall. The *lannula* also include the adherence surface of the leaflets. During diastole, the leaflets connect at this area and form a tight barrier. The pocket shaped load bearing structure, which lies between the edges of the leaflets and the connection to the aortic wall, is a thin and nearly translucent tissue with two different sides. A native heart valve is designed to withstand high pressure and great flow velocities. The microscopic structure of the single leaflet is one key point for accurate function. Thee layers form the leaflet: the *ventricularis*, *spongiosa* and *fibrosa* (Fig 2-2 a, b). The *ventricularis* faces the bloodstream coming from the LV. It is built of a collagen fibre network and layers of elastin filaments, which are radially aligned. During systole the elastin fibres seem to reduce the radial strain on the leaflet (Sacks et al. 2009). The *spongiosa* is the middle layer between the *fibrosa* and the *ventricularis*. It is primarily composed of hydrated glycosaminoglycans (GAG) and proteoglycans. It provides a buffer zone between the *fibrosa* and *ventricularis* to enable shear movement during systole and diastole. The *fibrosa* is the thickest layer. Its main components are crinkled Collagen Typ I fibres, which are organized in a dense network. The fibres are predominantly aligned in a longitudinal direction and for a small part also radially. Functionally, the *fibrosa* is the main load bearing layer. The circumferentially aligned collagen fibres increase stiffness and strength in this direction. (Jana et al. 2014)

The different histological structures of the three laminae facilitate the adaption of the leaflet to the physical forces to which the AV is exposed to during a cardiac cycle (Hasan et al. 2013). Moreover, the cells on the leaflets aid in the correct function of the valve. Native cells on the aortic valve leaflets can be differentiated into valvular endothelial cells (VEC) and valvular interstitial cells (VIC). VEC build a monolayer on the surface of the aortic valve leaflet and have the ability to adapt to different mechanical forces and the changing hemodynamic environment. Furthermore, they regulate the complex coagulation pathway, where they inhibit coagulation and ensure a free blood flow, as well as start the coagulation pathway when an injury occurs and react to the transmitters in the blood flow. (Butcher, Nerem 2007) VEC differ in certain qualities from the EC on the aortic wall. While vascular EC are parallel to the blood flow, VEC are oriented perpendicularly (Fig 2-3) (Butcher et al. 2004; Deck 1986). Furthermore, a study from Simmons *et al.* (2005) implies a difference in the gene expression of the VEC on the arterial and ventricular side. Experiments on porcine VEC show a significantly lower expression of the genes inhibiting vascular and valvular calcification in the EC of the arterial side.

Studies demonstrate, that VEC retain their ability from the prenatal phase to perform endothelial-to-

mesenchymal transformation. During the valvulogenesis EC in the endocardial cushion start to migrate into the valvular interstitium, gradually developing the contractile protein α-SMA and finally turning into VIC. (Paruchuri et al. 2006) It seems that endothelial-to-mesenchymal transformation provides a part of the renewal of the VIC in the course of physiologic valve remodeling (Hjortnaes et al. 2015). VIC present the majority of cells in the valve leaflets. They synthesize, maintain and remodel the ECM. When VIC are activated by mechanical stress or disease they become myofibroblast-like cells, while in their dormant state they resemble FB. Myofibroblasts are more contractile and release a number of different proteins (e.g. cytokines, chemokines, growth factors, ECM elements), when the valve is damaged. Moreover, VIC can also transform into osteoblast-like cells, which are associated with calcification of the valve. (Zhang et al. 2015)

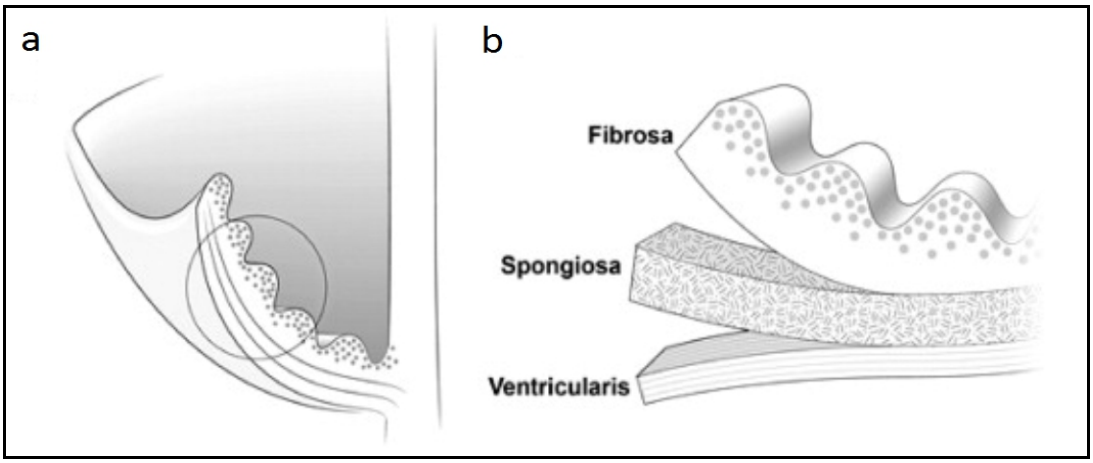

Fig 2-2 Schematic structure of an aortic valve leaflet *(a) displays the leaflet attached to the aortic wall. The crinkled side is the fibrosa (b), which contains mostly Collagen Typ I fibres, which are longitudinally aligned. It is the main load bearing layer. The spongiosa acts as buffer zone between fibrosa and ventricularis. Its main components are GAG. Its architecture enables a shear movement between fibrosa and ventricularis. The fibrosa is built from elastin and collagen fibres. During systole the elastin fibres reduce shear stress on the leaflet.*

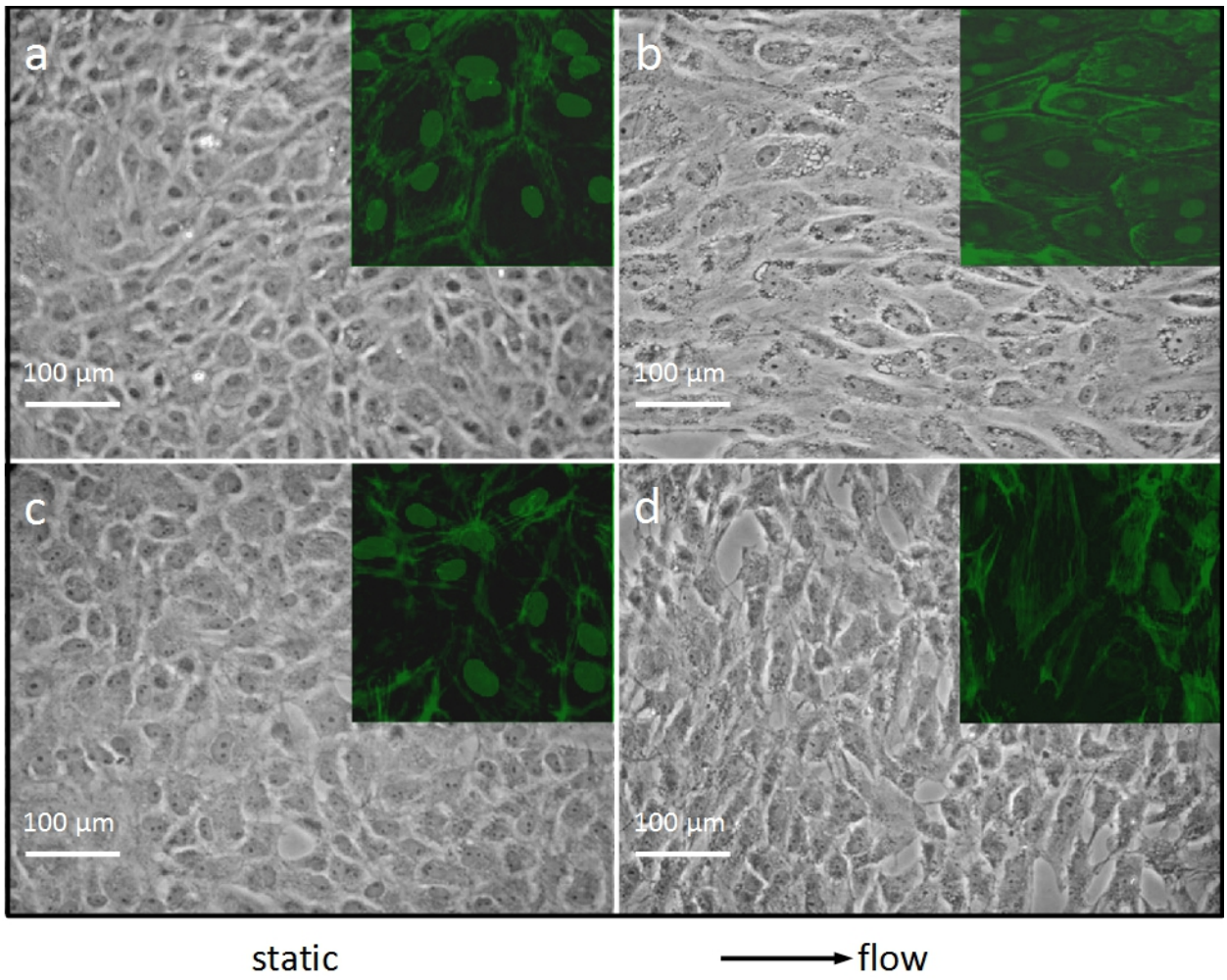

Fig 2-3 EC under static and dynamic conditions *The flow direction is indicated by the arrow at the bottom. The images (a) and (b) represent vascular endothelial cells, (c) and (d) represent the valvular endothelial cells. In (d) the perpendicular orientation of the valvular endothelial cells is visible, while in (b) the longitudinal orientation of the vascular endothelial cells is demonstrated. The green highlighted pictures depict F-Actin filament organization, which also changes orientation according to the flow direction.*

2.2.2. Pathophysiology

The causes for an aortic valve disease are varying. Degeneration, rheumatic fever and congenital deformities are abundant reasons for damages to the AV. At the present day degenerative calcification of the AV is the most frequent cause for an aortic valve stenosis (AVS) in the developed countries, while rheumatic fever is still the most common reason for AVS in emerging and third world countries (Carabello 2007; Coffey et al. 2016). The calcification process was thought to be a passive, degenerative disease. But studies show that the process of calcification of the AV is similar to that of atherosclerosis of the vessels (Otto et al. 1994; Zeng et al. 2016). Hemodynamic forces and common cardiovascular risk

factors (i.e. diabetes, hyperlipidaemia, hypertension) seem to play an important role in the development of an AVS (Simmons et al. 2005; Maganti et al. 2010).

Rheumatic fever usually occurs a few weeks after an infection with *streptococcus pyogenes*. The *streptococcus "M protein"* and cardiac proteins like Vimentin and Myosin have similar surface protein domains, thus creating a molecular mimicry and evoking an antibody response (Coffey et al. 2016). Although, Tandon *et al.* (2013) hypothesize that binding of the "*M protein*" to specific collagen structures is responsible for the antibody activation. Repeated subclinical infections then lead to fibrosis and inflammation, which eventually causes valve stenosis (Fig 2-4) (Coffey et al. 2016). While degenerative deterioration of the AV is most common in the older population (prevalence of 12.4 % in the population > 75 years), children between 5 and 15 years have the highest risk for a first episode of rheumatic fever. The highest prevalence of a rheumatic heart disease lies between the age of 25 to 45 years (Coffey et al. 2016; Remenyi et al. 2016).

Congenital malformations of the AV or the leaflets increase the risk for an early onset of valve degeneration and following AVS. Up to 75 % of the patients with a bicuspid aortic valve develop an AVS (Furukawa, Tanemoto 2015). The bicuspid aortic valve is the most common congenital heart valve defect (0.5 - 0.8 % of the newborn children are afflicted) (Coffey et al. 2016). Patients with a bicuspid aortic valve, which develops into an AVS, often require an invasive correction at an earlier age. The average age at surgery in these patients lies slightly below 50 years (Michelena et al. 2008). Furthermore, the bicuspid aortic valve is often associated with complications like AVS, aortic valve regurgitation, dilatation of the aorta and endocarditis (Furukawa, Tanemoto 2015).

During the progression of an AVS, the myocardium adapts to the change in transvalvular pressure. The myocardium of the LV thickens and contractility increases (Bonow et al. 2016). However, the benefit of these compensatory mechanisms is limited and eventually a decreased diastolic compliance, subendocardial ischemia and exhausted myocardial contraction reserve are the consequences. This ultimately leads to myocardial fibrosis and reduction of the LV ejection fraction. Diagnosis of AVS proves to be difficult, due to the lack of symptoms at an early stage. Heart murmurs, which are detected during a physical examination, are often the first indication for an AVS (Nishimura et al. 2014). Severe AVS often comes with the triad of dyspnea, angina and syncope. AVS combined with one of these symptoms is a strong indication for AV replacement. Studies show a very poor outcome for an untreated severe, symptomatic AVS (1-year-mortality up to 50 %, 5-year-mortality up to 90 %) (Bonow et al. 2016). The replacement of the AV in an asymptomatic AVS is recommended if the LV ejection fraction is decreased, the stenosis is severe (peak velocity > 4.0 m/s), or there is evidence for a rapid progression of the AVS (Nishimura et al. 2014).

Aortic valve regurgitation is less prevalent than AVS (Bonow et al. 2016). The patients, which present with this disease, are younger. Nevertheless, the incidence of a clinical significant regurgitation increases

with age, peaking at the sixth decade of life. (Maurer 2006) Congenital aortic valve regurgitation is often associated with an unicuspid, bicuspid, quadricuspid valve or a tricuspid valve with leaflet malformations. Furthermore infectious endocarditis (IE), congenital or acquired dilatation of the aortic root or the ascending aorta, rheumatic fever, and systemic lupus erythematosus can also cause insufficiency (Maganti et al. 2010). The normally mild onset and the slow progression of a congenital aortic valve regurgitation is in most cases well tolerated for many years (Bonow et al. 2016; Hoffman 2009). Nevertheless, progressive or severe aortic valve regurgitation leads to gradually increasing systolic LV dysfunction (Bonow et al. 2016). Aortic dissection or IE can cause an acute, severe aortic valve regurgitation. These conditions are emergencies and surgical treatment should not be delayed. (Nishimura et al. 2014)

IE has a yearly incidence of up to 10 in 100 000 people and is a rare condition (Cahill, Prendergast 2016). While the intact valvular endothelium is capable of fending of the daily bacteremia it is exposed to, conditions like rheumatic fever or valve sclerosis damage the endothelium and thus make is susceptible to infection. Also, heart valve prostheses increase the risk for an IE. 80 - 90 % of IE are caused by the gram-positive cocci of the staphylococcus, streptococcus and enterococcus species. Clinical symptoms for an IE are often unspecific, with fever (90 %) and a cardiac murmur (85 %) being the most common. Furthermore, evidence for complications like heart failure, stroke or metastatic infection can indicate an IE. While 50 - 60 % of IE cases can be treated with antibiotics, conditions like heart failure caused by regurgitation or stenosis, uncontrollable infection, sepsis and high risk of embolism are strong indications for a surgical treatment.

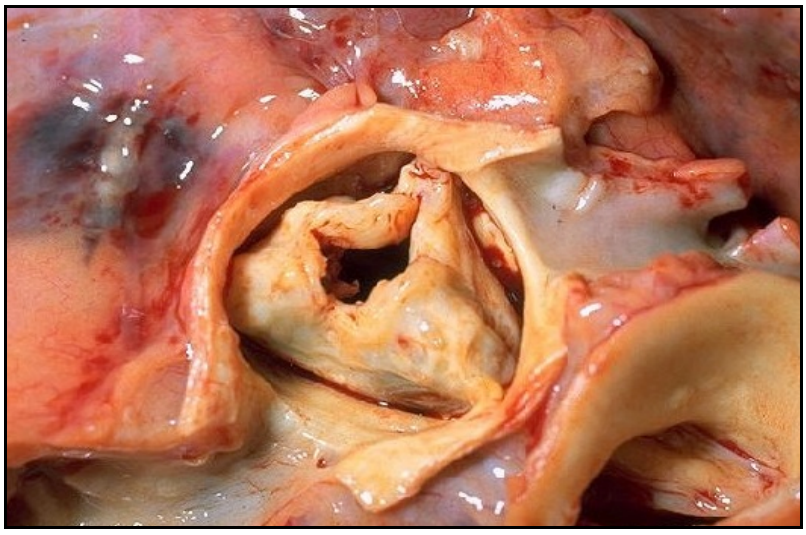

Fig 2-4 Aortic valve stenosis due to rheumatic infection *The three leaflets adhere tightly in the periphery and the effective orifice area is decreased.*

2.3. Aortic Valve Disease Treatment

2.3.1. Conservative Treatment

While there is actually no causal conservative therapy for an AVS, it is important to treat comorbidities like hypertension. Patients with decompensated AS and NYHA IV (angina pectoris and/or dyspnea at rest) eventually benefit from a treatment with vasodilatators to reduce afterload until surgery. Although, hyperlipidaemia is a risk factor for AVS, statine treatment does not successfully prevent progression of an AVS. (Nishimura et al. 2014)

2.3.2. Open Heart Surgery

Open heart surgery with cardioplegia and extracorporal circulation is the gold standard for aortic valve replacement (Bonow et al. 2016). The sternum is opened via a minimal or total median sternotomy. For cardio-pulmonary bypass an arterial cannula is placed in the aorta ascendens. The venous cannula is placed in the right atrium or in the inferior and superior venae cavae, if the patient suffers from severe tricuspid valve disease or has a cardiac shunt (Duran et al. 1991; Schmid 2014). Via the extracorporal circulation the core body temperature is lowered to 30-34 °C, if the duration of surgery is expected to last more than one hour (Schmid 2014). The aorta is cross clamped just under the arterial cannula and cold cardioplegia is instilled retrograde via the coronary sinus or antegrade via the aorta or the coronary ostia. For myocardial protection the heart is cooled to minimize the ischemic damage (Duran et al. 1991). The vent, a cannula to drain blood from the LV, is inserted into the right upper pulmonary vein to ensure a blood-free operation field (Schmid 2014). The wall of the aorta is horizontally cut open at the sinotubular junction. In case of an aortic stenosis the calcified leaflets of the valve are removed and surgical debridement is performed on the annulus. Abscess or fistula of the annulus, which are complications of an IE, often require extensive repair and the use of pericardial patches. The size of the AV prosthesis is measured intraoperative and the new valve is sewed in. CO_2 can be added in the situs during prosthesis implantation to avoid air embolism. The aorta is closed with a continuous side-to-side suture. Different valve prostheses are available for valve replacement (see *Chapter 2.4. Aortic Valve Prostheses).*

In some cases of aortic valve regurgitation it is possible to reconstruct the valve and thus sparing the patients the risks associated with AV prosthesis (Fig 2-5) (*Ch 2.4. Aortic Valve Prostheses*). It is important to evaluate if regurgitation is caused by a dilatation of the *aortic annulus* or a malformation of the valve itself. A dilatation of the *aortic annulus* with an associated aortic valve regurgitation can be surgically corrected with a subcommissural annuloplasty or the implantation of a prosthetic ring. Dilatation of the *aortic annulus* after aortic valve repair is a common reason for the recurrence of aortic valve regurgitation (Mazine et al. 2016). These findings emphasize the importance of securing the annulus

during surgery. A prolaps of the aortic valve leaflet is often associated with a bicuspid aortic valve. Different surgical methods are available for the repair of a leaflet prolaps. Triangular resection of the prolaps and suture of the median adhesion of the bicuspid valve shorten and elevate the cusp and enables a tight adaption. Other methods for the repair of an isolated leaflet prolaps include a cusp plication at the commissures (Minakata et al. 2004). Aortic valve regurgitation which is caused by the perforation of a leaflet can be fixed with a homologous pericardial patch (Mazine et al. 2016). However, an extensive lesion of the leaflet often requires a valve replacement. Reconstructive surgery of the AV is becoming more common in isolated aortic valve regurgitation today. Whereas reconstruction in AVS is in most cases not reasonable. (Schmid 2014).

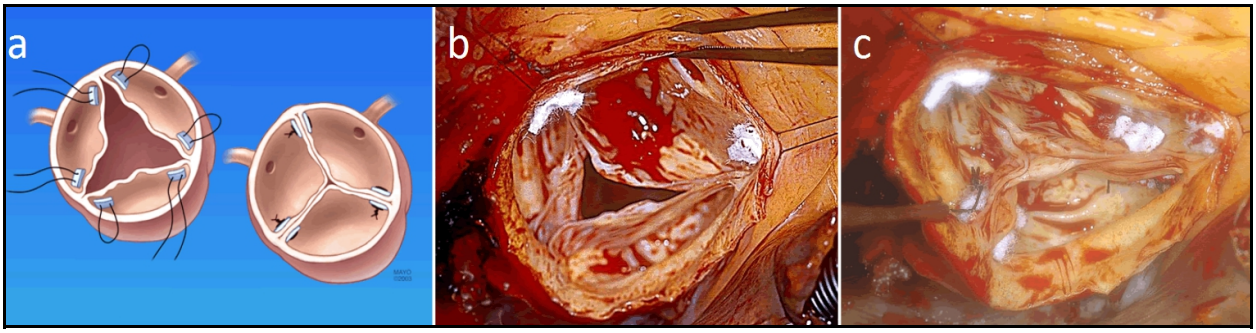

Fig 2-5 Reconstruction of an aortic valve regurgitation *(a) shows the layout of the reconstruction procedure. Just bellow the commissures the patches are applied and sutured in. (b) demonstrates the intraoperative picture before the reconstruction. The leaflets do not adapt. In (c) the subcommissural patches are applied and the leaflets adapt now.*

2.3.3. Transcatheter Aortic Valve Implantation

Initially, TAVI was intended for patients, who could not undergo conventional surgical aortic valve replacement due to their multiple comorbidities. The number of TAVI procedures is steadily increasing. Evolution of the implanting technique, decrease of procedure related complications and increasing evidence based research are reasons for the increase of TAVI procedures. (Bonow et al. 2016) Long-term results are still pending, thus making TAVI a procedure which is primarily performed in patients with contraindications for a conventional aortic valve replacement (Kuck et al. 2015).

Different surgical access points are possible for the insertion of the catheter for valve implantation. The transfemoral implantation route is most commonly used (Bonow et al. 2016). However, distinctive kinking of the pelvine arteries or aorta as well as severe peripheral arterial disease may be a contraindication for the transfemoral implantation. In those cases, the valve can be implanted transapical, transaortal via the ascending aorta, or transarterial via the subclavian or axillary artery. An interdisciplinary heart team is recommended to evaluate the appropriate access point for a TAVI.

In case of a transfemoral access, the femoral artery is punctured and a guiding wire is inserted. A sheath, which is used to insert the valve prosthesis, is introduced in the femoral artery after dilatation of the punctuation. The diameter of the sheath decreased during the last years. Large sized sheaths in femoral arteries, especially in elderly patients or patients with severe atherosclerosis, increase the risk of vascular complications (i.e. postoperative bleeding, dissection of the femoral artery) (Fanning et al. 2013). A guide wire, which is manually shaped to fit the form of the LV to decrease the risk of injury to the myocardium, is then advanced into the LV. In case of a severe aortic valve calcification, a balloon valvuloplasty (dilatation of the aortic valve without implantation of a valve prosthesis) can be performed before valve implantation. This procedure facilitates prosthesis implantation and expansion (Patsalis et al. 2013). The balloon is usually smaller than the aortic annulus to minimize the risk of an annulus rupture and severe aortic valve regurgitation. The balloon valvuloplasty and the valve implantation are performed during rapid ventricular pacing. The heart rate is raised to 160 - 220 bpm with a temporary pacemaker, which is usually implanted in the RV via the jugular or the femoral vein. The rapid movement of the LV during pacing reduces the LV ejection fraction and facilitates the placement of the balloon as well as the subsequent positioning of the valve prosthesis. During the balloon valvuloplasty the placing of the balloon is monitored using contrast-enhanced X-ray as well as transoesophageal echocardiography. The coronary flow is monitored with repeated contrast agent injection to avoid obstruction. After the balloon valvuloplasty the aortic valve prosthesis can be implanted. Before inserting the prosthesis through the sheath the crimping procedure is performed. Crimping reduces the diameter of the prosthesis so it fits the sheath and the vessel diameter. Current valve prostheses have to stay submerged in a liquid, because of the treatment with a fixative. This presently prevents the development of a preloaded delivery system, where the valve prosthesis is already crimped. (Alavi et al. 2014) Furthermore, the valve prosthesis deteriorates when crimped for a prolonged period of time (Kiefer et al. 2011). The crimper puts equal pressure on the sides of the prosthesis, thus enabling a symmetric decrease in diameter. Crimping is one particular problem of the TAVI procedure. The crimping of the prosthesis can damage the leaflet structure and thus can decrease valve durability (Alavi et al. 2014). Depending on the valve type, a balloon is needed to inflate the valve after crimping (Fig 2-6). Meanwhile, self expandable prostheses are available, which do not require rapid pacing during implantation (*Chap 2.4. Aortic Valve Prostheses*) (Fanning et al. 2013). Nevertheless, postdilatation may be necessary due to regurgitation after the expansion of the valve (Abdel-Wahab et al. 2014). Hemodynamic outcome and eventual paravalvular leakage are assessed with transoesophageal echocardiography and X-ray monitoring (Stortecky et al. 2012).

While the transfemoral approach can be performed under light sedation and local anesthesia, transapical and transaxillary access requires general anesthesia due to the more invasive procedure. For a transapical access, a mini-thoracotomy has to be performed. The cardiac apex is located with

echocardiography and the incision is placed at the 5th or 6th intercostal space. Purse string sutures, which are most commonly used, around the puncture site of the apex both hold the moving heart in place and facilitate closure of the wound after the procedure (Ziegelmueller et al. 2015). After the preparation of the operation field the myocardium is punctured and a guide wire inserted. It is important to keep the wire from entangling itself in the chordae of the mitral valve and eventually cause mitral regurgitation. Following the save deployment of the wire the sheath can be introduced and the following procedure is performed analogous to the transfemoral approach. A fragile LV myocardium can increase the risk for a ventricular rupture or building of a LV aneurysm after transapical device implantation (Stortecky et al. 2012). For a transaxillary or transsubclavian access the artery has to be surgically dissected. Delivering the valve prosthesis via a transaxillary or transsubclavican access may cause cardiac ischemia in patients, who have received a cardiopulmonary bypass surgery, where the internal mammary artery was used as bypass graft. The internal mammary artery is a branch of the subclavian artery and dissection of the vessel, which is a possible complication of the TAVI procedure, can cause ischemia. (Stortecky et al. 2012)

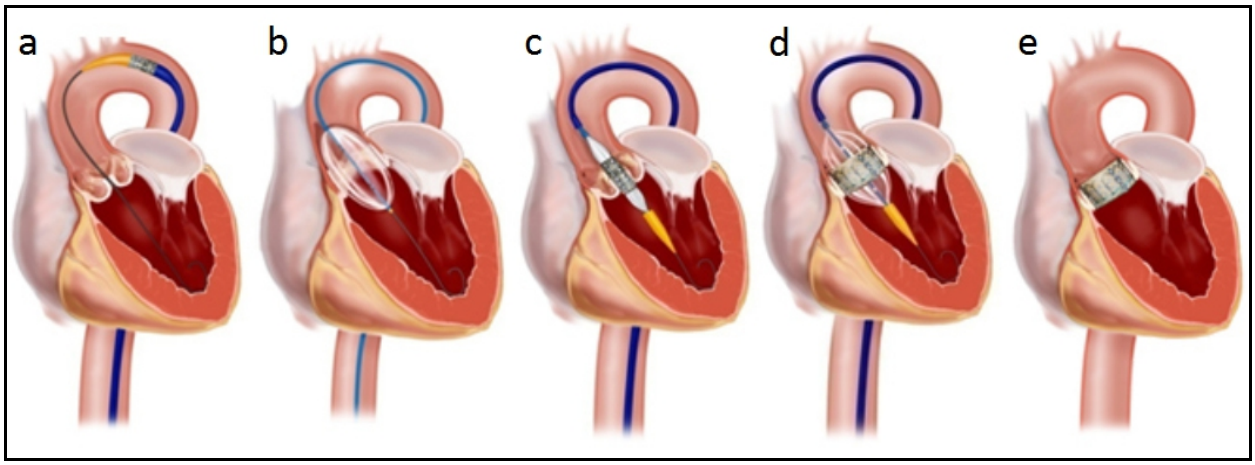

Fig 2-6 Transfemoral aortic valve implantation *(a) shows the guide wire placed in the left ventricle and the balloon, which is about to be placed in aortic position. (b) demonstrates the inflation of the balloon. After valvuloplasty the crimped aortic valve prosthesis is brought into position (c). Afterward the valve is expanded using a balloon (d). The position of the prosthesis can be confirmed via transoesophageal echocardiography and X-ray markers on the deployment device and the valve itself (e).*

2.4. Aortic Valve Prostheses

2.4.1. Mechanical Heart Valves

The main components of a mechanical heart valve (MHV) are either synthetic or nonbiological (Butany et al. 2003). Especially titanium and pyrolyte (a type of pyrolytic carbon) are frequently used materials (Gott et al. 2003). These materials have a very long durability, possibly up to 30-50 years (Ye et al. 2009). In most MHV, three main components can be distinguished: the occluder, the housing and the sewing ring. The occluder is the movable part of the prosthesis. Depending on the valve type it can be a ball, a disc or a leaflet. The housing provides support and fixation for the occluder. The housing of the caged-ball valves, as the name implies, is a cage, which guides and hold the ball in place. The valves with discs or leaflets require a ring of titanium or pyrolytic carbon as housing, where the moving parts are mounted. The sewing ring enables the implantation of the MHV. The opening and closing of the MHV is passive and depends on the blood flow as well as the pressure gradient. (Butany et al. 2003) Looking at the hemodynamic properties of the different MHV types, they can be categorized into two groups: valves with lateral flow patterns such as caged ball valves (Fig 2-7 a) and valves with a more central flow such as the tilting disc and bileaflet valves (Fig 2-7 b, c)(Yoganathan et al. 2005). The Starr-Edwards caged ball valve is the only caged ball valve, which is currently used. While it demonstrates good reliability its hemodynamic properties are unsatisfactory. The pressure drop of a caged ball valve is higher compared to a tilting disc or bileaflet valve. (Yoganathan et al. 2004) Moreover, its high-profile configuration and the occluder-induced turbulence are disadvantageous (Dasi et al. 2009) Nevertheless, all MHV generate flow patterns significantly different compared to a native AV. High velocity and shear stress are part of these flow patterns which consequently cause damage to blood cells. Low flow regions caused by recirculation increase the possibility of clot formation. (Yoganathan et al. 2005) To decrease the risk of clot formation, especially in the region of the hinges in bileaflet valves, the leaflet edges and the housing, a certain degree of insufficiency upon valve closure is admitted to allow retrograde flow (Butany et al. 2003). Aside from the thrombogenicity caused by abnormal flow patterns, the reduced hemocompatibility of the used materials is another risk factor for clot formation (Ye et al. 2009). To prevent thrombus formation a life long anticoagulation therapy is mandatory. Vitamin K antagonists like warfarin are utilized for this purpose (Eikelboom et al. 2013).

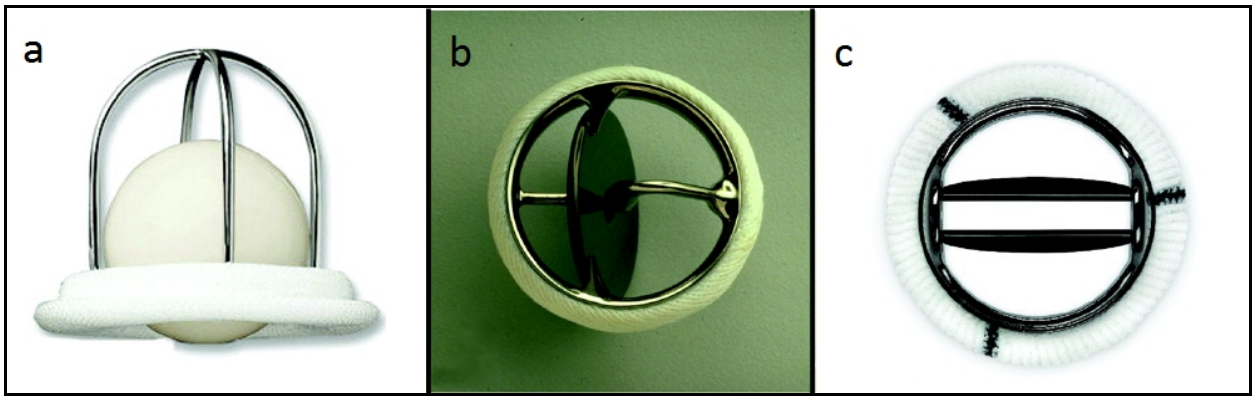

Fig 2-7 Different models of mechanical heart valves *(a) depicts a caged ball valve (Starr-Edwards). (b) shows a tilting disc MHV (Medtronic Hall) and (c) displays a bileaflet MHV (St Jude)*

2.4.2. Biological Heart Valves

Different types of biological heart valves (BHV) are available for aortic valve replacement. Autografts are organs or tissue which are removed from their original position in the human body and placed in another position in the same body. One example is the Ross procedure. The malfunctioning aortic valve is replaced with the patient's own pulmonary valve. A homograft is implanted in the pulmonary valve position. Due to the moderate pressure in the pulmonary circulation, biological valve prostheses in this position have a extended durability. The pulmonary trunk is able to grow with the patient, thus making it especially beneficial for very young patients. However, late valve failure often requires repeated surgeries which are associated with a higher operative risk. (Bloomfield 2002)

Tissue which is obtained from a human body and placed in another human is considered a homograft. Homografts can be harvested from cadavers, from organ donors or from the explanted heart of a heart transplant recipient. A study from Fan *et* al. (2012) which evaluated the bacterial contamination status of homografts of different origins, described a lower contamination rate for homografts, which where harvested from recipients of a heart transplant. After explantation the homografts were disinfected in an antibiotic solution and then either fresh-wet stored at 4 °C or cryopreserved in liquid nitrogen. A cryopreserved homograft can stay frozen over a prolonged period of time. However, special care must be taken during the rewarming process to achieve a homogeneous thawing of the complete homograft to avoid forming of interstitial ice crystals. Crystallization of interstitial water can cause later degeneration. During fresh-wet storage more donor cells on the homograft stay viable. These residual cells might increase the immunogenic response of the recipient (Gulbins et al. 2003b). Homografts and native aortic valves were thought to have the same durability. However, a calcification process limits the durability of homografts. 20 years after implantation, about 30 - 40 % of the homografts are still functioning. The use of homografts is very restricted today. The considerable drawbacks of these prostheses include their

limited availability, the slightly more complex implantation procedure, and limited durability. (Delmo Walter et al. 2012; Bloomfield 2002)

Xenografts are valves, which originate from another species. These valves are either manufactured from bovine pericardium or a whole porcine valve (Pibarot, Dumesnil 2009). There are porcine valves which are fabricated either with a stent (Fig 2-8 a) or without (Fig 2-8 b). The word “stent” in regard to a “stented valve” refers to a frame, which provides mechanical support and an attachment to the aortic wall (Sacks et al. 2006). Theory stated, that the absence of the sewing ring and stent enables the implantation of larger valves, and therefore improves the effective orifice area. However, the missing sewing ring raises the complexity of the implantation. (Cohen et al. 2010) Recent studies regarding the benefits of stentless valves for the patient (e.g. reducing LV mass, better hemodynamic properties, lower transvalvular gradients) could validate a significant difference compared to stented valves (Kobayashi 2011). Bovine valves are fabricated from flat sheets of bovine pericardium (Fig 2-8 c). During the fabrication process, the focus lies on maximizing the opening area during systole and optimizing the coadaptation area of the leaflets during diastole. This results in improved hemodynamic properties of the bovine valves compared to porcine valves (Vesely 2003). To reduce antigenicity and to stabilize against proteolytic degradation, bovine and porcine valve prostheses are treated with glutaraldehyde. This process cross-links and masks the antigens, thereby reducing the immunologic response (Badylak 2004). Nevertheless, xenografts and homografts elicit an immune response from the host body (e.g. Alpha-Gal antibodies against xenografts; cell mediated immune response activated by antigen presenting cells against homografts) (Badylak, Gilbert 2008; Moroni, Mirabella 2014). This induces an inflammation reaction, which also contributes to the limited durability of the BHV. Moreover, glutaraldehyde itself mediates a calcification process which further adds to the restricted life time of a bioprosthetic valve. (Vesely 2003) Contrary to MHV, BHV do not require a life long anticoagulation thus decreasing the risk for major bleeding (Brennan et al. 2013).

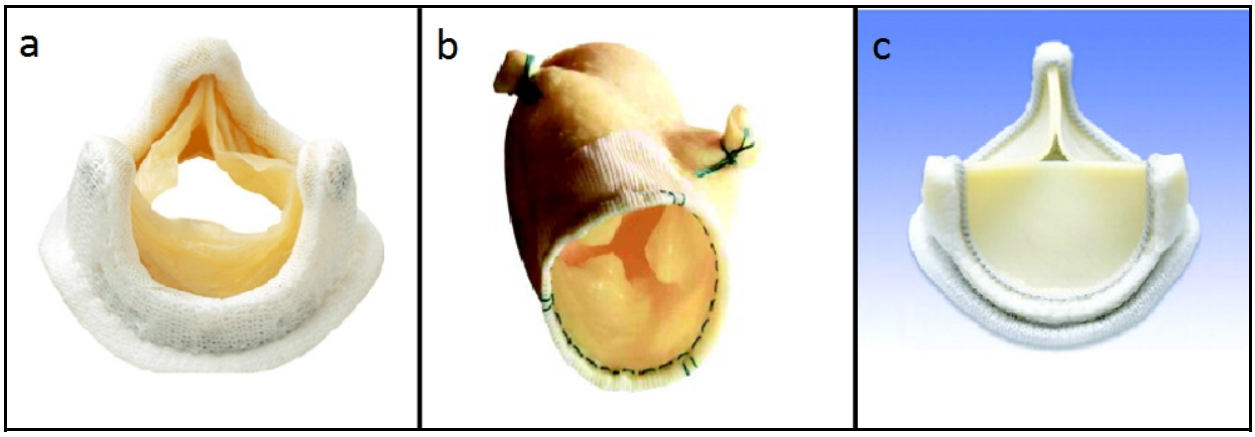

Fig 2-8 Different models of biological heart valves *(a) shows a stented porcine valve (Medtronic Mosaic), (b) a stentless porcine bioprosthesis (Medtronic Freestyle) and (c) a stented pericardial bioprosthesis (Carpentier-Edwards Magna)*

2.5. Heart Valve Tissue Engineering

2.5.1. Introduction

About 1 % of neonates are born with a congenital heart disease. More than 30 % of these malformations affect the aortic or pulmonary valve. This establishes a significant demand for artificial heart valves especially for pediatric patients. (Schoen 2011) Currently a dysfunctional heart valve can be replaced with either a BHV or a MHV. However, there are limits to the possibilities of the valves. Both valve types lack the possibility for growth, remodel or repair. The replacement of a malfunctioning heart valve in young patients often requires multiple subsequent valve replacement surgeries. The combination of cells, scaffolds and bioreactors enables tissue engineering to overcome the limits of conventional heart valve prostheses. The ideal tissue engineered valve enables growth, remodeling and even repair of the valve. Designed from the patient's own cells the thromboembolic potential is minimal and the optimal hemodynamic attributes do not require anticoagulation. (Sanz-Garcia et al. 2015)

2.5.2. Heart Valve Scaffolds

A scaffold is a three dimensional supporting structure which enables cell adhesion, migration and growth. Biocompatibility of the applied scaffold material as well as mechanical integrity and sterilizability are essential requirements (Jana et al. 2014). Furthermore, a scaffold should facilitate cell nutrition and allow dynamic changes of its architecture (Dohmen, Konertz 2009). A scaffold can be fabricated from two different sources: a decellularized heart valve scaffold, either of xenogenic or allogenic origin, or an artificial scaffold, manufactured from synthetic or natural polymers. Artificial scaffold material can be further classified by their structure, which is either porous, fibrous or hydrogelic. (Jana et al. 2014)

Decellularized Heart Valve Scaffolds

Decellularized heart valves preserve the complex structure of the ECM of a native aortic valve, which is one possible advantage over artificial scaffolds. Xenogenic and allogenic heart valves are sources for decellularized valves. The short supply on human heart valves is the primary reason for the more frequent use of xenogenic heart valves, despite their higher antigenic potential. (Jana et al. 2014) The host body identifies xenogenic and allogenic cell material as foreign and initiates an immune response (Gilbert et al. 2006). ECM proteins, however, are shared within the species and are thus tolerated in xenogenic species. The optimal decellularization process removes the native cellular and nuclear material from the valve while the ECM and the ECM proteins stay intact and preserve their functionality (Khorramirouz et al. 2014). The decellularization process often combines different procedures, including physical, chemical and enzymatic treatments. A decellularization protocol includes the physical or chemical lysis of the cell membrane, enzymatic or chemical disconnection of the cell-ECM connection and the removal of any cell debris, which may elicit immunologic responses (Gilbert et al. 2006).

Physical methods for the decellularization include freeze-thaw cycles, agitation and immersion and the use of pressure (Keane et al. 2015). During the freezing process ice crystals form intracellular, which rupture the cell membrane and induce cell lysis. The remaining intracellular and membranous components have to be removed by consecutive processing. (Crapo et al. 2011) The temperature drop has to be monitored closely to avoid the formation of ice crystals in the ECM as well. (Gilbert et al. 2006) Aortic valve homografts showed signs of microscopic and macroscopic fissures after rapid thawing processes, most likely due to the temperature differences between the outer and inner wall during freezing and thawing processes (Wassenaar et al. 1995). Agitation and immersion of the sample in enzymatic, chemical and/or detergent solvents is a commonly used decellularization protocol. The duration of the process depends on multiple factors, including the strength of the agitation, the type of enzymatic, chemical or detergent solution, which is utilized, and the thickness and density of the tissue. (Keane et al. 2015) Pressure can aid in the distribution of decellularization agents into the tissue and remove the cellular remains from the tissue. Applying pressure gradients during the decellularization of hollow organs (e.g. blood vessels, intestines, urinary bladder) can be advantageous. (Keane et al. 2015) Montoya *et al.* (2009) decellularized human umbilical veins using a convective flow protocol and compared it to rotary agitation. Immunohistological analysis showed residual cell debris in the samples which were subjected to rotary agitation. The vessels which were exposed to convective flow at 5 mmHg and 50 mmHg were free of cells. The circumferential collagen structure stayed intact. However, at higher pressures (150 mmHg) the basement membrane was disrupted to a certain degree.

Non-ionic detergents such as Triton X-100 sever lipid-lipid and lipid-protein interactions. Protein-protein interactions stay intact, thus proteins within tissues maintain their functionality. Triton X-100 is known for its moderate impact on the tissue structure itself. It is widely used in various decellularization

protocols. (Gilbert et al. 2006) The valvular structure of an aortic valve stayed intact after 24 h treatment with Triton X-100. The nuclear material was completely removed from the valve. However, cell remnants were detected in the attached myocardium and the aortic wall. Regarding the ECM, treatment with Triton X-100 causes a nearly complete loss of GAG and a decrease of the quantity of laminin and fibronectine in the heart valve. (Grauss et al. 2005) The loss of GAG highly depends on the tissue, which is decellularized. While heart valve tissue loses most of its GAG after a 24 h treatment with Triton X-100, the GAG of the anterior cruciate ligament stayed intact even after a 4 day period of processing. Treatment with Triton X-100 can be a very effective decellularization, but its effectiveness depends on the tissue, which is processed and the combination with other decellularization methods. (Gilbert et al. 2006)

Ionic detergents like sodium dodecyl sulfate (SDS) and sodium deoxycholate (SD) solubilize cytoplasmatic and nuclear cellular membranes, but can also cause denaturation of proteins by dissolving the protein-protein connections. SDS displays a very efficient removal of cell components from tissue, compared to other detergents. Nuclear remnants and cytoplasmatic protein are also removed. However, the GAG concentration and collagen integrity decrease after the use of SDS. SD also exhibits efficient cell removal qualities, but causes even more disruption in the structure of the native tissue compared to SDS. (Gilbert et al. 2006) Nonetheless, SDS and SD efficiently remove cells from tissue as well as enable host cell repopulation after decellularization (Rieder et al. 2004; Khorramirouz et al. 2014).

Enzymatic decellularization includes the processing with proteases (e.g., trypsin), nukleases (e.g. DNase, RNase) and esterases (phospholipase A2) (Keane et al. 2015). During the enzymatic decellularization with trypsin peptide bonds on the carbon side of arginine and lysin are separated if the next residue is not proline (Voet 2002). Studies show different results regarding the decellularization efficiency of trypsin. While some report a limited success of cell removal compared to the decellularization with a SD 1 %/SDS 1 % mixture (Khorramirouz et al. 2014), others describe a nearly complete cell removal after a 24 h treatment of the valve with trypsin 0.05 %/EDTA 0.02 % (Schenke-Layland et al. 2003). DNase and RNase catalyze the hydrolization of deoxyribonucleotides and ribonucleotide chains. During the decellularization process, they are often utilized to remove residual DNA when the detergent decellularization showed incomplete decellularization. (Keane et al. 2015) After the decellularization of rat aortic valves with SDS 0.1 % for 24 h at 4° C Grauss *et al.* (2003) added an enzymatic decellularization step with RNase and DNase to remove any residual substances. They achieved a complete removal of cells through the whole valve tissue. The elastic laminae as well as the collagen fibres seemed to be intact. However, fibronectin and chondroitin sulfate were completely washed out from the leaflet albeit still present in the base of the valve. The pancreatic phospholipase A2 hydrolyzes the ester bond of membrane glycerophospholipids. Wu *et al.* (2009) demonstrated almost complete cell removal after the decellularization of porcine corneal stroma using a combination of SD 0.5 % and phospholipase A2

200 U/ml. The collagen fibres stayed intact as well as a sufficient amount of proteoglycans.

An important step during the decellularization process is the removal of the residual chemicals after decellularization. High concentration of chemicals in the decellularized tissue are toxic to the cells and prevent the host cells from seeding the tissue after implantation or *in vitro*. (Gilbert et al. 2006) Rieder *et al.* (2004) demonstrated the toxic effect of SDS on cells. Porcine pulmonary and aortic valves were decellularized with SDS 0.1 % for 24 h. The residual cell material was removed by subjecting the specimen to RNase (100 µg/ml) and DNase (150 IU/ml) treatment for 24 h. The samples were washed with M-199 medium for 24 h at 4° C. After the decellularization human EC were seeded on the specimen. Within 24 h no cell attachment was observed but a massive cell lysis took place. Histological analysis showed no confluent cell layer after 5 days of incubation.

The efficiency of cell removal and the potential damaging of the scaffold tissue during the decellularization process depend to a great extent on the tissue. While using the same decellularization protocol, with only variation in the concentration of trypsin (0.5 % vs. 0.05 %), Grauss *et al.* (2005) described ineffective removal of cells from the rat aortic valve, while Schenke-Layland *et al.* (2003) reported successful removal of cells from the porcine pulmonary valve. The subtle changes in the protocol do not fully explain the highly divergent results. It seems the success of a decellularization and the changes to the ECM differ depending on the tissue source, the composition of the tissue, the density and other factors. Therefore, a tissue adapted decellularization protocol for each different scaffold seems necessary, to achieve complete cell removal and reduce damage to the ECM. (Gilbert et al. 2006)

Artificial Heart Valve Scaffolds

Considering the diminishing supply of homograft heart valves for scaffolds and the lack of small-size homo- and xenografts, artificial heart valve scaffolds can provide a nearly endless supply of valves in all sizes (McMullan et al. 2006). Decreased immunogenicity and thrombogenicity of artificial scaffolds may pose advantages as well as control over biodegradability, mechanical properties and durability (Jana et al. 2014). However, problems arise when the complex architecture and the functionality of the heart valve have to be copied. Scaffolds with porous, fibrous or hydrogelic structures are available for the fabrication of an artificial heart valve with the ability to mimic the ECM and the performance of a native valve. (Jana et al. 2014)

Porous scaffolds provide an interconnected network of homogeneous pores, which facilitates a continuous sustenance of nutrients and drainage of metabolic waste (Jana et al. 2014). The porous structure imitates the native ECM, enabling interaction of cells with their environment (Dhandayuthapani et al. 2011). The ideal pore size of the scaffold depends on the respective tissue and cell (Wei, Ma 2004). Small pores may form a dense network, but they can hinder cell migration and eventually impede the building of large tissue. Large pores stimulate vascularization of the scaffold,

however during *in vitro* cell seeding these scaffold showed low cell holding and eventually biomechanical failure due to the large unfilled volume. (Ghavidel Mehr et al. 2014) Polyglycolic acid (PGA) and polylactic acid were among the first polymers used for tissue engineering (Jana et al. 2014). These materials support cellular adhesion and ECM synthesis. After single leaflet replacement in sheep, they performed adequately. But due to their high stiffness and rigidity, cell proliferation of the applied cells could not be achieved. (Jana et al. 2014) Polyhydroxyalkanoates (PHA) are soft elastomeric polymers with high elasticity and mechanical integrity. Stock *et al.* (2000) used polyhydroxyoctanoate (PHO), a member of the PHA group, to overcome the lacking pliability of the PGA. Using the salt leaching technique they manufactured a porous PHO leaflet, which was sutured to a non porous PHO conduit with a layer of a PGA felt. Accordingly the scaffold was coated with ovine vascular cells and implanted in sheep for 24 weeks. The examination after 24 weeks revealed an increase in ECM and no thrombus formation whereas a non seeded control valve showed a severe thrombus formation on all three leaflets in the doppler echocardiography starting after 4 weeks. PHA are of great interest due to their tunable mechanical properties and high biocompatibility. By incorporating different pendant groups the mechanical properties of the PHA can be varied. For instance, elongating the hydroxyvalerate group of poly(3HB) leaves the polymer more elastomeric. (Jana et al. 2014)

Polyglycolic sebacate (PGS) consists of an accordion-like honeycomb microstructure. The unique structure of the PGS generates a native-like myocardium tissue and conveys an anisotropy to the cells, which Engelmayr *et al*. (2008) showed for neonatal rat heart cells. The mechanical and degradation characteristics of PGS can be controlled by varying the polymerization parameters. Furthermore, the material displays high biocompatibility. (Jana et al. 2014) The limited water uptake capability of PGS can be improved by using polyethylene glycol (PEG) and form PGS-co-PEG polymers (Patel et al. 2013). Coating of the PGS scaffolds with laminin, fibrin, Collagen I, fibronectin or elastin also improved the cellularity, production of ECM and regulation of the cell phenotype (Sales et al. 2007). Although these experiments reported positive results, the manufactured 3-D porous scaffolds showed a deficiency in shape and elastomeric flexibility compared to a native valve. However, new techniques like bioprinting may enable the fabrication of scaffolds with these characteristics. (Jana et al. 2014)

Fibrous scaffolds mimic the fibre structure of the ECM very closely (Jana et al. 2015). In terms of cell adhesion, migration, proliferation and differentiation they are superior to non-fibrous scaffolds (Jana et al. 2014). Electrospinning is a widely used technique to create fibrous scaffolds. This technique can be used on most polymers, is ease to handle and versatile. The function of the electrospinning process is based on the principle of electrostatic. The machine is essentially made of a syringe with a nozzle, a counter electrode (e.g. metal plate), an electrical field source and a pump. The electrical voltage of the nozzle and of the counter electrode is different. The polymer is introduced via the nozzle and is exposed to the voltage difference between the nozzle and the electrode. The polymer globules then assume a

cone shape, which is caused by the electrical voltage. When the polymer reaches the counter electrode, the liquid part of the polymer has evaporated and a solid continuous filament is obtained. (Braghirolli et al. 2014) The scaffold is built fibre-by-fibre, enabling a tight control of the fibre diameter, fibre alignment, macroscopic scaffold geometry and scaffold porosity for cell infiltration of each layer (Capulli et al. 2016). PGA is a polymer, which is often used in nanofabricated fibrous scaffolds. While the high mechanical stiffness is a considerable drawback of PGA, biocompatibility and bioabsorbility are favorable properties of this material. (Jana et al. 2014) The high hydrophilicity of PGA enables a degradation of the material in less then 4 weeks, promoting collagen and ECM production by providing an effective environment and stimulation (Atala, Mooney 1996). Zünd *et al.* (1998) seeded FB on a PGA mesh scaffold. EC, which were seeded on these construct, built a monolayer without the growth of capillaries. To improve biocompatibilty PGA meshes were dip-coated with a 1 % solution of poly(4HB), a homopolymer with a reduced degradation rate compared to PGA, thus restricting the degradation rate of PGA. After 20 weeks of cultivating ovine FB and EC on the scaffold, the results showed a higher ECM and DNA expression of the coated scaffolds. (Hoerstrup et al. 2000) The rate of degradation is an important factor for the development of a scaffold. Degradation reduces the mechanical properties of the scaffold, which can be balanced by the ECM production. (Jana et al. 2014)

While electrospinning has many advantages, the high currents, which are used, limit the usable materials to polymers which are solvent in a conductive solution (Capulli et al. 2016). This also includes the restricted use of natural proteins, due to the denaturating effect of high voltage on the 3-D structure of proteins. (Capulli et al. 2016) Rotary jet spinning is a fabrication method, which was developed to overcome the shortcomings of electrospinning. Instead of using high voltage, rotary jet spinning uses centrifugal force to create nanofibres. Natural and synthetic polymers can be mixed to adapt mechanical properties and degradation rate of the scaffold. (Capulli et al. 2016) A polymer-protein hybrid scaffold was created by Badrossamay *et al.* (2014) using Poly-ε-caprolactone/collagen nanofibres. The scaffold displayed better mechanical and biodegradation characteristics compared to other hybrid scaffolds or unaltered polymer scaffolds as well as better cell adhesion.

Hydrogels are characterized by their high water content and the swollen polymer chain networks (Jana et al. 2014). Their structural similarity to the natural ECM make them usable for tissue engineering and regenerative medicine (Hoerstrup et al. 2000). Hydrogels promote cell migration and angiogenesis, have a high water content and enable rapid nutrient diffusion (Bryant, Anseth 2001). The polymer chains, which the hydrogels are composed of, can be either of synthetic or natural origin. The crosslinking of hydrophilic homopolymers, copolymers or macropolymers defines the structural integrity of the hydrogel. (Drury, Mooney 2003) Hydrogels can be created using varying methods. Free radical polymerization promotes fast reaction and building of the hydrogels. However, the reaction takes place uncontrollable and results in inhomogeneous characteristics of the hydrogel. Another method is the

conjugate addition reaction, which is based upon the reaction of acrylated monomers, esters or amids combined with thiols. This method in turn comes with an increased risk of side reactions by competing nucleophiles from biological conglomerates, such as living cells. The click chemistry method shows a mild reaction condition while retaining a high selectivity, thus achieving better results in hydrogels compared to the standard methods. (Jana et al. 2014) Click chemistry refers to varying chemical reactions, which meet the following criteria; the reaction is modular, has a broad range, they produce a high yield and their by-products are inoffensive and can be easily removed. The intention of click chemistry reaction is to create selective and modular "blocks" that can be readily applied. The reaction itself is characterized by its simple reaction conditions, easy to come by starting materials and reagents, the relinquishment of solvents or only using solvents, which are benign (e.g. water) and easy product isolation. (Kolb et al. 2001) Different natural and synthetic monomers can be utilized to form hydrogels. Examples for synthetic monomers are poly(ethylene oxide), poly(vinyl alcohol) (PVA) and polypeptides. Natural monomers include agarose, alginate, chitosan, collagen, fibrin, gelatin, and hyaluronic acid. (Drury, Mooney 2003) The encapsulation of cells in a hydrogel increases the cellular efficiency by enhancing the cell adhesion, differentiation and proliferation (Jana et al. 2014). Flanagan *et al.* (2006) demonstrated better cell surface coverage in collagen-chondroitin sulfate hydrogels compared to collagen only hydrogels. A major drawback of the hydrogels is their weak mechanical stiffness. In consequence, the mechanical properties of cell-encapsulated hydrogels have to be enhanced to function as stand-alone scaffolds. (Jana et al. 2014) The physical properties like stiffness and degree of swelling of poly(ethylene glycol) diacrylate (PEGDA) hydrogels can be modified by manipulating the molecular weight, the weight fraction of macromer in solution and the crosslinking time (Durst et al. 2011). The characteristics of PVA hydrogels are similar to those of soft tissue. When physically crosslinked by repeated freeze-thawing cycles the mechanical properties of PVA become more similar to those of a native porcine valve. (Wan et al. 2002) Adding structure and orientation to the hydrogel is another technique to enhance the stiffness. Hockaday *et al.* (2012) fabricated heterogeneous and cytocompatible hydrogels from PEGDA using a 3-D-printing/photocrosslinking method. Although, PEGDA in its unmodified form is known for its non-adhesion properties, porcine aortic valve interstitial cells adhered and spread on the printed PEGDA hydrogels. Moreover, the stiffness of the modified PEGDA hydrogel was ten times bigger compared to the original hydrogel. While bioprinting seems to be a promising technique to build valve scaffolds, challenges remain concerning the flexibility and mechanical properties of the current valves. The low-viscosity solution, used by modern bioprinters, may not be able to completely imitate the native heart valve. Although crosslinking can enhance the physical properties of the valves, it interferes with cell compatibility. These problems are still to be faced and more studies have to be done to enable *in vivo* experiments with hydrogel scaffolds. (Jana et al. 2014)

2.5.3. Bioreactors for Heart Valve Tissue Engineering

The *in vitro* conditioning of tissue engineered valves is an essential step towards the development of functional tissue *in vivo*. The biomechanical and biochemical conditioning of the heart valve serves two purposes: to enable the maturation of the tissue *in vitro* and to prepare the valve to function immediately after implantation. (Parvin Nejad et al. 2016) A bioreactor can provide these biochemical and biomechanical stimuli in a controlled environment. When appropriate stimuli are applied on cells, they can proliferate, differentiate, migrate and align themselves according to the stimulus. Furthermore, cells may build, reabsorb and organize ECM in a desired way. The change from the original scaffold material to autologous ECM is also a critical point in the acceptance of the tissue engineered valve after implantation. (Spoon et al. 2013) Moreover, *in vitro* testing of durability and function in the bioreactor can identify structural weaknesses in the valve scaffold prior to implantation or testing *in vivo* (Parvin Nejad et al. 2016). Bioreactors enable control of the environmental parameters of the *in vitro* testing. Common in bioreactors is the regulation of O_2, CO_2, temperature and nutrient supply. Two types of bioreactors can be categorized, depending on the absence or presence of mechanical stimuli: static bioreactors, which give control over the environment and dynamic bioreactors, which additionally subject the valve construct to biomechanical stimuli. (Parvin Nejad et al. 2016) Dynamic bioreactors can expose the valve construct to a variety of biomechanical stimuli, including stretch, flexure, shear and pressure. The different impulses have varied effects on the cells and the valve. While cyclic stretching can increase cell proliferation, collagen synthesis, stiffness and GAG content, cyclic flexure has a positive impact on cell migration, collagen synthesis and stiffness. Oscillating fluid shear stress has shown to increase inflammation resistance, strength, alignment and protection against calcification. (Spoon et al. 2013) Another benefit of the dynamic bioreactor is the capability to evenly distribute cells and nutrient on a 3-D scaffold. A study conducted by Nasseri *et al*. (2003) demonstrated that cell seeding on a tubular polymer scaffold in a rotating bioreactor enabled better nutrient and oxygen distribution and favorable conditions for cell attachment and tissue growth. The residual medium showed 7 % unattached cells after 24 h of seeding. After 5 days the inner and outer surface of the tubular construct was covered in a confluent layer of myofibroblasts. Cardiac valve tissue engineering uses different types of dynamic bioreactors for conditioning. Spoon *et al*. (2013) categorized three general types based on their objective: flow-based whole valve conditioning bioreactors, which simulate the systole and diastole of a cardiac cycle, strain-based whole valve conditioning bioreactors, which aim to perform the diastolic pressure and isolated cusp stimulation bioreactors, which put isolated leaflets under predefined mechanical stimuli. A flow-based whole valve conditioning bioreactor generally consists of a flow source, resistance and a compliance module (Ruel, Lachance 2010). A computer guided pump is utilized to generate the pressurized pulsatile flow which mimics the systole and diastole during a cardiac cycle

(Spoon et al. 2013). The resistance imitates the blood flow hindrance caused by arteries and capillaries (Ruel, Lachance 2010). In most cases the compliance module consists of an air filled chamber, representing the elastic function of the large arteries (Dumont et al. 2002). A valve chamber, media reservoir and a gas exchanger are also common in many bioreactors of this type. Advanced bioreactors also include sensors for flow, pressure, temperature, pO_2, pCO_2, glucose lactate and valve deformation. Depending on the construct, pictures and videos of the valve can be taken using digital cameras, endoscopes or microscopes. (Spoon et al. 2013) Hoerstrup *et al*. (2000) designed the first flow-based bioreactor (Fig 2-9). The design consisted of an air chamber and a medium chamber. The chambers were separated by a silicone diaphragm, the valve was located in a third chamber. By pumping air into the air chamber, the medium on the other side was pushed into the valve perfusion chamber and through the valve. The flow mimicked the systole. A pause in the medium flow changed the pressure gradients, thus closing the valve leaflets and imitating the diastole. The diaphragm pump generated a flow ranging from 50 to 2000 ml/min, as well as a resulting pressure range from 10 to 240 mmHg. However, the design denied an independent pressure control (Spoon et al. 2013). Dumont *et al*. (2002) constructed one of the first flow-based bioreactors, which enabled independent control over resistance and compliance, thus giving control over pressure and flow. They varied the compliance by letting air in and out of the compliance chamber. The resistance was modulated using a clamp on an elastic tube in the system. Both of these elements create an afterload on the valve by imitating the compliance of the large arteries and resistance of the capillaries. (Spoon et al. 2013) Hildebrand *et al*. (2004) developed an improved system, where they incorporated flow and pressure sensors. By installing a feedback control loop to automatically adjust the driving pressure and resistance the bioreactor could maintain the mean pressure and flow without a manual intervention. The bioreactor designed by König *et al.* (2012) reduced the often unwieldy design of the bioreactors to a smaller form. Their bioreactor was created to gradually adapt an EC layer on an aortic valve to simulated physiologic flow conditions. Earlier experiments showed a shortcoming of statically incubated EC to acclimate to sudden flow changes. The EC layer was already damaged by flow rates below physiological thresholds. Three main parts form the bioreactor: the core, which houses a Teflon™ support unit, the actuation unit and the monitor unit (Fig 2-10). An aortic valve sample can be fixated in the Teflon™ support unit and put into the core element. The medium is channeled in a laminar flow trough the valve. This establishes sufficient flow and pressure conditions. The actuation unit creates a pulsatile flow via an air chamber and a membrane. The air, which is pushed from the actuation unit in the air chamber, moves the diaphragm, which results in a medium flow. The small size of the bioreactor enables the placement of the bioreactor in a standard incubator. The avoidance of tubes and screws in this design facilitates sterilization as well as the handling and assembling of the bioreactor. A monitor unit enables the real time surveillance of the movement of the valve with an endoscope.

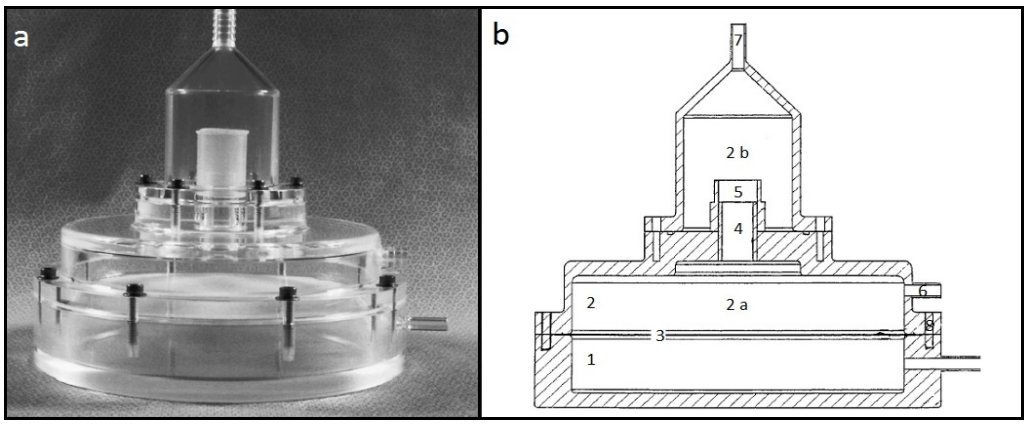

Fig 2-9 A pulsatile bioreactor and schematic overview designed by Hoerstrup et al. (2000) *The main components of this bioreactor are the two chambers (1,2) at the base. The air chamber (1) and the fluid chamber (2) are separated by a silicone membrane (3). By periodically inflating air into the air chamber, the membrane is set into motion and the fluid is pumped upwards from the lower compartment (2a) through a tube (4) into the valve perfusion chamber (2b). The valve can be secured in a second silicone tube (5), which is removable and enables easy fixation of the valve. The medium flows through a valve inlet (6) and valve outlet (7) into a medium reservoir. The bioreactor was constructed of three acrylic glass components, which were fixated using stainless steel screws (8).*

Strain-based whole valve conditioning bioreactors were created to simulate the diastolic pressure conditions. Mol *et al*. (2005) constructed one of the first strain-based bioreactors, the diastolic pulse duplicator, which put the valve under cyclic pressure in its closed state to mimic diastole. Results from previous studies demonstrated excellent growth and maturation of tissue engineered blood vessels in bioreactors that only worked with dynamic wall straining and without pulsatile flow (Niklason et al. 2001; Seliktar et al. 2000; Kim, Mooney 2000). The dynamic strain on the valve was created by repeatedly pressing the surrounding media against the closed valve. Results showed a successful tissue conditioning with the use of the diastolic pulse duplicator. Initially, Mol *et al*. (2005) estimated the amount and distribution of the strain on the leaflets using finite element analysis. However, this method gave no control over the tissue deformation and the monitoring possibilities were limited. Additionally, the tensile properties of the leaflet changed with the growing ECM and scaffold degradation. These changes could not be accounted for in the original diastolic pulse duplicator. (Parvin Nejad et al. 2016) To address these problems, Kortsmit *et al.* (2009a) installed a control system, which calculated the tissue strain based on the volumetric deformation of the leaflet. The volumetric deformation accounted for the changes in volume due to the deformation of the leaflet and was measured using a flow sensor. An additionally installed feedback loop enabled the adaption of the system to the growing ECM and the biomechanical changes of the maturing tissue. Using the volumetric deformation, the feedback control mechanism allowed the evaluation and regulation of the induced deformation of the heart valve leaflets.

(Kortsmit et al. 2009b) A variation of the control system from Vismara *et al*. (2010) used the compliance of the scaffold as a parameter for its biomechanical behavior. The compliance was estimated assuming a linear volume pressure relation. Syedain *et al.* (2009) bypassed the need for a feedback control system, when they mounted the heart valve inside a latex conduit. The cyclic injection of culture medium into the latex tube created a distension on the leaflets and thus a mechanical strain. The stiffer latex tube dominated the mechanical response and thus the strain experience of the leaflets, which resulted in a consistent strain on the valve, regardless of the changes in the heart valve leaflet during ECM maturation.

Bioreactors are also used to put single valve leaflets under predefined mechanical stimuli. This option enables the analysis of specific mechanical stimuli and their effects on the valve leaflet to establish the optimal conditions for tissue proliferation and differentiation. (Parvin Nejad et al. 2016) Valve leaflets can be subjected to a variety of different biomechanical stimuli (e.g. flow, pressure or a combination of different stimuli) (Spoon et al. 2013). Gould *et al*. (2012) demonstrated that cyclic strain anisotropy can enhance the turnover of valvular interstitial cells and α-SMA expression. Furthermore, it influences cell and collagen fibre to orientate in the direction of the strain. In contrast applying cyclic flexural strain on a non-seeded PGA/PLLA scaffold resulted in a decreased stiffness and damage to the scaffold architecture (Engelmayr et al. 2003). In both studies cyclic strain seems to play a role in initiating cell differentiation and orientation as well as biomaterial conversion (Parvin Nejad et al. 2016). Another study conducted by Engelmayr *et al*. (2006) demonstrated a synergistic effect of laminar flow and cyclic flexure on the bone marrow mesenchymal stem cell mediated tissue formation. Isolated cusp stimulation gives important information on the influence of different mechanical stimuli on the cells and the scaffold material. Comparing these results to the performance of a native valve gives further information about the desired behavior of the tissue engineered valve. (Parvin Nejad et al. 2016)

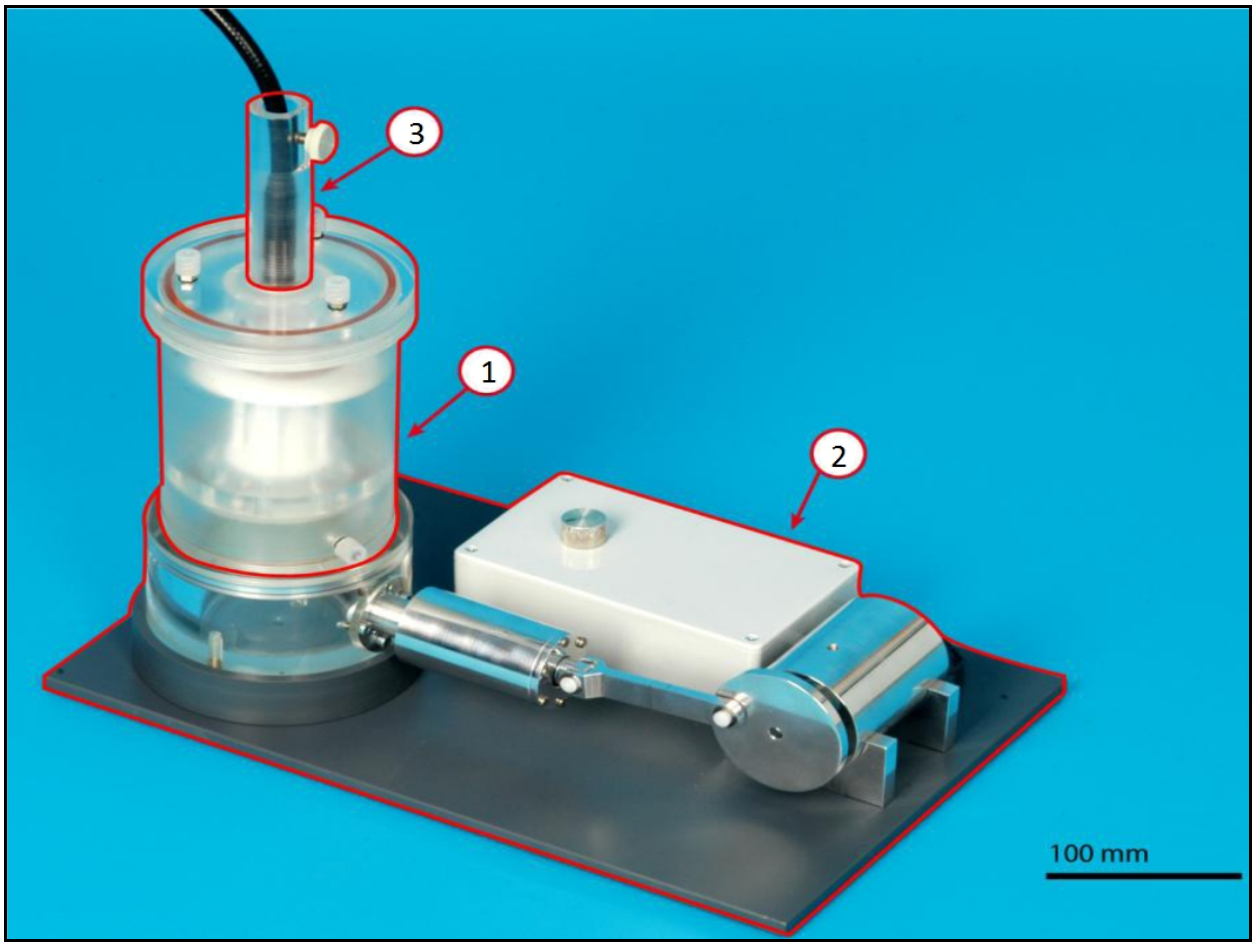

Fig 2-10 A pulsatile bioreactor for whole valve conditioning designed by König et al. (2012) *(1) is the core, where the Teflon™ support unit and the valve is fixated, (2) the actuation unit and (3) the monitor unit. The monitor unit allows the insertion of an endoscope and real time surveillance.*

2.5.4. Cell Sources for Heart Valve Tissue Engineering

Optimal autologous cells for tissue engineering should readily adopt the function of the original cells and be easy to harvest. Adult as well as progenitor/stem cells are utilized for the recellularization of heart valve scaffolds. Cells, which are used for heart valve tissue engineering in humans, include mesenchymal stem cells (MSC), umbilical cord-derived progenitor cells, valvular interstitial cells and vascular EC. (Spoon et al. 2013)

MSC are multipotent cells, which can be harvested from varying tissue including adipose tissue, the umbilical cord and cord blood as well as bone marrow (Ugurlucan et al. 2009). When they receive the adequate stimulus, they can differentiate into phenotypes of a diversity of cells like the connective tissue of organs, tendons and other mesenchymal cells (Patel, Genovese 2011). A study conducted by Iop *et al.* (2009) demonstrated successful *in vitro* recellularization of decellularized porcine heart valves with human bone marrow MSC. The cells formed an EC monolayer and differentiated into FB, myofibroblasts and smooth muscle cells without pre-seeding differentiation. Weber *et al.* (2011) showed in a nonhuman

primate model, that tissue engineered heart valves, which were loaded and then incubated for 10 min with bone marrow MSC, displayed a nearly confluent layer of EC and VIC 4 weeks after implantation. However, cell tracking analysis revealed that none of the seeded bone marrow MSC where still present on the valve. Although, these cells are easy to obtain from the bone marrow, the *in vitro* cultivation requires time and the proliferation speed depends most likely on age. Moreover, fibrosis and calcification processes were noted in stem-cell based treatment with these cells. (Ugurlucan et al. 2009)

The umbilical cord is composed of one vein and two arteries. These vessels, the cord blood and the so called "Wharton's jelly", a mucoid tissue which surrounds the vessels, are sources for endothelial progenitor cells and fibroblast like MSC. (Weber et al. 2012) The MSC, which are derived from the vessels, have the capability to differentiate into adipose tissue, EC, cardiomyocytes and osteomyocytes. A high number of immature stem/progenitor cells can be found in the cord blood. (Ugurlucan et al. 2009) Schmidt *et al.* (2006) used MSC harvested from the Wharton's jelly as well as endothelial progenitor cells accumulated from the umbilical cord blood to seed a non-woven PGA scaffold. The valves were statically as well as dynamically incubated for 28 days. Results showed a microscopic architecture close to that of native valve with EC covering the surface and synthesis of collagen in the deeper layers. The valve samples, which where put under dynamic stimulation, had several tissue layers resulting in a more mature tissue formation compared to the static samples. Tissue banks have become more common in the last couple of years. They process and preserve umbilical cord and blood stem cells to enable their use for future therapies. (Ugurlucan et al. 2009)

Adult cells, which are used for heart valve tissue engineering, include human vascular EC and human valvular interstitial cells (Spoon et al. 2013). Yang *et al*. (2012) seeded human vascular cells harvested from the saphenous vein on a decellularized bovine pericardial patch and conducted *in vitro* and *in vivo* analysis in a mouse model. 30 days after implantation, the immunohistochemical analysis showed a confluent cell layer on the surface as well as differentiation of the cells into EC, smooth muscle cells, and FB. Schnell *et al*. (2001) compared venous to aortic myofibroblasts. They harvested human vascular EC and myofibroblasts from the vena saphena magna as well as from the ascending aorta. Cell harvest from the ascending aorta of a living patient can only be performed during a cardiac surgery. Harvesting cells from a peripheral vein is less invasive. The human body tolerates the loss of a peripheral vein better than the loss of an artery. Even if the patient does not undergo cardiac surgery, the vein can be obtained via a small skin incision. The cells were seeded on a biodegradable polyurethane scaffold and incubated for 6 weeks. The mechanical testing demonstrated excellent stability of the VEC during axial traction compared to human aortic myofibroblasts. Both cells built a viable, multilayered tissue, while the VEC created more ECM. Gulbins *et al.* (2005) seeded human saphenous EC and FB on a complex 3-D model, an aortic root. They used a special rotation incubator to distribute the cells evenly on the valve and the leaflets. Results showed a confluent and viable EC layer on the valves. Valves, which were preseeded

with FB demonstrated a higher content of Collagen IV and laminin, which improved the adhesion of EC. Table 2-1 gives a short overview of the advantages and disadvantages of each cell type.

Tab 2-1 An overview of the different cell types used in heart valve tissue engineering

Advantage	Disadvantage
Mesenchymal stem cells	
Can be harvested from various tissues	In vitro cultivation takes time
Can differentiate into various tissues	Proliferation speed decreases with cell age
Umbilical cord/blood cells	
Can differentiate into various tissues	Can only be harvested at birth
Young cells, which are free of consequences of aging	Currently not available for everyone
Valvular interstitial cells	
Express good behavior seeded on scaffolds	Autologous cells are difficult to harvest
	Function of cells altered in valvular heart disease
Vascular endothelial cells	
Autologous cells are easy to harvest	Further investigation regarding the feasibility and effectivity is necessary
Good performance on seeded scaffolds	

2.6. Aim of this Study

Currently available heart valve prostheses have some critical disadvantages. Apart from the limited durability on one side and the need for anticoagulation on the other side the lacking ability for growth and repair is one of the major drawbacks. A tissue engineered valve would not have these handicaps. Furthermore, a minimal invasive implantation via the TAVI procedure might even be possible.

Before we think about implanting a tissue engineered valve into a human body via the TAVI procedure we must know the reaction of the valve and the cells to this treatment. The tissue engineered valve has the advantage to be built from the patient's own cells. These cells and the cell layer have to be intact upon implantation. We wanted to know how these valves and the cells would react to the crimping process and the perfusion. Currently the creation of a tissue engineered valve takes some time. If the TAVI procedure critically damages the cell layer the advantages of these valve prostheses (e.g. reduced thrombogenicity, possible growth, reduced inflammatory reaction) may be for naught. So, how does the cell layer of a tissue engineered valve reacts to crimping and perfusion? Based on the study performed by Scheuer *et al.* (2013) we expected no major changes in the cell layer on the heart valve.

Human FB and vascular EC were harvested from the vena saphena magna. These cells were seeded on a decellularized aortic valve. To mimic the physiological conditions of a native aortic valve, the FB were seeded first. The homograft itself demonstrates favorable characteristics as scaffold. The ECM composition and mechanical properties of the homograft are very close to the native valve. The bioreactor, which was used, enabled the simulation of physiological conditions and gradually increasing flow rates. To assess the reaction of the cell layer immunohistochemical as well as SEM analysis was performed and quantitatively evaluated.

3. Methods

3.1. Cell Culture

General Conditions

Work with cells was performed under sterile conditions under a laminar work flow. The used solutions were sterile and heated to 37 °C. The cell culture was incubated at 37 °C, 5 % CO_2 content and 95 % humidity unless stated otherwise.

3.1.1. Cell Cultivation

EC and FB were isolated from excess veins from coronary bypass operations performed at the cardiac-thoracic surgery department of the University Hospital of Munich, Großhadern. All donors signed an informed consent (see *"Appendices 1. Informed Consent"*), which approved of the use of the left over veins for an experimental study. The veins were irreversible anonymized. The regional ethic committee accepted the use of the anonymous excess vein pieces.

After the removal of the veins from the patients the residual segments were stored at 4 °C in a *storage solution* (M 199 20 ml, penicillin/streptomycin 1 ml) for a maximum of two days. The veins length varied between 5 and 7 cm. The cells were harvested using a modified method described in previous studies (Miyata et al. 1991; Bader et al. 1998; van Kooten et al. 1994; Gulbins et al. 2006). The veins were cannulized and secured at the cannula on one side with a surgical suture. Next they were rinsed with 15 ml *rinsing solution* (M199 194 ml, heparin 5000 IE/ml 1 ml, gentamycin 10 mg/ml 5 ml) to remove plaques and erythrocytes. During this step the tightness of the veins was also verified. The *rinsing solution* was pressed into the vein, while the other side was clamped. Eventual leakages of *rinsing solution* would imply a fissure in the vein. Then they were filled with *collagenase solution EC* (collagenase 240 U 10 mg, human serum albumin 20 % 8 ml) and stored in 200 ml PBS in an incubator for 30 min. This isolation step dissolved the EC layer. The process was inactivated by rinsing the veins with 15 ml *stopp solution* (M199 500 ml, fetal calf serum 20 % 125 ml). The EC solution was collected in a tube and centrifugated at 500 RPM for 7 min at room temperature (RT). After centrifugation the supernatant was removed and the cell pellet was resuspended in 5 ml *EC growth medium* (ECGM) (growth medium 500 ml, EC supplement 10 ml, fetal calf serum 6 % 30 ml, penicillin-streptomycin 1 ml). The solution was transferred to a 12.5 cm^2 culture cell flask.

For FB isolation the *collagenase solution FB* (collagenase 240 U 20 ml, human serum albumin 20 % 8 ml) was used and the veins were incubated for 40 min. Otherwise the FB isolation was performed analogously to the first isolation step. To increase the FB harvest the veins were horizontally sliced and the adventitia was removed. The venous tissue was separated into small slices (2 - 4 mm^2) and

positioned under a cover slip (2.5 cm x 2.5 cm) on a culture dish (A = 9.6 cm^2). The cover slip and consequently the tissue segments were secured with four drops of sterilized silicone. Finally 2.5 ml *FB growth medium* (FBGM) (growth medium 500 ml, FB supplement 10 ml, fetal calf serum 11 % 55 ml, penicillin/streptomycin 1 ml) were added to support FB outgrowth. The cell cultivation and proliferation was conducted in the incubator. The cell growth medium (CGM) was exchanged every second day. As soon as the cell layer reached confluency, a splitting of the cells was performed. The CGM was removed and the cell culture was rinsed with PBS. Trypsin at 37 °C was added and incubated for 3 min to break the cell-to-cell bonds. The according volume of PBS, Trypsin and *stopp solution* can be read from the table (Tab 3-1) below. After controlling the enzymatic treatment with a phase contrast microscope, the reaction was stopped adding 3 ml *stopp solution*. The cell/trypsin solution was then pipetted into a 50 ml tube and centrifugated at 500 RPM for 7 min at RT. The supernatant was removed, the cell pellet resuspended in 8 ml CGM and then seeded in a new culture flask (ratio 1:6 in passage 1, ratio 1:3 in subsequent passages).

Tab 3-1 According volume of PBS, trypsin and stopp solution for cell trypsinization

	Flask 12.5 cm^2	**Flask 75 cm^2**	**Flask 162 cm^2**
Solution	**Volume**		
PBS	6 ml	10 ml	14 ml
Trypsin	1 ml	2 ml	3 ml
Stopp solution	3 ml	9 ml	14 ml

3.1.2. Cryopreservation of the Cells

Cells, which were not immediately used for further experiments, were cryopreserved at the third or fourth passage. For cryopreservation a method established in previous studies was used (Polchow et al. 2012).

The cells were first trypsinized as described above. After centrifugation the cell pellet was resuspended in *cryomedium* (CGM 1.05 ml, FCS 11 % 0.3 ml , DMSO 0.45 ml, 1.5 ml *cryomedium*/vial) and stored in a freezer immediately. The cells were cooled down to the temperature of -80 °C at a rate of approximately -1 °C/min. For long term preservation the cryovials were then stored in liquid nitrogen at -196 °C after one week. For reuse of the cells they were thawed. Two cryovials were shortly placed (10 sec) in a 37 °C water bath. DMSO has a cytotoxic effect, so a fast handling of the cell solution was critical. The cells were resuspended in the *defreezing solution* (CGM and fetal calf serum 6 % 10:1) and centrifugated at 500 RPM for 7 min at RT to remove the cytotoxic DMSO. The supernatant was removed, the cell pellet resuspended in CGM and seeded in a cell culture flask.

3.2. Processing of the Aortic Valve

Aortic valves were thawed, decellularized, stented and reseeded with FB and EC. Following they were crimped and exposed to physiologic flow conditions in a high flow bioreactor (Fig 3-1).

Samples for scanning electron microscopic and immunohistochemial analysis were taken from the native, the decellularized, reseeded and after perfusion valve.

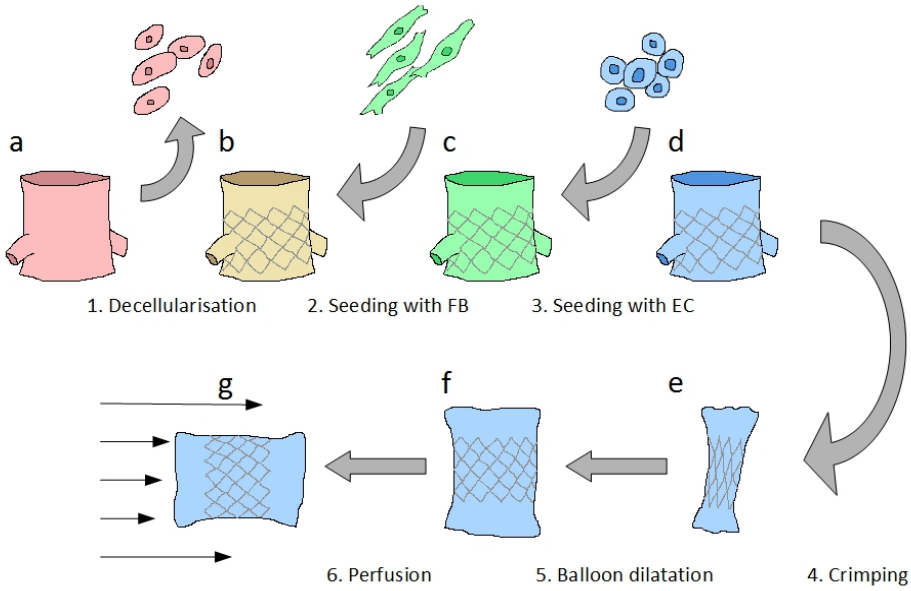

Fig 3-1 Processing of the aortic valve *After the decellularization (1. Decellularization) of the native valve (a) the stent was sutured on the valve (b). Then the dynamic seeding procedure was performed. First the FB (c) were seeded on the valve, then the EC (d). The valve was crimped for 10 min (e) and dilated (f) to perform the perfusion study (g)*

3.2.1. Removal of the Heart Valves

Aortic homografts from organ donors, which were not suitable for *in vivo* implantation, were used for the *in vitro* experiment. After explantation the hearts were stored in 700 ml M199 at 4 °C for transport. The aortic valve was dissected under sterile conditions and stored in three plastic bags to ensure sterile packaging. The inner bag was filled with 60 ml *cryopreservation solution* (M199 200 ml, DMSO 22.6 ml). The valve was enveloped in gauze, placed in the bag and another 100 ml cryopreservation solution were added. After air removal the bag was sealed. The inner bag was placed in two more bags. The aortic valve was then stored at -196 °C in liquid nitrogen. A quick freezing process was important to prevent the formation of ice crystal and damage to the aortic wall.

3.2.2. Thawing

2 l Ringer's solution, in two different containers, each with 1 l, were heated up to 56 °C. Thawing solution (M199 500 ml, penicillin/streptomycin 1 ml) was warmed up to 37 °C. After confirming the integrity of the outer package, the outer envelope of the frozen homograft was removed under non sterile conditions. The remaining two packages containing the aortic homograft were put in 56 °C Ringer's solution for 5-7 min. The second package was removed under sterile conditions and the inner bag containing the frozen aortic valve was thawed in sterile 56 °C Ringer's solution in a sterile container. After 5-7 min the last bag was removed and the homografts were then thawed in sterile 56 °C Ringer's solution in a new sterile jar. Following the enveloping gauze was removed and the valves were put in 37 °C M199. Before cell seeding the homografts were stored in 250 ml *storage solution AV* (M199 249 ml, penicillin/streptomycin 1 ml) for 24 h. Samples for analysis were taken from the vessel wall.

3.2.3. Decellularization

To remove any residual cell material and debris the decellularization step was conducted. First the fatty tissue and the remaining myocardial tissue were removed with a scalpel and a surgical scissor. The valve was then put in 500 ml *decellularization solution* (PBS 500 ml, SD 2.5 g, SDS 2.5 g) for 24 h on a 3-D rotating table at RT. To remove any remaining detergent the valve was rinsed 6 times with PBS for 24 h at RT respectively. After washing the valves were placed in 250 ml *storage solution decell* (M199 500 ml, Penicillin/Streptomycin 1 ml) for 24 h.

3.2.4. Stenting and Fixation to a Teflon™ Support Unit

To enable the crimping and expanding process the homograft was fixed in a stent. The compressed cobalt-chromium (CoCr, NP35N) stent was first expanded using a hegar's dilator to the diameter of the respective homograft. Then the stent was securely fixed to the vessel with single button sutures at the top and the bottom. In between the stents were sewed in with less single button sutures (Fig 3-2 a). Afterwards the valve was positioned in a Teflon™ frame (Fig 3-2 b) and secured with a single circumferential suture to the Teflon™ frame at the myocardial part of the vessel (Fig 3-2 c, d). The mounting on a Teflon™ unit enabled easier handling and positioning in the bioreactor for recellularization.

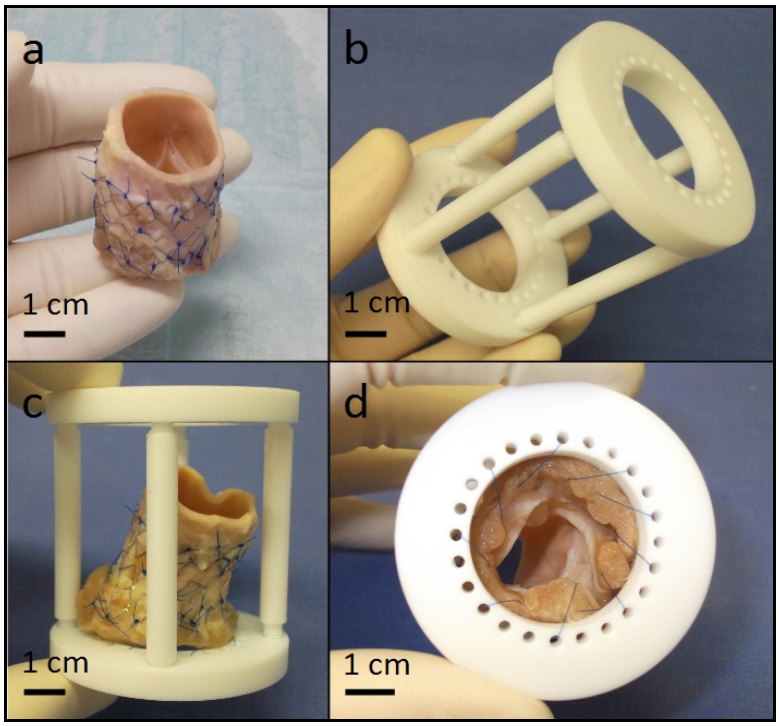

Fig 3-2 Stenting and mounting of the decellularized valve *To enable the crimping process a cobalt-chromium stent was sutured on the outside of the aortic homograft (a). For easier handling and to enable placement in the dynamic seeding bioreactor the homograft was mounted on a Teflon™ unit (b). The valve was secured with a single circumferential suture in the Teflon™ unit ((c) homograft from the side, (d) homograft from the ventricular side, remnants of the myocardial tissue are still visible)*

3.2.5. Recellularization

For the recellularization of the homografts about 1.5 x 10^6 cells/cm^2 were used. The approximate surface value of the homograft was calculated assuming the homograft as a cylinder and the valve leaflets as circles. This calculation was done for each valve individually. The mean surface area of the valves amounted to 43.49 ± 7.8 cm^2. This resulted in a mean cell number of 65.23 ± 11.7 x 10^6 cells per valve. A culture flask 162 cm^2 holds approximately 3-3.5 x 10^6 cells. So the optimal number of flasks for seeding could be determined. The homografts were first seeded with FB and than with EC. To detach the cells from the culture flask the trypsination method described in *Chap. 2.1.3. "Culturing and trypsinizing of the cells"* was applied. After processing the cells they were resuspended in as little CGM as possible to achieve a high concentration of cells. Before seeding the number of cells was determined following the method described in *Chap. 4.2. "Cell counting"*. To achieve a homogeneously distributed cell layer a dynamic cell seeding bioreactor (Fig 3-3 a) was utilized. After trypsination and counting the cell/CGM solution was pipetted onto the valve leaflets in closed position. The homograft was carefully placed inside the bioreactor and the bioreactor was completely filled with CGM without cells. Special attention was given to avoid disturbing the already placed cell/GCM solution on the leaflets. After sealing the lid

on the bioreactor eventual remaining air bubbles were removed by gently pressing the down side located membrane. An outlet with an attached three-way stopcock on top of the lid enabled the removal of the air. The rotating bioreactor enabled a rotation around the y- as well as z-axis. The rotation facilitated a 3-D distribution of the cells over the homograft. To ensure attachment of the cells the reactor's movements were halted during the holding phase for 20 min. The different orientations during the holding phase ensured a homogeneous spreading. The duration of the running phase of the reactor took 2.5 min. The whole bioreactor was placed in an incubator for 24 h at 37 °C/5 % CO_2. After completing the dynamic seeding phase the remaining cells in the CGM were counted to assess the number of cells attached to the valve. Afterward the homograft mounted on the Teflon™ frame was put under statical incubation in a jar for 6 d at 37 °C/5 % CO_2 (Fig 3-3 b). CGM was exchanged every third day. The procedure was repeated for the seeding of the EC. Samples for analysis were taken of the vessel wall after recellularization with FB and EC.

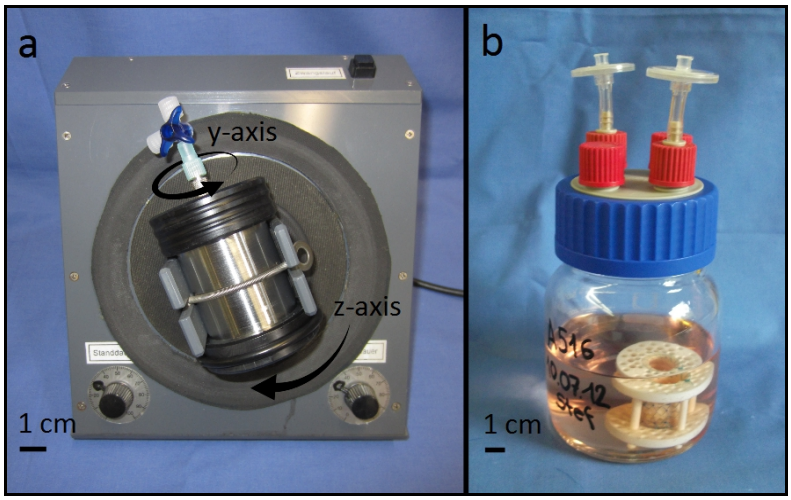

Fig 3-3 Recellularization of the aortic valve homograft *(a) shows the dynamic seeding reactor. It was capable at rotating around its y- as well as z-axis simultaneously. This enabled a homogeneous distribution of the cells. To allow attachment in between the 2.5 min running phases, the reactor stopped for 20 min. This procedure was executed for 24 h. Afterward the valve was incubated in a jar (b) for another 6 d.*

3.3. Perfusion Procedure

3.3.1. Crimping

Before inserting the homograft in the bioreactor, the crimping procedure was performed. The recellularized homografts were detached from the Teflon™ support unit and a balloon catheter was inserted in the middle of the valve (Fig 3-4 a). The mounted valve was positioned in a conventional heart

valve crimper (Fig 3-4 b). A crimper is a device which is used during the TAVI procedure to decrease the diameter of the valve by applying concentric pressure on the valve. The valve was crimped to the smallest possible diameter (approximately 7 - 9 mm) with a concentric force of about 10-15 kg (Fig 3-4 c). Fast handling of the valve was critical to avoid damage from dryness to the cell layer. After the crimping process the valve was placed in 37 °C CGM for 10 min to simulate the delivery process *in vivo* during the TAVI procedure. Finally the valves were expanded again by injecting water into the balloon catheter.

Because of better hemodynamic properties the valve was placed in a special designed acrylic glass unit (Fig 3-4 d). This unit omitted the need to suture the valve to a Teflon™ frame again, which minimized the necessary handling. An indention on the inside of the acrylic glass unit enabled the sutureless fixation of the valve. Moreover, the closed sides of the the acrylic glass unit supported a laminar CGM flow. The Teflon™ frame had open sides . After crimping and fixation of the valve, it was placed in the high flow bioreactor for perfusion (Fig 3-4 e).

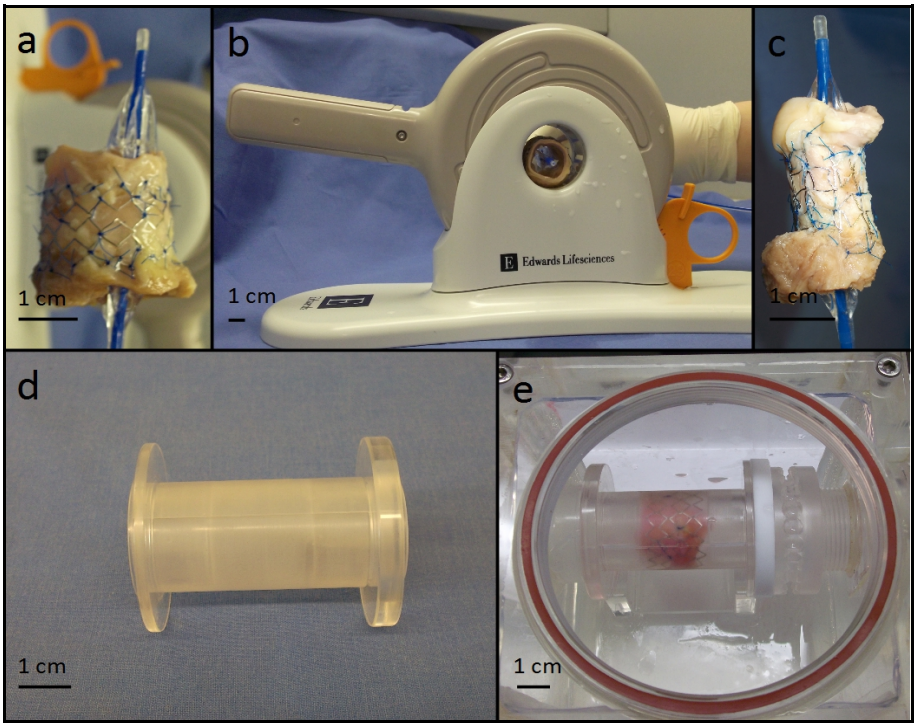

Fig 3-4 Overview of the crimping procedure and the acrylic glass unit for mounting in the bioreactor*(a) shows the recellularized valve placed on a balloon catheter. (b) depicts the mounted valve in the heart valve crimper. The valve was crimped to a diameter of 7-9 mm (c). The valve was then stored in CGM for 10 min at 37 °C. The acrylic glass unit was designed to enable the sutureless fixation and improve the flow conditions. (d) demonstrates the assembled acrylic glass unit. The placement in the bioreactor can be seen in picture (e). A white spacer was inserted to guarantee a safe placement in the bioreactor. The closed sides of the valve enabled a laminar and therefore more physiologic blood flow compared to the Teflon™ frame, which had open sides.*

3.3.2. High Flow Bioreactor and Perfusion

A high flow bioreactor (Fig 3-5 a-c) performed the pulsatile perfusion on the seeded homograft. To copy a physiologic flow the Berlin Heart EXCOR® system (Fig 3-5 d), a left ventricular assist device (LVAD), was utilized. This LVAD system uses pneumatic compression to create a pulsatile flow. A membrane separates an air filled chamber from the blood (or medium) and transfers the pulsatile movements on the blood. Two valves in the LVAD guarantee an unidirectional blood flow. The LVAD was connected to a computer guided actuation unit (Fig 3-6 a, b), which created a pulsatile flow. Via the inlet and the outlet of the bioreactor and silicone tubes the LVAD was connected to the bioreactor (Fig 3-5 d). The homograft was subjected to the pulsatile flow over a period of three days. During these three days the flow was increased every 24 h. The program started with 1 l/min, then the flow was raised to 1.5 l/min and finally to 2 l/min.

To minimize the risk of bacterial or fungal contamination the removable parts of the bioreactor were kept to a minimum. Altogether seven parts of the bioreactor were movable. The whole body and the corresponding parts were gas sterilizable. The setup of the bioreactor was performed under sterile conditions. All connections to the open air were sealed with a three-way stopcock and a sterile micro-filter (pore size 0.22 µm), to allow gas exchange and prevent contamination. The whole bioreactor fitted in an incubator, thus temperature, gas content and humidity could be controlled. The medium flowed via the inlet to the homograft. After the reseeding procedure the Teflon™ frame was removed and the valve was mounted in an acrylic glass unit. The acrylic glass unit minimized the necessary handling of the valve and ensured a laminar medium flow through the valve. The valve chamber had a round lid, which enabled the insertion of the homograft. It was locked with a rubber seal. The long acrylic glass tunnel connected two compliance cylinders, which mimicked the elastic function of the large arteries. Right before the compliance cylinders an endoscopic access was located. It provided life video footage of the performance of the valve (Fig 3-7 a, b). After the connection tunnel two medium reservoir chambers were placed. A movable wall between these chambers simulated the resistance of the small vessels. Via a screw the resistance value could be changed. The reservoir chambers provided enough GCM to nourish the valve over a period of three days. This reduced the need for medium exchange and thereby decreased the risk of contamination. After the medium reservoir the outlet was attached, which guided the medium back to the LVAD. The bioreactor had a CGM capacity of 5 l. It was filled with 2.5 l ECGM and 2.5 l M199. For the duration of the perfusion the whole bioreactor was stored in an incubator. After perfusion samples were taken from supravalvular, valvular and subvalvular parts of the aortic wall and from the leaflets.

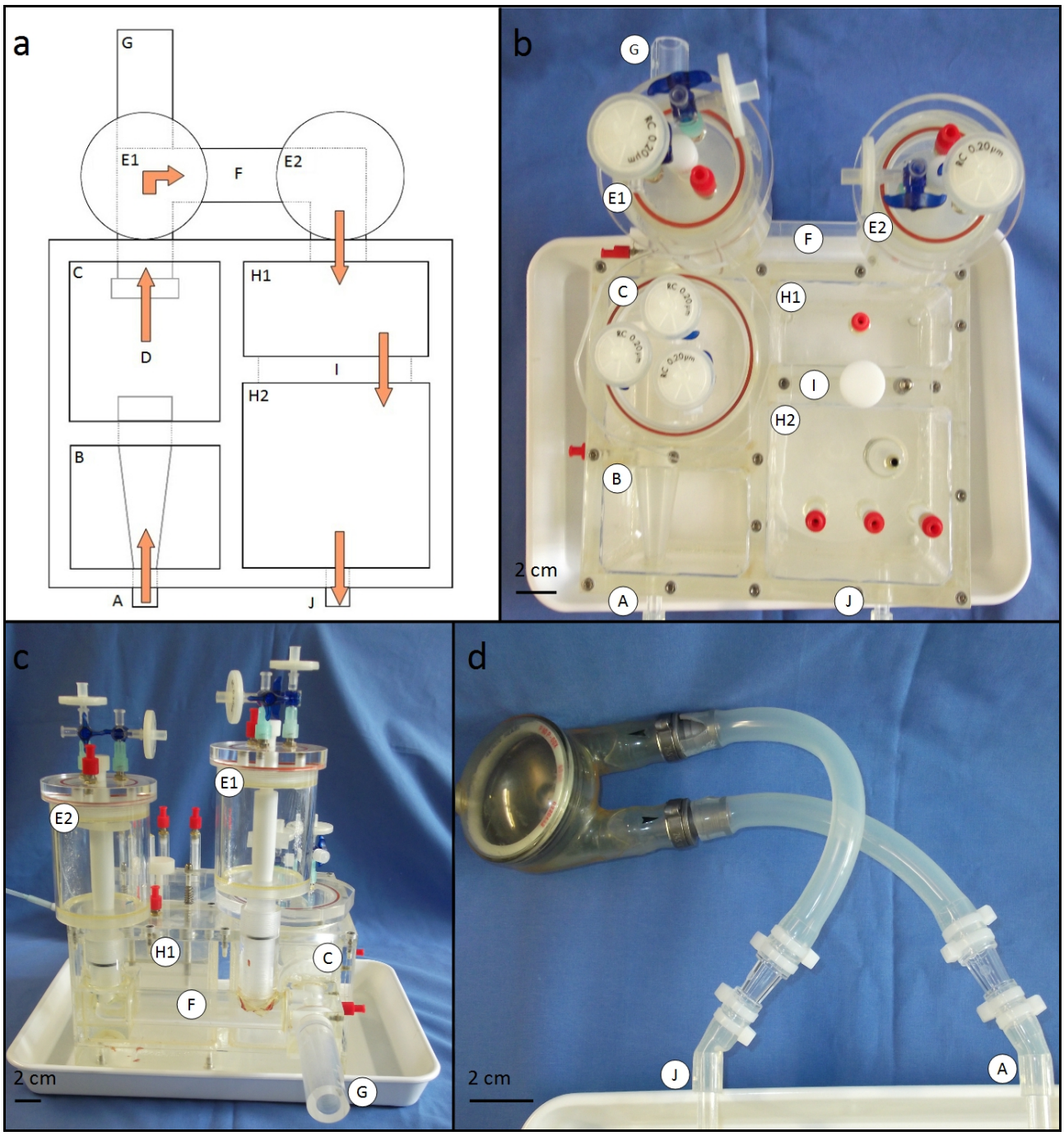

Fig 3-5 The high flow bioreactor which was used for the perfusion phase of the study *Picture (a) shows the outline of the high flow bioreactor. The medium flows (indicated by the orange arrows) through the inlet (A) into the bioreactor. A cone shaped tunnel (B) diverts the GCM flow. The homograft is attached to the in- and outflow (D) of the valve chamber (C). The medium is then guided into the tunnel (F) where the compliance cylinders (E1 and E2) are attached. Via the endoscopic access (G) a live video can be obtained to monitor the performance of the valve. In the medium reservoir chamber (H1 and H2) enough medium can be stored to supply nutrients for the recellularized valve over the period of three days. A movable wall (I) between the reservoir chambers simulates the peripheral vascular resistance. The outlet (J) guides the medium back to the attached LVAD. Picture (d) shows the Berlin Heart EXCOR®. It is connected via two silicone tubes to the outlet and inlet of the high flow bioreactor. Two small arrows indicate the flow direction in the Berlin Heart EXCOR®. Placing the Berlin Heart EXCOR® in the right direction is important because two valves in the LVAD direct the flow and create and unidirectional flow of medium.*

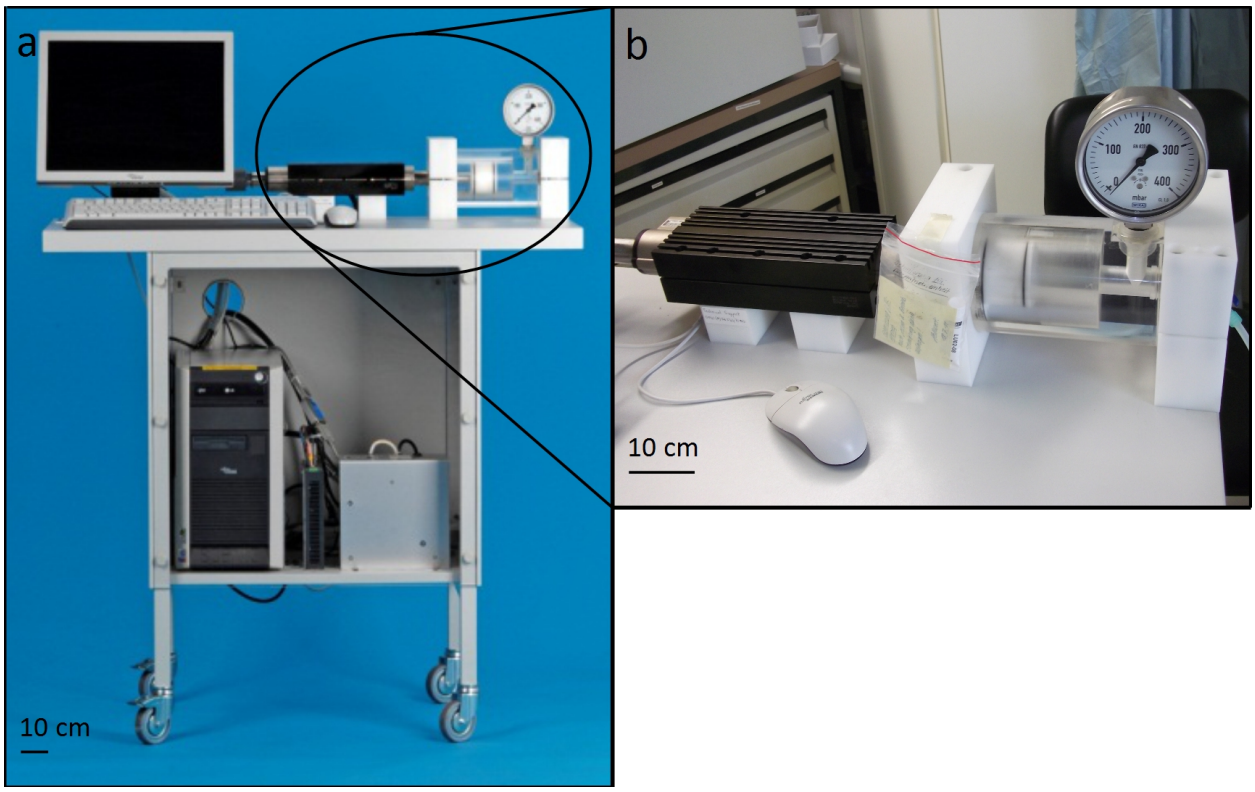

Fig 3-6 The control unit and the pump *The computer guided actuation unit (a), which set the flow rate, and an enlarged picture of the pump system, which created the pulsatile flow (b).*

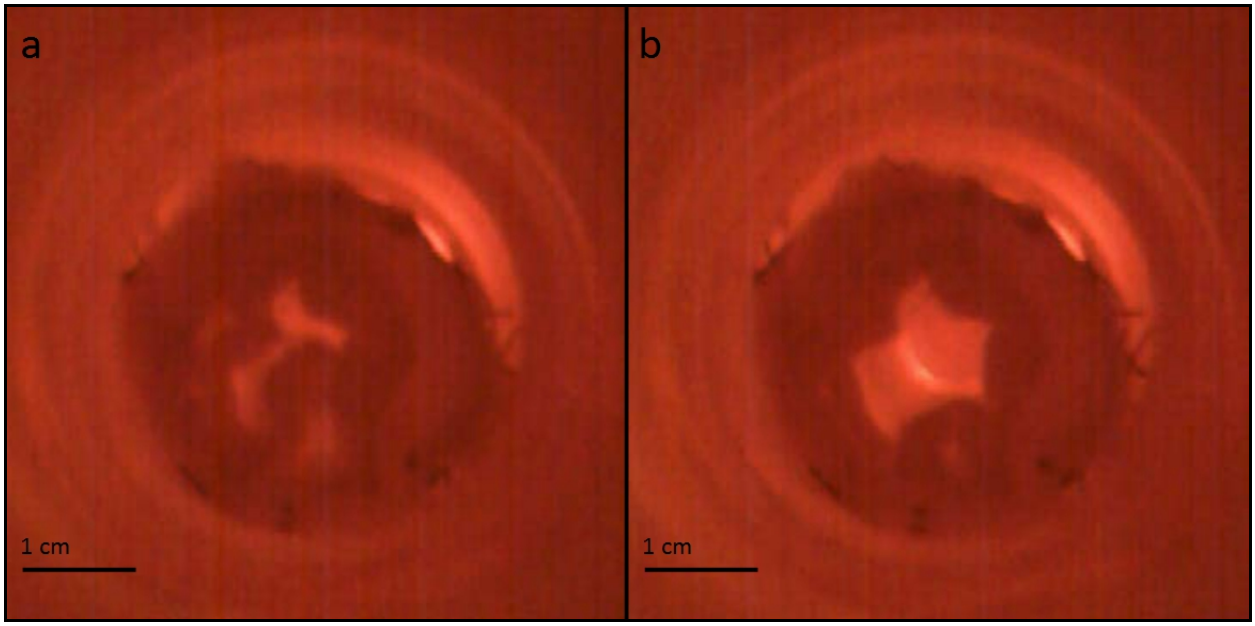

Fig 3-7 The closure and opening of the aortic valve during perfusion *(a) depicts the closed valve. The three leaflets can be distinguished. (b) shows the opened valve and the leaflets, which align themselves at the aortic wall.*

4. Analysis

4.1. Phase Contrast Microscopy

Phase contrast microscopy is an advanced technique compared to microscopy to evaluate the state of transparent objects. When light travels through a transparent object changes in the amplitude and phase appear. However, the human eye can only process the changes in amplitude. Phase contrast microscopy makes these changes visible by manipulating the background light of the sample and the light, which is scattered by the sample and defines most of the details of the specimen. (Zernike 1942) For the monitoring of the progress of cell cultivation and proliferation (Fig 4-1 a, b) as well as the trypsination process (Fig 4-1 c), phase contrast microscopy was utilized. The cells were examined in a 200x optical magnification.

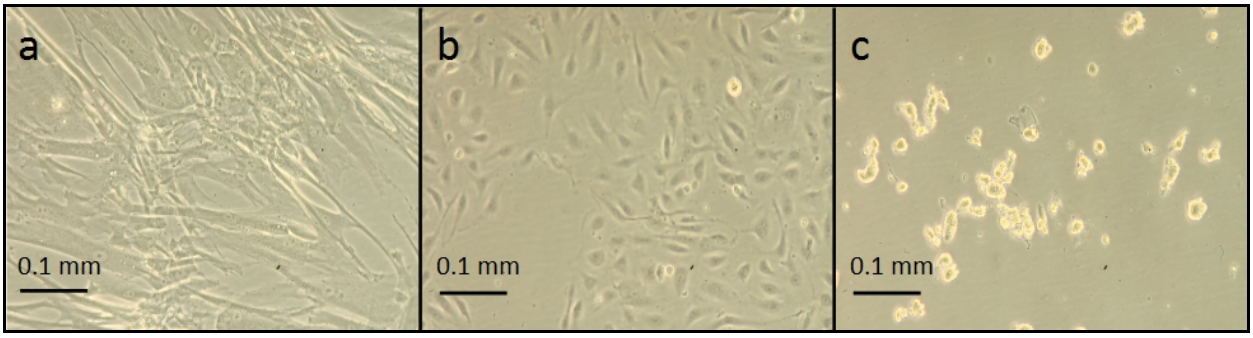

Fig 4-1 FB and EC in culture *FB (a) can be differentiated from EC by their spindle like form as well as their tendency to build multilayers, which is shown by their overlapping appendices. EC (b) tend to keep a rounder shape compared to FB and do not build multilayers. Cells during the trypsination process (c). After detaching the cells from the culture medium they have a round shape and float freely in the medium.*

4.2. Cell Counting

For cell counting a Neubauer counting chamber was used (Fig 4-2). During the trypsination process 250 µl cell suspension were removed to perform cell counting. 50 µl each were diluted 1:2, 1:4 and 1:8 with trypan blue. Trypan blue enabled the differentiation between vital and dead cells. Due to the damaged cell membrane, dead cells absorb the blue color while vital cells stay uncolored. (Strober 2015) The number of cells was calculated according to the following formula:

$$NL = \frac{N \times 10^4 \times d \times V}{S}$$

NL	Number of living cells
N	Number of cells counted
d	Dilution factor
V	Volume of original cell suspension
S	Number of squares counted

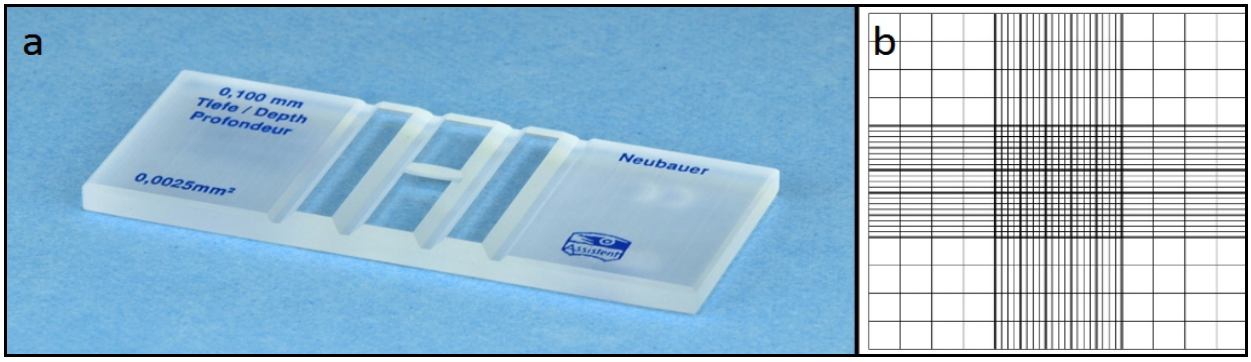

Fig 4-2 Neubauer counting chamber *Looking at a Neubauer counting chamber (a) through the light microscope, the grid (b) becomes visible. To count the living cells, every non-coloured cell in the space of one big grid in one of the four corners has to be counted. The dimension of the grid depends on the Neubauer counting chamber, which is used.*

4.3. Immunohistochemical Staining

Immunohistochemical analysis was performed to identify the different surface proteins and ECM proteins within the tissue of the heart valve and the cells. This analysis uses the interaction between antigens and antibodies to apply color, which can be seen through a microscope. Antibodies, which are produced from different animal race (e.g. mice, rabbits) bind to a specific, predefined protein. After the first incubation with the animal antibody, a second incubation was performed. This time an antibody against the animal antibody, which is linked with the enzyme peroxidase, was applied. After the second incubation hydrogen peroxide (H_2O_2) was added to the sample. This triggered a reaction with the peroxidase, which finally resulted in a brown-red coloring of the sought proteins. Specific antibodies were used to identify different cell structures. CD31 identified EC. TE-7 was used for FB. SMC-Myosin and α-Actin are found in smooth muscle cells. VE-Cadherin and Connexin-43 were utilized to identify intercellular connections. Collagen IV and Fibronectin were used to label ECM proteins. ICAM and VCAM are cell adhesion molecules, which are expressed during an inflammatory reaction.

The procedure can be divided into three phases: *Phase 1* (preanalytical) The tissue preparation. This includes the fixation, trimming, and embedding of the tissue section. The embedded tissue was cut into small sections with the microtome. *Phase 2* (analytic) begins with the deparaffination of the tissue sections. Furthermore, eventual preincubation steps (e.g. antigen retrieval, blocking of non-specific antigens) and the incubation with the first antibody are conducted. During the final step the tissue was counterstained with the second antibody and the cover slip was attached. *Phase 3* (interpretation) The results are interpreted and the IHC controls are evaluated. (Ramos-Vara, Miller 2014)

4.3.1. Cell Culture Preparation

For the staining of the cell cultures FB and EC cultures were cultivated in cell culture treated 8-well plates until they reached confluency. The medium was removed and the whole plates were put into -80 °C ethanol 96 % for at least 24 h.

4.3.2. Tissue Preparation

The samples, which were taken from the homograft, were put into formalin 10 % at 4 °C for 10 days to achieve a sufficient fixation. Following the specimens were put into paraffin and after cooling the paraffin blocks were cut into sections between 5 - 8 µm using a microtome. The paraffin slices were loaded on a slide and were put in a heater at 40 °C for 24 h to dry.

4.3.3. Deparaffination

The specimen were heated to 55 °C and then repeatedly rinsed with Xylene to remove the paraffin. The samples were rehydrated by a descending alcohol grade. The descending alcohol series started with ethanol 96 % followed by ethanol 70 %, 50 % and at last 30 %. At each alcohol concentration the specimen were incubated for 10 min. Finally the samples were permeabilized with 0.5 % Triton-X in PBS for 10 min at RT. Before antibody application the specimens were rinsed with aqua destillata and PBS for 6 min each to remove the residual ethanol.

4.3.4. Antibody Application

The samples were first treated with Triton-X to enable a permeabilization of the cell membrane. Samples for staining against VE-Cadherin, Connexin-43, Fibronectin and Collagen IV were put under a proteolytic treatment with protease 10 % for 3 min at RT. This process enabled an intensification of the specific staining by facilitating the detection of the tissue antigens (Linnoila, Petrusz 1984). A denaturation of proteins occurred during the fixation process. To expose the antibody binding sites of the proteins, a proteolytic demasking was performed. For proteolytic demasking of ICAM, VCAM and TE-7, the specimen were put into 0,1 mM EDTA buffer (pH=8.0) and boiled for 15 min. Samples were boiled in 10mM Tris/1mM EDTA (pH=9,0) solution for 15 min to demask α-Actin. The staining for Connexin-43, CD31, SMC-Myosin and VE-Cadherin required a treatment with Target Retrieval solution (pH=6.0) and boiling for 15 min. Endogenous peroxidase of the cells was blocked with 0.4 % H_2O_2 in PBS. Following the samples were incubated for 24 h at 4 °C with primary antibodies, which were diluted according to the producer information. After the rinsing with PBS the second antibody, which was linked with horse radish peroxidase, was applied and the samples were incubated for 10 min. The application of a color/H_2O_2 mixture for 10 min enabled the colorization of the sample. For better differentiation of the

cell nucleus the specimen were stained with hematoxylin and then rinsed for 2-5 min with deionized water. Finally aqueous mounting solution was applied and the cover slips were put on the samples. The stained specimen were observed under the light microscope.

4.4. Scanning Electron Microscopy

Introduction

Scanning electron microscopy (SEM) uses an electron beam to display the topography of samples. An electron source, a lanthanum hexaboride (LaB_6) cathode, emits electrons, which pass through a combination of different lenses and scanning coils or deflector plates to create a focused beam. The deflector or scanning coils deflect the beam in its x- and y-axis to create a scanning raster over the sample. To avoid interaction of the electron beam with air molecules the scan has to be performed in a high vacuum. When the electron beam hits the sample, the electrons are reflected and lose their energy. Three types of radiation are generated: the elastic scattering, which creates high-energy electrons, the inelastic scattering, which results in secondary electrons, and the electromagnetic radiation. These different radiations and particles can be detected by specialized detectors. A map of the surface topography of the sample can be created from the information on the position of the electron beam on the sample and the intensity of the emitted radiation/particles.

SEM analysis can only be performed on samples which are vacuum resistant, dry, and conductive. Therefore, wet samples have to be processed before analysis. The normal drying process often involves a change of the sample structure. To avoid this, the physical effect of phase transition is utilized. During critical point drying the status of a substance has the same density in its liquid as well as gaseous phase under a predefined pressure and temperature. Under these circumstances the sample can be dried avoiding the transition from the liquid to the gaseous phase and eventual damage caused by this change. However, due to the loss of fluid, the sample can shrink and fissures can occur. Non-conductive materials can be locally charged either negatively or positively during the scanning process. To prevent this, the sample has to be coated with a layer of a conductive element. In most cases gold is used. The layer has to be ultra thin to enable a correct scan during SEM. To transfer the gold atoms from the target (gold) to the sample, a high vacuum and the inert gas argon are utilized. A high vacuum is generated in the sample chamber and the target and the specimen are ionized. The target becomes the negative and the specimen the positive electrode. Following, argon gas is insufflated into the sample chamber. The inert gas atoms become ionized and accelerate towards the negatively charged target. Small gold particles are released from the target and a fine gold dust forms. This dust casts down on the sample and envelopes the surface.

4.4.1. Fixation

Samples for SEM were stored in FIX II solution (Aqua bidest. 456 ml, glutaraldehyd 43.5 ml, HCl 0.75 ml, Na-CaCO 5.65 g) at 4 °C for at least 48 h. Next the samples were dehydrated in an ascending alcohol series (30 %, 50 %, 70 %, 96 %) for 10 min each. During the final step the alcohol 96 % was replaced with acetone at -20 °C.

4.4.2. Critical Point Drying and Sputtering

The samples were placed in the specimen chamber and filled with acetone at -20 °C. Afterward the acetone was gradually replaced with liquid carbon dioxide. As soon as the acetone was completely replaced with carbon dioxide, pressure and temperature in the specimen chamber was altered (42 °C, 9.0 MPa) to surpass the critical point of carbon dioxide. At this point carbon dioxide changed from liquid to gaseous phase without forming a phase boundary. Following, the gaseous carbon dioxide was slowly released over a period of 30 min. The dried specimens were then put in the sputtering chamber, where a vacuum was generated. The inert gas argon was added and the samples were exposed to gold ions (180 sec, 10^{-5} mbar, 24 °C). Analysis of the samples was performed with the scanning electron microscope Evo LS10 from Zeiss.

4.5. Image Evaluation with ImageJ

ImageJ is an open source image processing program specifically designed for processing scientific images. ImageJ enabled a quantitative evaluation of the immunohistochemical samples. The surface covered with cells was measured and the ratio between the covered/not covered surface was calculated. The immunohistochemical staining for CD 31 and TE-7 were utilized for cell coverage evaluation. This method added a quantitative evaluation of the immunohistochemical samples to the qualitative evaluation of the coloring.

5. Results

5.1. Cytology

5.1.1. Phase Contrast Microscopy

Phase contrast microscopy was utilized to observe cell proliferation during culturing, trypsination process and to differentiate between EC (Fig 5-1 a) and FB (Fig 5-1 b). EC show a rather irregular shape. They have a ball-shaped middle, where the cell nucleus is located, and in some cases tails on the sides. While FB can grow in overlapping layers, so called multilayers, EC form monolayers. FB are spindle-shaped. Their elongated body contains the cell nucleus in the middle.

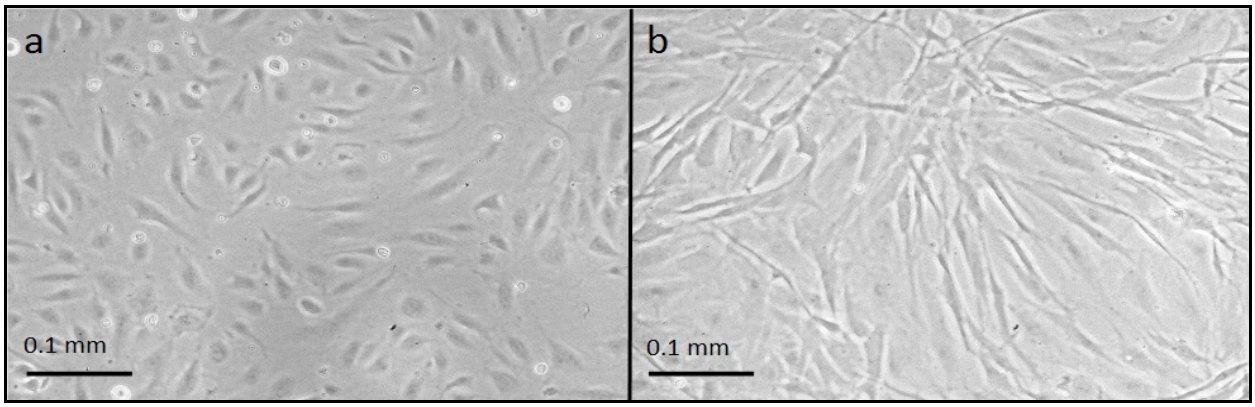

Fig 5-1 EC and FB cultures in phase contrast microscopy *EC (a) show a cuboid body with short tails on the sides. FB (b) have a typical elongated shape and can build multilayers.*

5.1.2. Immunocytochemical Analysis

To verify the specification of the utilized cell cultures, antibody staining was performed. Staining against CD 31 and VE-Cadherin indicated EC cultures (Fig 5-2 a, b). For a negative control EC cultures were stained against TE-7, which remained negative (Fig 5-2 c). FB cultures were stained analogously. Protein expression of TE-7, Fibronectin and negative expression for CD 31 demonstrated FB cultures (Fig 5-2 d, e, f).

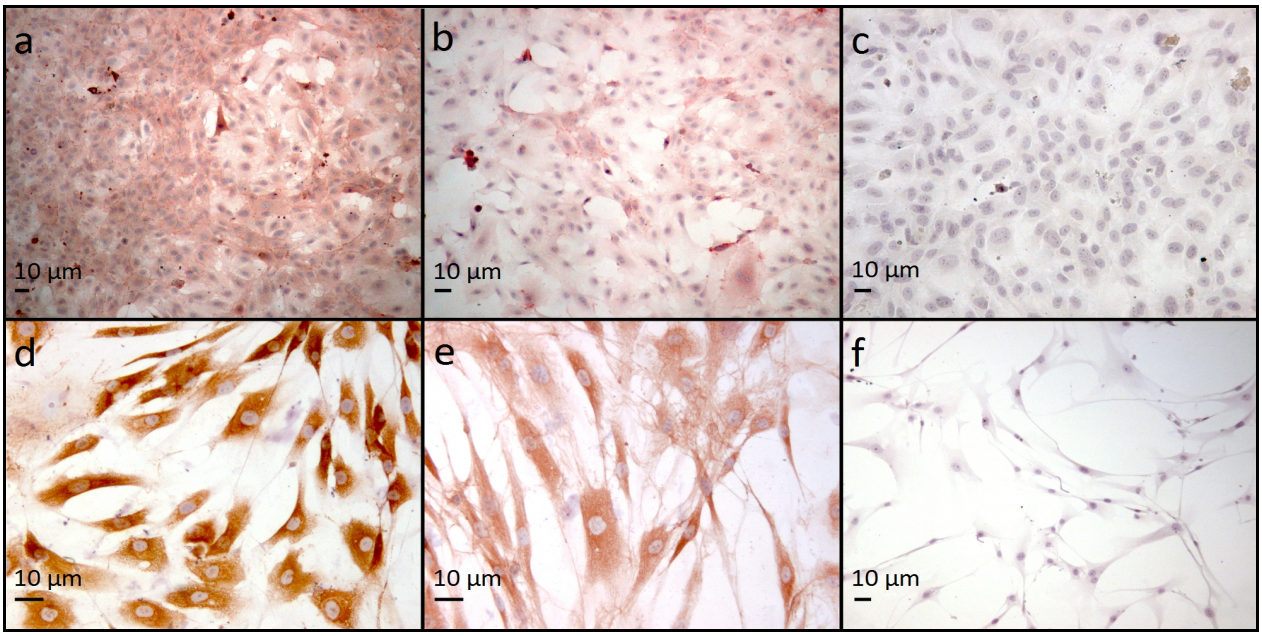

Fig 5-2 Immunocytochemical staining of a representative EC and FB culture *EC specific CD 31 is positive (a). The intracellular adhesion protein VE-Cadherin expression also demonstrates an EC culture (b). The negative staining against TE-7 (c) in the EC culture was the control. TE-7 staining is strongly colored, demonstrating FB culture (d). Fibronectin expression is also highly positive (e). The staining against CD 31 in the FB culture remained negative (f)*

5.2. Macroscopic Examination of the Aortic Homografts during Processing

The homografts, which were used for the study had a diameter of 2.28 ± 0.15 cm and a length of 2.38 ± 0.42 cm. Macroscopic inspection after thawing of the homografts displayed no damages (Fig 5-3 a, b). Remains of the myocardium were still attached to the aorta. The two coronary arteries were severed at approximately 0.5 – 1.0 cm (Fig 5-3 a, black arrow) on every sample. The homografts had a pink-yellow coloring. This may be due to the pink color of M199, which was used in many solutions and the medium. After the decellularization, the homografts lost their pink color and a yellow structure remained (Fig 5-3 c, d). The homografts stayed intact and well preserved. Immunohistological and SEM analysis was performed to evaluate the decellularization (see *Chapter 5.3.4. "Homograft wall after Crimping and Perfusion, Chapter 5.4.4. "Walls of the Homograft after Crimping and Perfusion"*). Remnants of the myocardium were dissected to facilitate the following recellularization. The recellularization process colored the valve slightly pink (Fig 5-3 e, f). The macroscopic structure of the leaflet and the wall seemed undamaged and fully functional.

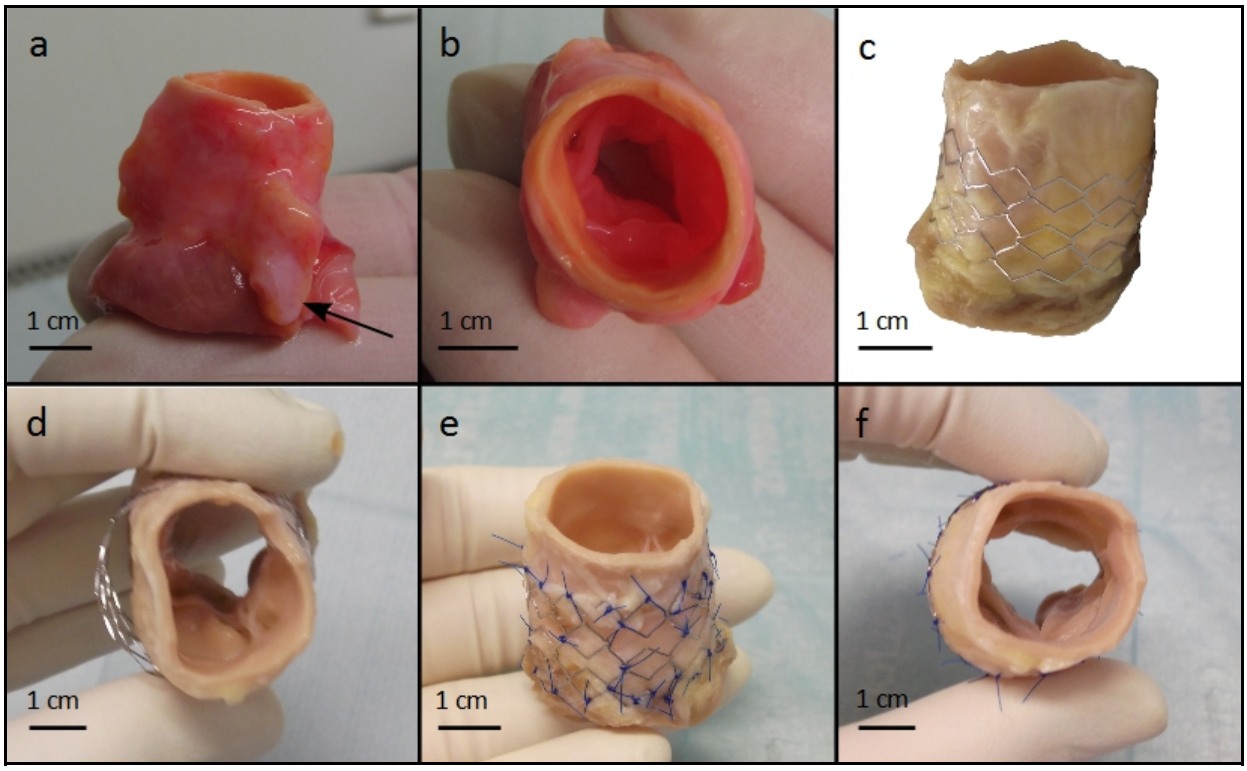

Fig 5-3 Macroscopic views of the aortic homograft during processing *In picture (a) and (b) the valve is inspected after thawing. No tears or fissures, which may be caused by the thawing process, are visible. The arrow in (a) marks a coronary artery. The leaflets are also undamaged and intact. After the decellularization the valve lost its pink color (c, d). A stent was dilated to fit the valve size (c, d) and sewed in with single knot sutures (e, f). The structure of the aorta and the leaflets are unscathed after recellularization (e, f). The valve regained a slightly pink color after recellularization.*

5.3. Homograft Topography

For qualitative analysis of the cell layer integrity and ECM substance, SEM analysis as described in *Chapter 4.4. "Scanning Electron Microscopy"* was performed.

5.3.1. Native Homografts

The luminal surface of the native homografts after thawing appeared inhomogeneous (Fig 5-4 a). The surface on the outer wall was covered in a corrugated layer (Fig 5-4 b). Both surfaces alternated between higher and deeper plateaus, leaving the surface very irregular and undulated. The depths and highs of the luminal surfaces were smaller. Particles of different size adhered to inner surface (Fig 5-4 a, whites circles) and were visible on all homografts.

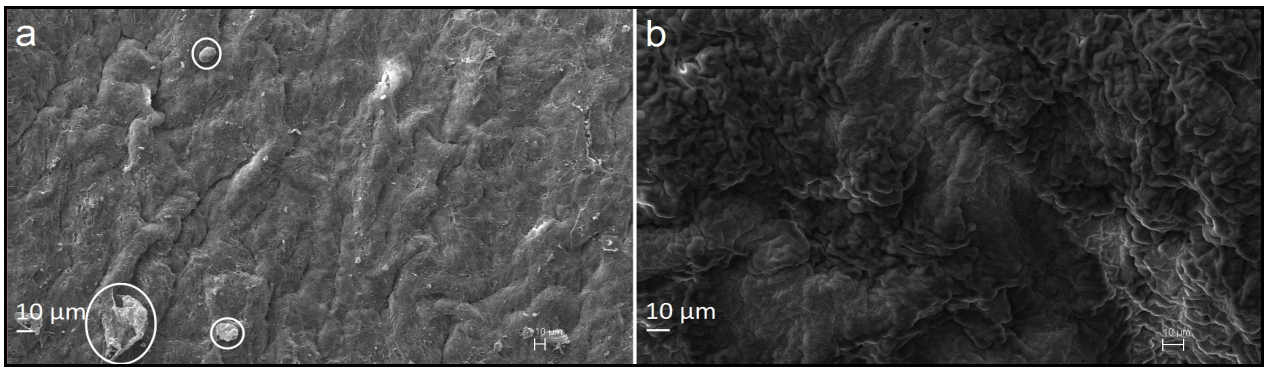

Fig 5-4 SEM image of the native homograft surface *The luminal surface is covered with an inhomogeneous layer. The whole area appears undulated. Round particles in different sizes adhere to the surface (a, white circles). The undulating is more pronounced on the outer surface (b). These are representative images of four independent experiments, each performed with heart valves and cells from a different donor.*

5.3.2. Decellularized Homografts

After the decellularization process, the luminal side (Fig 5-5 a) appeared rougher. Large and small particles in different shapes adhered to the surface (Fig 5-5 a, white circles). The outer wall showed a woven-like structure, indicating fibres (Fig 5-5 b).

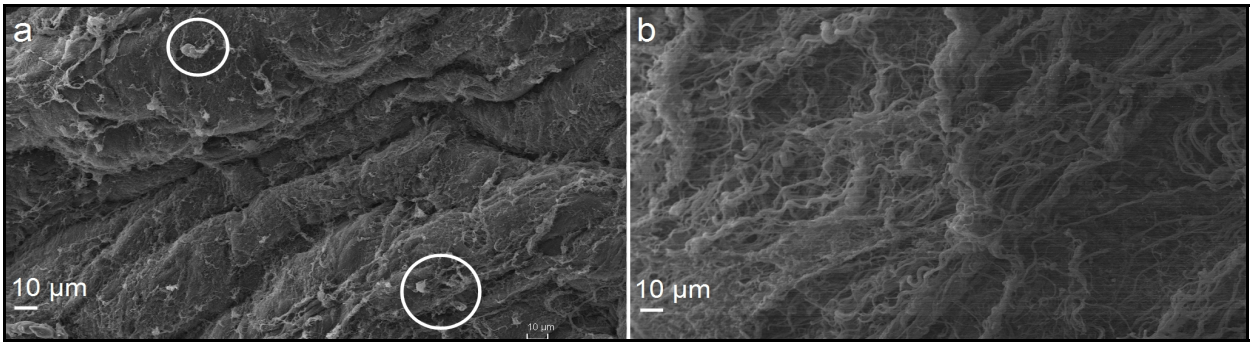

Fig 5-5 SEM image of the homograft surface after decellularization *The luminal surface appears rougher and more irregular (a). Particles in long shapes are attached to the surface (a, white circles). Fibres in a woven structure define the outer wall of the homograft (b). These are representative images of four independent experiments, each performed with heart valves and cells from a different donor.*

5.3.3. Recellularized Homografts

The recellularized surface of the homografts showed an intact, homogeneous cell layer (Fig 5-6 a). The EC demonstrated the typical cobblestone pattern of their distribution, but no orientation in a distinct direction. Occasionally, fragments and particles adhered to the surface, but these findings were seldom

and are most likely artifacts, which occurred during SEM processing. One sample displayed tears in the otherwise intact cell layer (Fig 5-6 c). Reason for these fissures was most likely the manipulation during the processing for SEM imaging. The outer side of the wall was also covered with cells (Fig 5-6 d). The distribution of the cell layer was not as homogeneous as on the inner side. Deep tears broke the cell layer in which the fibre structure of ECM was visible.

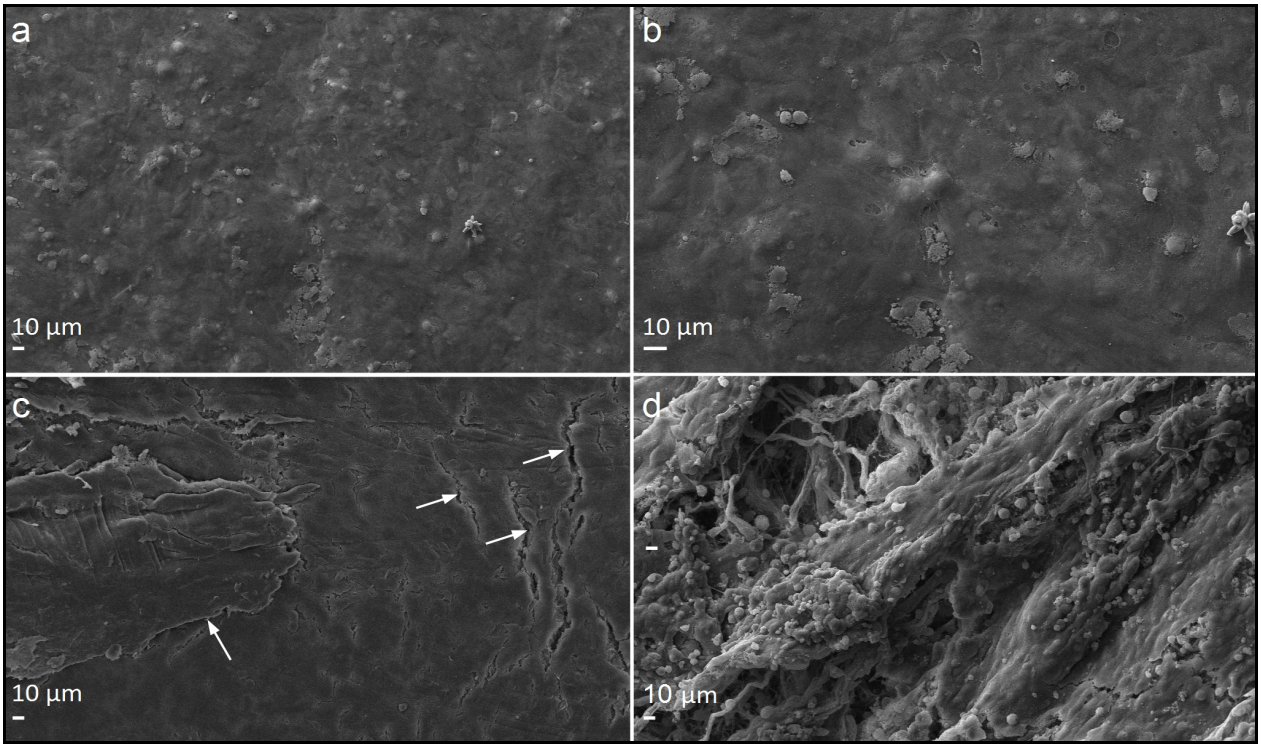

Fig 5-6 SEM image of the homograft after recellularization *A confluent and homogeneous cell layer covers the surface of the aortic wall (a). The higher resolution of the image shows a cobblestone pattern, which is characteristic for EC (b). The ruptures (c, white arrows) developed most likely during drying. On the outer wall a layer of cells is visible (d). Occasionally deep tears occurred, in which the fibre structure of the tissue was visible. These are representative images of four independent experiments, each performed with heart valves and cells from a different donor.*

5.3.4. Wall and Leaflet of the Homografts after Crimping and Perfusion

Wall

For SEM analysis the aortic homograft was divided into four sections: The supravalvular, valvular and subvalvular part of the aortic wall and the valve.

Large patches of a cell layer covered most of the supravalvular wall surface. In between, fissures and cracks were visible. Occasionally, the fibre structure of the ECM or another cell layer was visible. Dumps on the layer indicated cell nuclei. However, a cobblestone pattern was not identified. Fragments and

particles adhered to the surface. The amount of these particles varied between the samples.

Parts of the walls of the valvular part of the vessel were also coated in a layer. Although it was not as even as the layer of the recellularized valve. A cobblestone structure was also not visible. Fragments in different sizes and shapes were scattered all over the specimen. The amount of fragments differed from sample to sample. Whole cell layers were teared off the wall. The uncovered areas exposed underlying cell layers and parts of the ECM (Fig 5-7 c, d).

The surface of the subvalvular specimen varied to a certain extend. Two samples demonstrated a structure, which resembled a cobblestone pattern and indicated an EC layer (Fig 5-7 e, white circle). However, part of the cell layer was ripped off (Fig 5-7 e, white arrows). Another sample's layer was torn (Fig 5-7 f). Elongated cells, which indicated FB, were disrupted and parts of the filamentous ECM were in view. Particles of different sizes were scattered over the surfaces. Quantities of particles were inhomogeneously distributed over the surface.

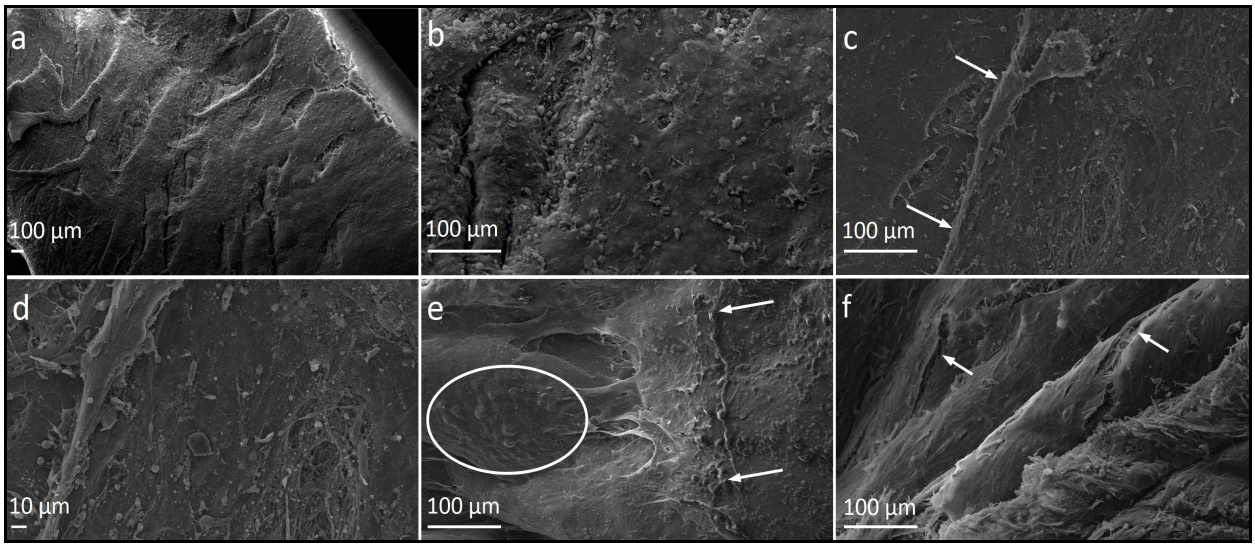

Fig 5-7 SEM image of the aortic wall after crimping and perfusion *Supravalvular (a, b), valvular (c, d) and subvalvular (e, f) samples. The side of the supravalvular wall which faces the bloodstream is covered by a cell layer (a). Multiple fissures permeate this layer. Through these ruptures other cell layers and to some extend ECM are visible. Particles of different sizes are scattered all over the surface (b). The valvular wall displays similar findings. A large cell layer (c, white arrows) is detached from the underlying tissue. Cell remnants are scattered over the layer (d). A part of the cell layer in (e) form a cobblestone pattern (e, white circle). A wide cell layer scales off from the layer below in this part of the wall as well (e, white arrows). Longitudinally shaped cells, which only partially demonstrate a homogeneous alignment, cover the surface of the subvalvular wall part (f). Fissures can be found all over the area (f, white arrows). These are representative images of four independent experiments, each performed with heart valves and cells from a different donor.*

Leaflet

The arterial and ventricular sides of the leaflet were analyzed. However, due to processing after crimping and perfusion there was no reliable technique to differentiate arterial and ventricular sides. The leaflets surface was mostly covered in a cell layer. Small fissures and cracks appeared all over the surface. Three different samples demonstrated a partial cell layer (Fig 5-8 a, white circle), which could be classified as cobblestone structure and indicated partial coverage with EC. The FB coverage of the surface was inhomogeneous. 50 % of the samples showed a smooth surface. The distinct shape and cell nuclei of some of the cells was apparent (Fig 5-8 b, c). On the other half, the cell layer was partially torn and the ECM underneath was visible (Fig 5-8 d). Cell remnants in different amounts were attached to the surface of every sample.

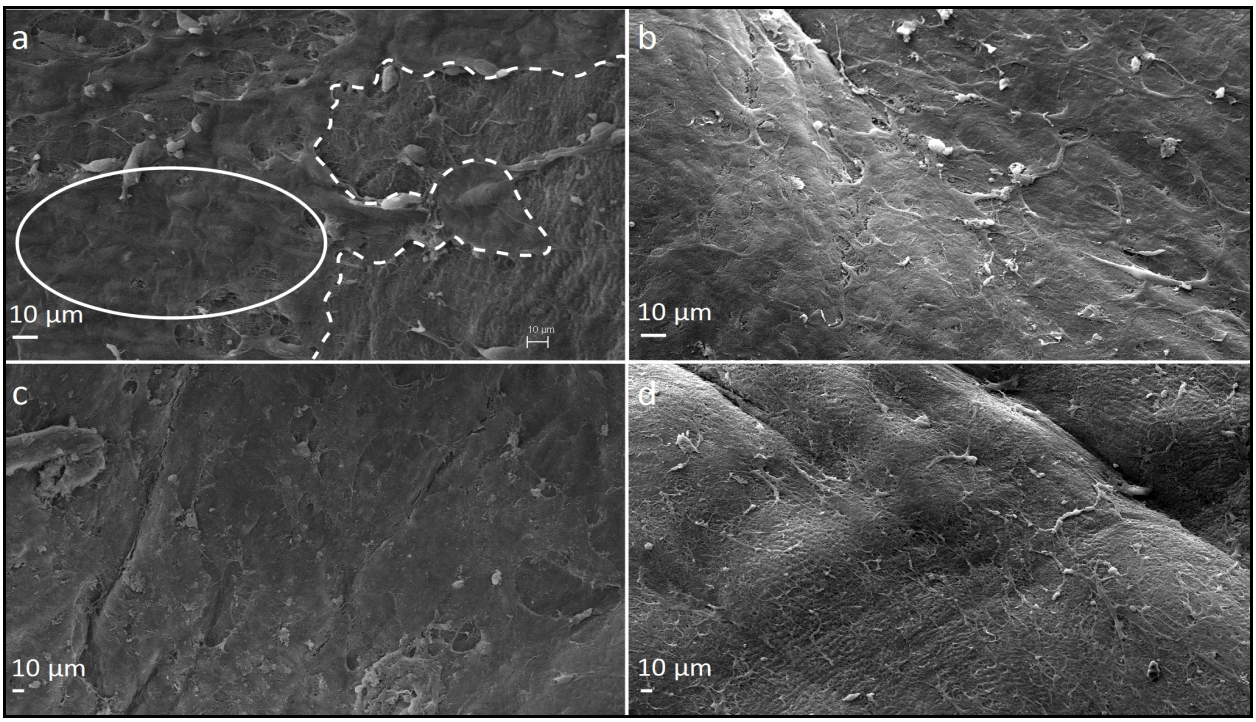

Fig 5-8 SEM image of the aortic valve leaflets after crimping and perfusion *The sample (a) demonstrates a structure, which can be classified as cobblestone pattern (a, white circle) and indicates an incomplete coverage which EC. The dotted white line roughly outlines the borders of the cell layer. All samples were covered with a FB layer. The spindle form of the FB can be seen in (b). The FB layer was in some case less continuous (c). Parts of the layer are disrupted and the ECM beneath shows (d). These are representative images of four independent experiments each performed with heart valves and cells from a different donor.*

5.3.5. Summary of SEM Analysis

TABLE 5-1: SUMMARY OF SEM RESULTS

Process stage		*Cell layer integrity*
Native		o
Decellularized homografts		FBL --- / ECL ---
Recellularized homografts		ECL +++
Homografts after crimping and perfusion	supravalvular	FBL ++-/ ECL ---
	valvular	FBL +-- / ECL ---
	subvalvular	FBL ++- / ECL +--
	leaflet	FBL ++- / ECL +--

Key: o = cell layer not definitive discernible, FBL = fibroblast layer, ECL = endothelial cell layer, --- = 0-30 % cell layer cover, +-- = 30-60 % cell layer cover, ++- = 60-90 % cell layer cover, +++ = 90-100 % cell layer cover

5.4. Immunohistochemical Analysis

5.4.1. Native Homografts

CD 31 (Fig 5-9 a) and TE-7 (Fig 5-9 b) protein expression was negative for a confluent cell layer on the surface of the wall samples after staining. TE-7 stains were moderately colored in a band along the *tunica intima* of the aortic walls in 50 % of the specimen. Although positive, this colorization only occurred within the wall and not on the surface. The staining against the intercellular adhesion proteins, Connexin 43 and VE-Cadherin, was negative. ICAM and VCAM expression was also negative. The immunohistochemical staining showed positive staining against Collagen IV, SMC-Myosin, α-Actin and Fibronectin in the wall of the aorta. Collagen IV and SMC-Myosin (Fig 5-9 c, d) staining showed strong dyeing in all samples.

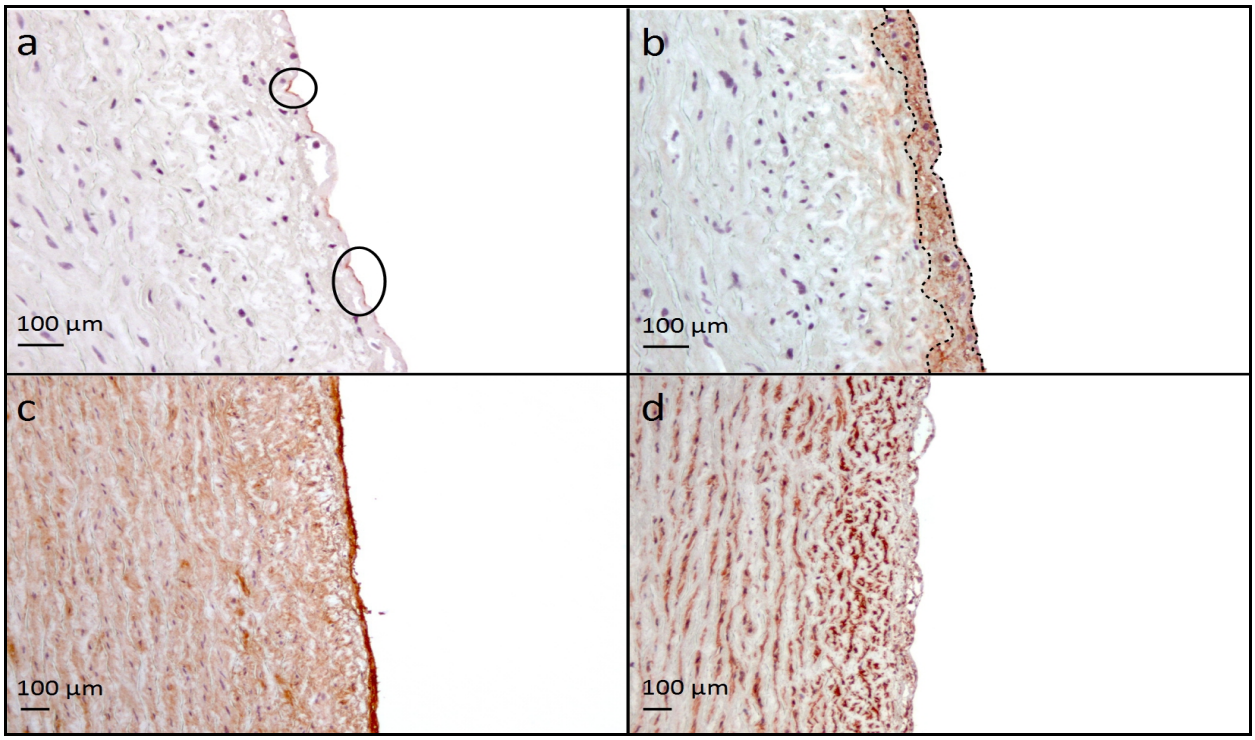

Fig 5-9 IHC staining of a representative native homograft *cell nuclei staining with hematoxylin Occasional staining against CD 31 appears on the samples (a, black circle), but no confluent cell layer is visible. The broad band of color (b, dotted line) displays the TE-7 staining in the tunica intima of the aortic wall. In (c) the red color indicates a strong reaction against Collagen IV antibodies. SMC-Myosin is also highly colored within the aortic wall (d).*

5.4.2. Decellularized Homografts

The decellularization process removed the cells on the aortic wall surface. Staining against CD 31 (Fig 5-10 a) and TE-7 (Fig 5-10 b) proteins were negative on the wall's surface. The staining against the ECM proteins (α-Actin, Collagen IV, Fibronectin, SMC-Myosin) (Fig 5-10 c, d) were positive, which indicated at least a partial preservation of the ECM.

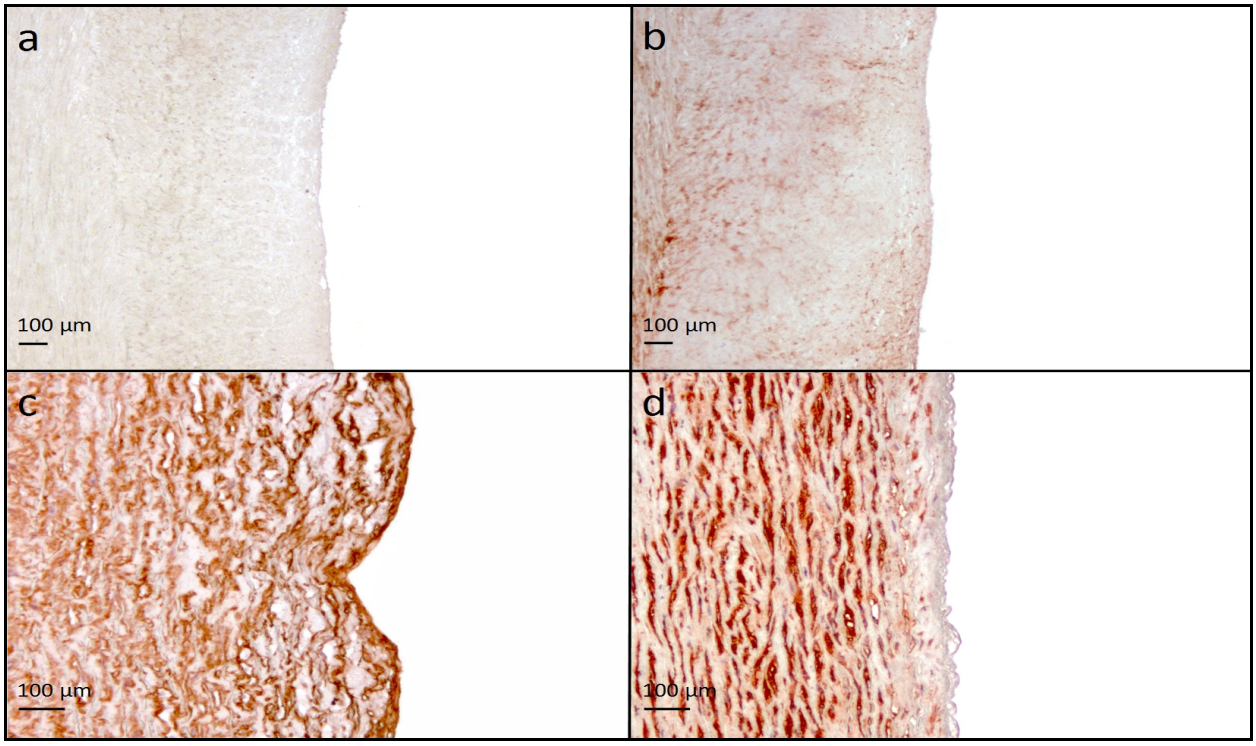

Fig 5-10 IHC staining of a representative homograft after decellularization *cell nuclei staining with hematoxylin. After decellularization no cells were detectable on the surface of the wall, which faces the blood stream. CD 31 staining is negative (a). In (d) a few scattered cell nuclei are visible in the deeper layer of aortic wall. TE-7 proteins are stained in the deeper layer of the aortic wall, but staining against TE-7 is not visible on the surface (b). The staining against Collagen IV (c) and SMC-Myosin (d) is highly positive.*

5.4.3. Recellularized Homografts

After the recellularization the staining against CD 31 showed a strong reaction (Fig 5-11 a). The red-brown staining covered the surface of all samples. The staining against TE-7 demonstrated a confluent FB layer underneath the EC layer (Fig 5-11 b). CD 31 and TE-7 staining was positive on all samples. The intercellular adhesion proteins (Connexin 43, VE-Cadherin) colored slightly on 100 % of the samples (Fig 5-11 b, c). The coloring of ICAM (Fig 5-11 e), a protein which mediates inflammatory response, was positive in all samples, while the staining against VCAM was negative (Fig 5-11 f). SMC-Myosin showed a reaction in the deeper layer of the walls, while Collagen IV also demonstrated a colorization near the surface in 50 % of the specimen (Fig 5-11 g, h). The staining showed a confluent cell layer.

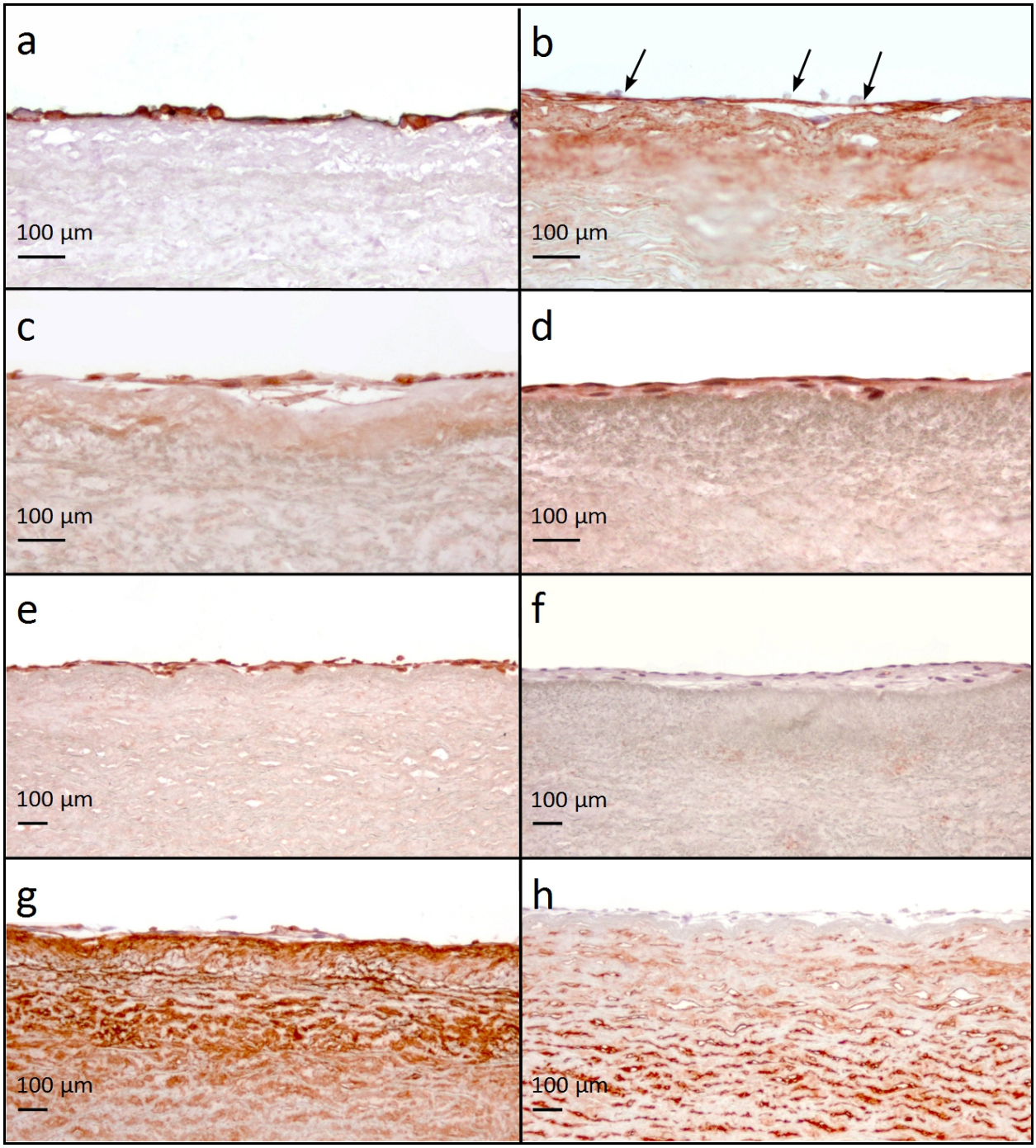

Fig 5-11 IHC staining of a representative homograft after recellularization *cell nuclei staining with hematoxylin. The staining against CD 31 demonstrates a strong reaction. The red layer on the wall surface (a) shows a confluent EC layer, which is visible on all samples. TE-7 staining verifies a FB cell layer on all samples (b). The black arrows in (b) mark EC on top of the FB layer. The intercellular adhesion proteins Connexin 43 (d) and VE-Cadherin (d) color in a faint red layer on the surface of 100 % of the wall samples. ICAM (e) also demonstrates an expression on all samples, while VCAM (f) expression is not detected on any sample. The staining for Collagen IV was strongly positive, especially in the tunica intima of the aortic wall (g). In 50 % of the samples, the protein reaction was also positive close to the surface. SMC-Myosin expression stained throughout the aortic wall (h). It was positive in 100 % of the samples. There is no detection of SMC-Myosin in the cell layer on the surface.*

5.4.4. Wall of the Homografts after Crimping and Perfusion

Cell Layer

The staining against CD 31 displayed no confluent cell layer on the supravalvular, valvular or subvalvular part of the aortic wall. On one sample about 18 % of the wall were covered in cells. However, they formed only small patches and no confluent layer (Fig 5-12 a), which covered the whole wall. TE-7 expression was visible on all parts of the aortic wall. The FB layer covered more of the aortic wall than the EC layer (Fig 5-12 b). A mean of 55 % of the aortic wall was covered with FB. On one sample nearly 100 % of the luminal surface was covered with FB. On the three remaining samples about 40 % of the surface was coated with FB.

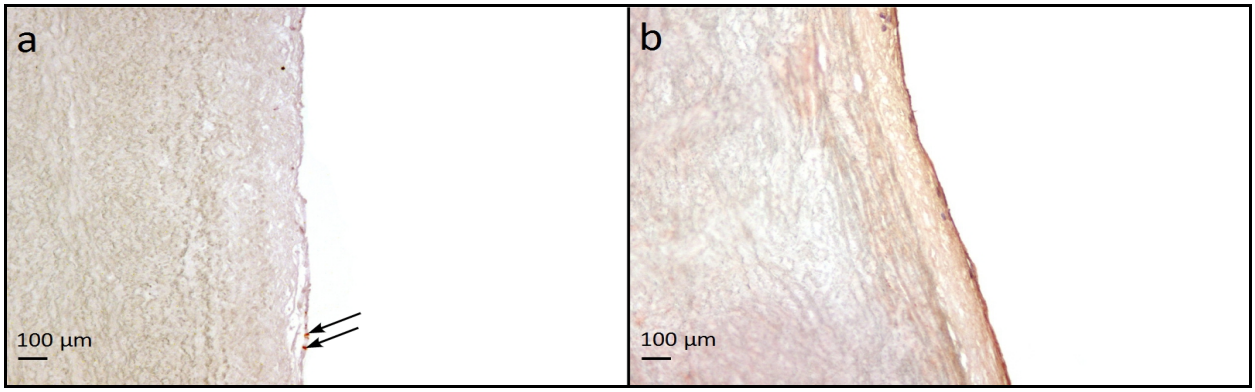

Fig 5-12 Cell layer after crimping and perfusion on a representative homograft *cell nuclei staining with hematoxylin. A confluent EC layer is not detected on any of the samples. Although, some red spotted dots are visible on the wall's inner surface (a, black arrows), a continuous layer can not be discerned. The FB layers coats about 55 % of the aortic wall (b). One sample displays a nearly 100 % covering (b), while in the other samples approximately 40 % of the surface is coated.*

Intercellular Adhesion Proteins

The expression of the EC specific VE-Cadherin (Fig 5-13 a) and Connexin 43 (Fig 5-13 b) was positive in the remaining EC. Although, the samples showed no confluent cell layer compared to the samples after recellularization, the expression of VE-Cadherin and Connexin 43 was highly colored.

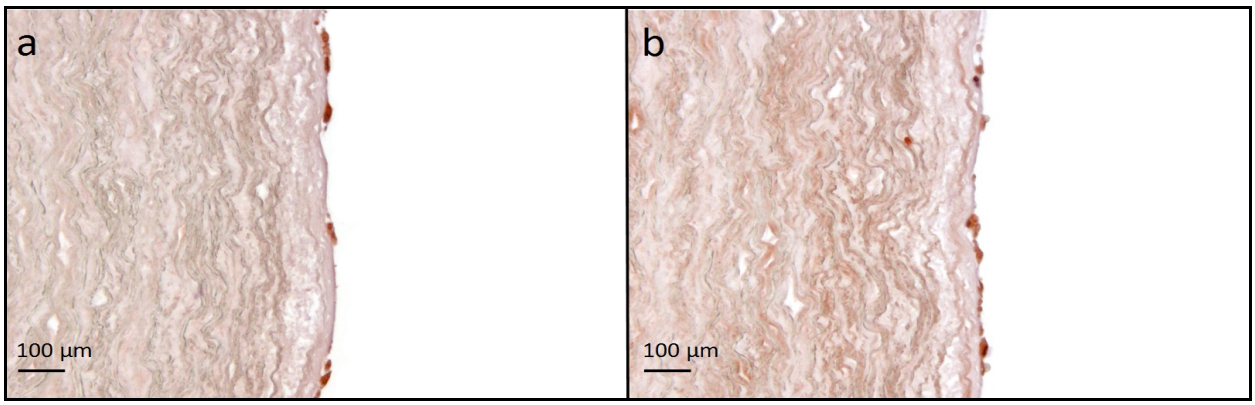

Fig 5-13 Intercellular adhesion molecules after crimping and perfusion on a representative homograft *cell nuclei staining with hematoxylin. The cells, which remained after perfusion, show a distinctive colorization for VE-Cadherin (a) and Connexin 43 (b).*

Inflammation modulatory Proteins

The crimping and perfusion procedure elicited an ICAM expression in the remaining cells on the surface (Fig 5-14 a). Compared to the expression of ICAM after seeding, the expression remained on the same level. In contrast, the inflammation protein VCAM was not detectable on the surface (Fig 5-14 b). The remaining cells (Fig 5-14 b, black arrows) stayed negative for the VCAM expression.

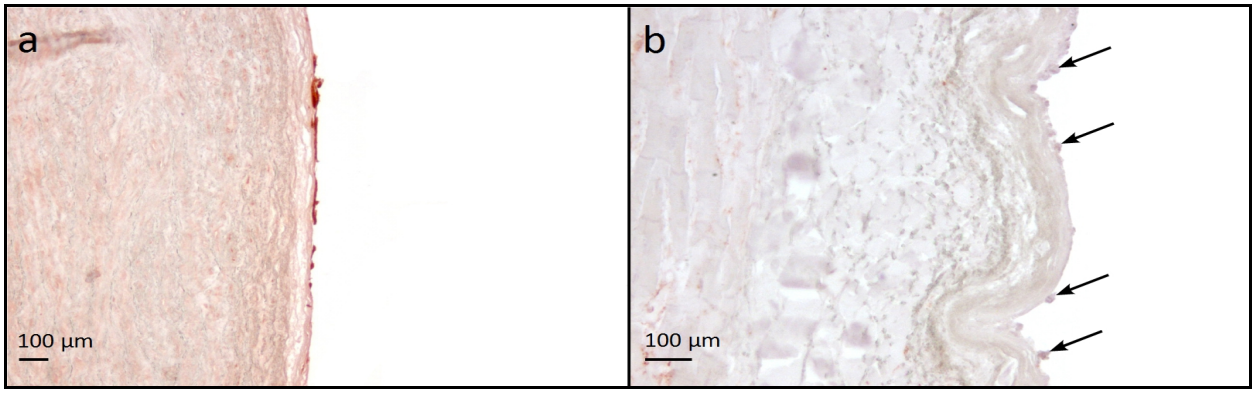

Fig 5-14 Inflammation reaction after crimping and perfusion on a representative homograft *cell nuclei staining with hematoxylin. The red staining on the surface is the reaction from the ICAM protein (a). The remaining cells stain strongly for this protein. This reaction is detected on all samples that still maintained cells. The inflammation protein VCAM does not show on the samples (b). Although cell nuclei were colored (b, black arrows) there was no VCAM expression.*

Structural Proteins of the ECM

The coloring of Collagen IV increased in strength after crimping and perfusion. Especially the coloring of the *tunica intima* intensified. 92 % of the samples displayed a strong red colored band just beneath the cell layer on the wall's surface (Fig 5-15 a, black dotted line). The staining against Fibronectin was not as strong as Collagen IV but also increased in the *tunica intima* (Fig 5-15 c). A faint but distinct reddish band can also be detected lining the inner surface of the aortic wall.

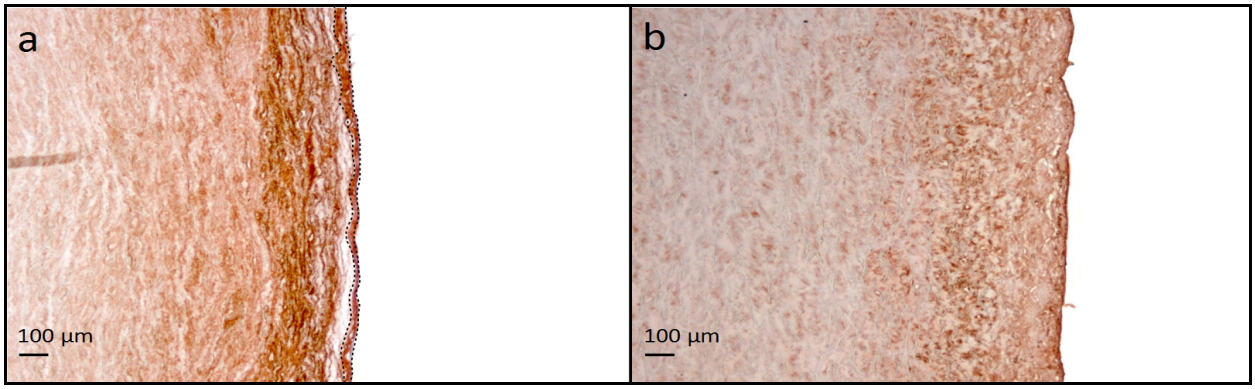

Fig 5-15 ECM protein expression after crimping and perfusion on a representative homograft *cell nuclei staining with hematoxylin. The coloring of Collagen IV intensified after crimping and perfusion (a). A distinct red band is visible just beneath the cell layer of the aortic wall (a, dotted line). 92 % of the specimens display this band. Also the staining against Fibronectin reveals this broad line (b). However, the coloring is not as strong as the Collagen IV colorization.*

5.4.5. Leaflet of the Homografts after Crimping and Perfusion

Cell Layer

Staining against CD 31 on the aortic leaflet after crimping and perfusion showed no EC layer (Fig 5-16 a, b). Single EC were scattered over the surface, but did not form a confluent layer neither on the ventricular nor on the arterial side of the leaflet. These findings were congruent on all four samples.
TE-7 staining decreased on the arterial side of the leaflet as well (Fig 5-16 d). While 100 % of the wall were covered in FB after recellularization, after crimping and perfusion an average of 70 % of the wall were coated. On the ventricular side of the leaflet about 90 % of the surface were covered in FB (Fig 5-16 c). Three of the samples demonstrated a 100 % cell layer confluency, one showed 60 %. Although cell nuclei are present in this last sample, the cells did not stain against CD 31 or TE-7 (Fig 5-16 e, f, dotted line, black circle). The missing staining against TE-7 may be contributed to a staining failure.

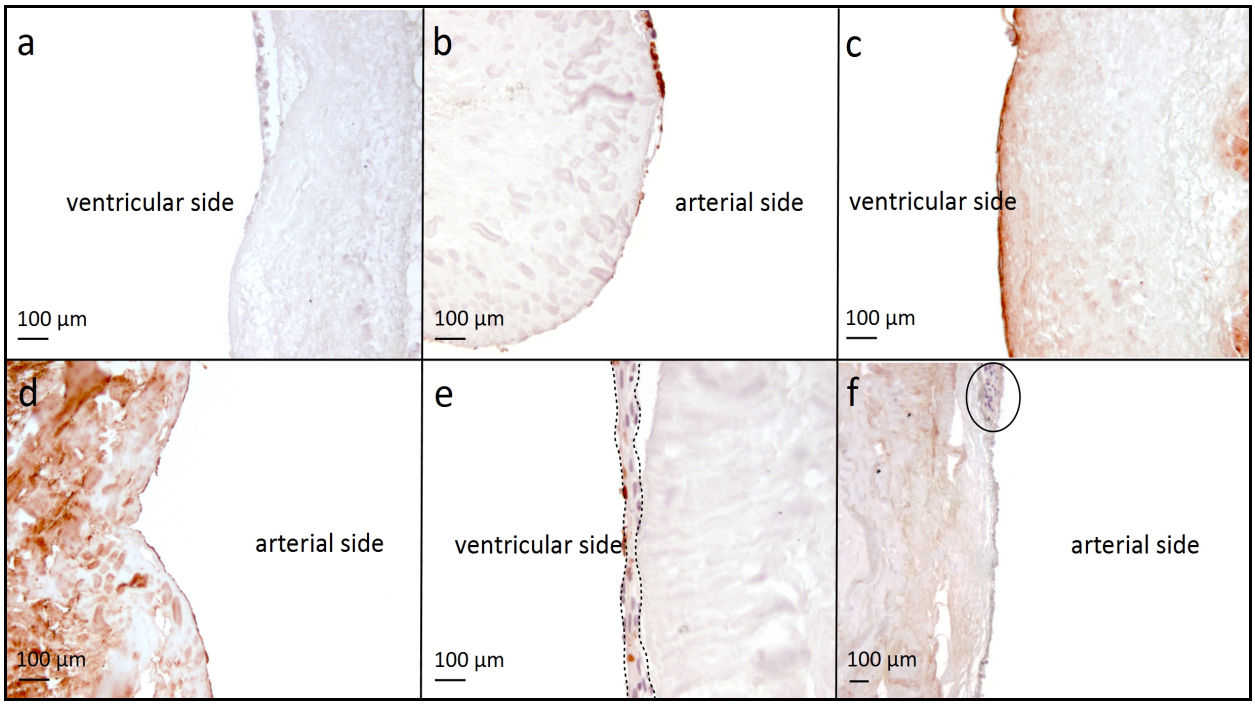

Fig 5-16 Staining against CD 31 and TE-7 on a representative aortic leaflet after crimping and perfusion *cell nuclei staining with hematoxylin. The cell staining against CD 31 shows no intact cell layer on the surface of the leaflet (a, b). Single cells are visible (b) but neither of the samples show a confluent layer, regardless of arterial or ventricular side. The staining against TE-7 displays a red-brown colorization. The cell layer on the ventricular side is confluent (c). Small disruptions of the cell layer integrity are rare. The arterial side of the leaflet sustained more damage after crimping and perfusion (d). Interruption of the cell layer are common. This one specimen shows a cell layer which does not stain for CD 31 (e, area between the dotted lines). Although the cell conglomerate is clearly visible (f, black circle) it does not stain for TE-7. This is most likely caused by a failure of the antibody staining.*

Intercellular Adhesion Proteins

The cells, which were still adherent after crimping and perfusion, did clearly stain for the intracellular adhesion proteins Connexin 43 (fig 5-17 a, b) and VE-Cadherin (fig 5-17 c, d). Due to fewer cells on the surface, the Connexin 43 reaction was not as strong as in the recellularized samples. VE-Cadherin expression, typical for EC, was strongly positive in the remaining EC. The intensity of color did not change from recellularized state to the crimped and perfused state.

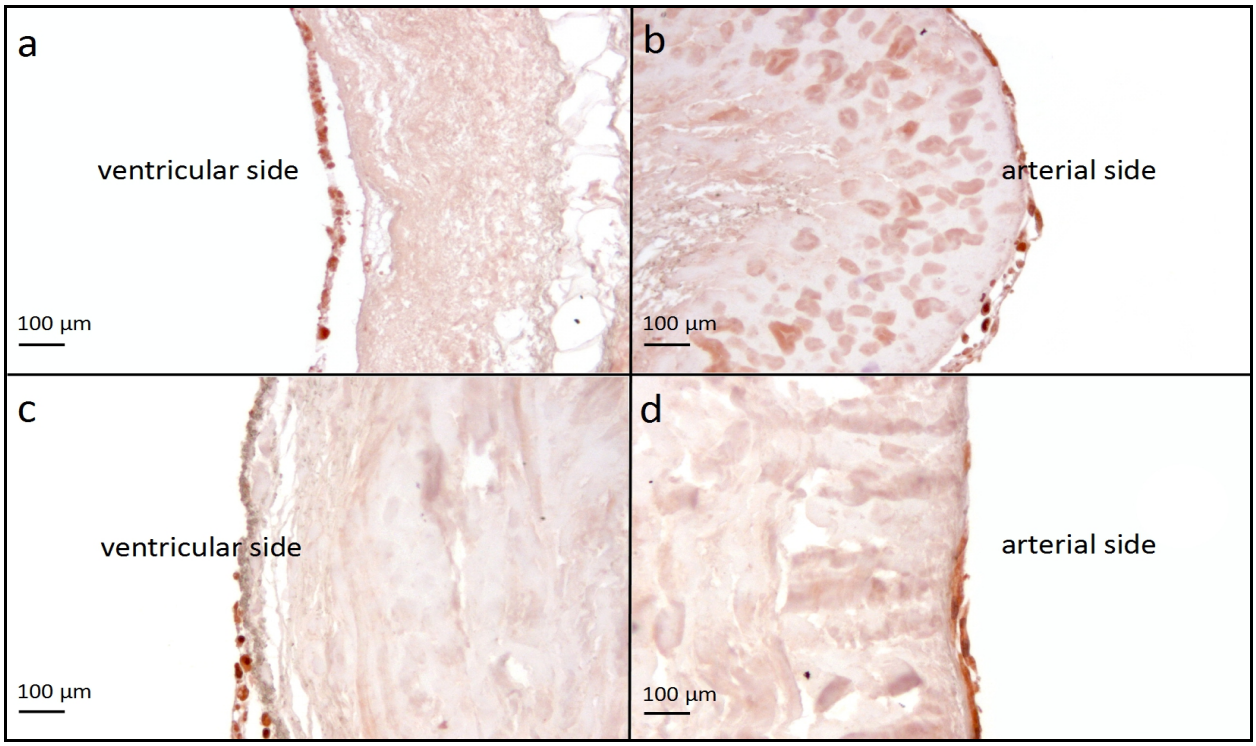

Fig 5-17 Intracellular adhesion protein Connexin 43 and VE-Cadherin on a representative leaflet after crimping and perfusion *cell nuclei staining with hematoxylin. The staining against Connexin 43 demonstrates a deep colorization on both sides of the valve leaflet (a, b). Although, the cell layer is not confluent and only a few scattered single cells are attached to the surface. The EC-typical VE-Cadherin shows strong colorization in the remaining EC (c). Remnants of the EC can be found on both sides of the leaflet (c, d).*

Inflammation modulatory Proteins

ICAM and VCAM expressions were determined to evaluate the inflammation reaction of the cells. ICAM expression did not increase compared to the recellularized homografts but stayed on the same level (Fig 5-18 a, b). Likewise VCAM antibody reaction remained negative (Fig 5-18 c, d). A faint reddish colorization in deeper layers of the leaflet may be due to processing artifacts (Fig 5-18 d).

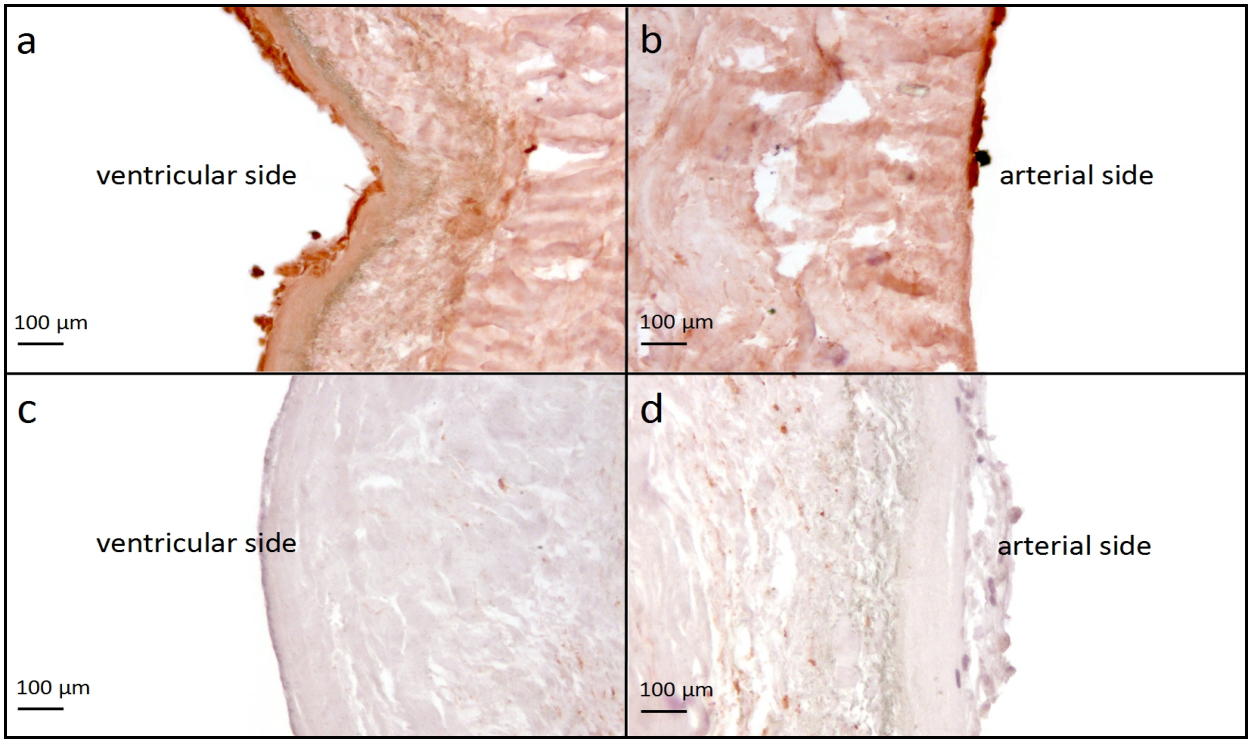

Fig 5-18 ICAM and VCAM expression on a representative leaflet after crimping and perfusion *cell nuclei staining with hematoxylin. The cells, which are still attached to the leaflet, show a reaction with ICAM antibodies (a). The color strength compares to those on the aortic wall samples after recellularization. The cells on the surface of the leaflet do not express VCAM (c, d) and therefore do not color after antibody application. The reddish color in the deeper layer of the leaflet may be contributed to processing artifacts.*

Structural Proteins of the ECM

The ECM protein Collagen IV staining showed a deep colorization along the surface of the leaflet (Fig 5-19). This reaction occurred on both sides of the leaflets. These results were similar to those of the aortic wall after crimping and perfusion. Compared to the outcome of the staining after recellularization, Collagen IV expression increased near the surface. The Fibronectin expression was clearly visible as a red band which covered the surface (Fig 5-19 c, d).

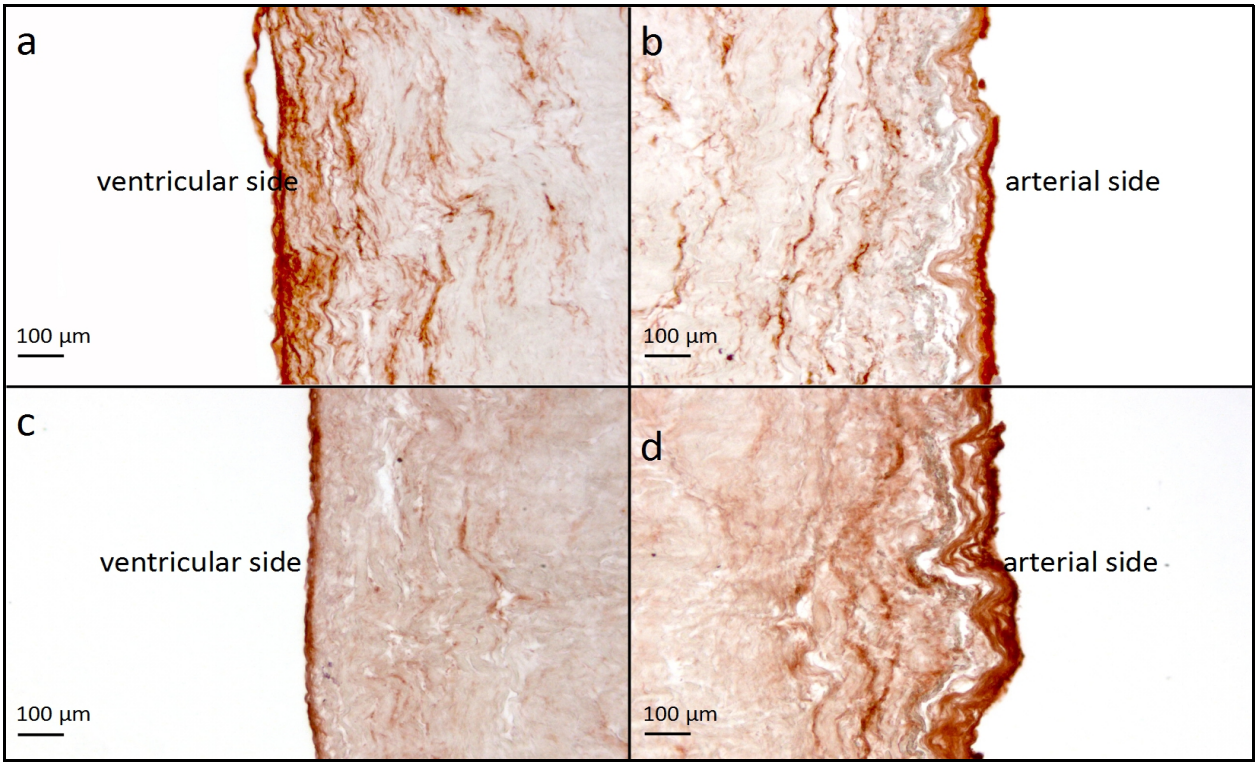

Fig 5-19 Collagen IV and Fibronectin expression on a representative leaflet after crimping and perfusion *cell nuclei staining with hematoxylin. The Collagen IV staining is especially dominant in the region near the surface of the leaflets (a, b). These results are similar to those of the Collagen IV expression in the aortic wall. Intensity and area of colorization were similar on both sides of the leaflets. The staining against Fibronectin (c, d) is also more intense close to the surface of the leaflet.*

5.4.6. Summary of Immunohistochemical Analysis

Table 5-2: Summary of immunohistochemical Results listed in tabular Form

Protein expression	*Process stage*					
	Native	*Decellularized homografts*	*Recellularized homografts*	*After crimping and perfusion*		
				Wall	*Leaflet VS*	*Leaflet AS*
Cell verification						
CD 31	+--	---	+++	+--	+--	+--
TE-7	+--	---	+++	++-	++-	+--
SMC-Myosin	+++	++-	++-	++-	---	---
Intercellular adhesion proteins						
Connexin 43	+--	---	++-	++-	++-	++-
VE-Cadherin	+--	---	++-	+--	+--	+--
Inflammation modulatory proteins						
ICAM	+--	---	+++	+++	+++	+++
VCAM	---	---	---	---	---	---
ECM proteins						
Collagen IV	++-	+++	++-	+++	++-	++-
Fibronectin	++-	++-	++-	+++	+++	+++
Intracellular structural proteins						
α-Actin	++-	++-	++-	++-	---	+--

The intensity of the color was categorized. The color strength correlates with the quantity of protein expression.

Key: --- = no expression, +-- = minimal expression, ++- = moderate expression, +++ = strong expression

5.4.7. Quantitative Cell Layer Confluency Analysis

Quantitative cell layer confluency analysis was performed as described in *Chap. 4.5. "Image Evaluation with ImageJ"*. CD 31 and TE-7 protein expressions were utilized for EC respectively FB proof. Cell layer integrity of the different parts of the valve and the leaflet were compared. The quantitative analysis of the FB coating of the wall demonstrated an inhomogeneous distribution. While sample 4 retained nearly full coverage of all wall sections (Fig 5-20 b), the confluency of the FB layer on the other samples decreased. On the valvular part of sample 2 no cell layer was detected. EC covered less surface of the aortic wall (Fig 5-20 a). Three samples kept EC on the surface, however, the percentage of covering was low. There was a distinct reduction of the EC on the surface after crimping and perfusion. The EC cover of the aortic valve leaflets is similar to the aortic wall (Fig 5-20 c). The FB layer on the leaflet's surface was better preserved compared to the wall. Further analysis showed a better preservation of the FB on the ventricular side in three of four samples.

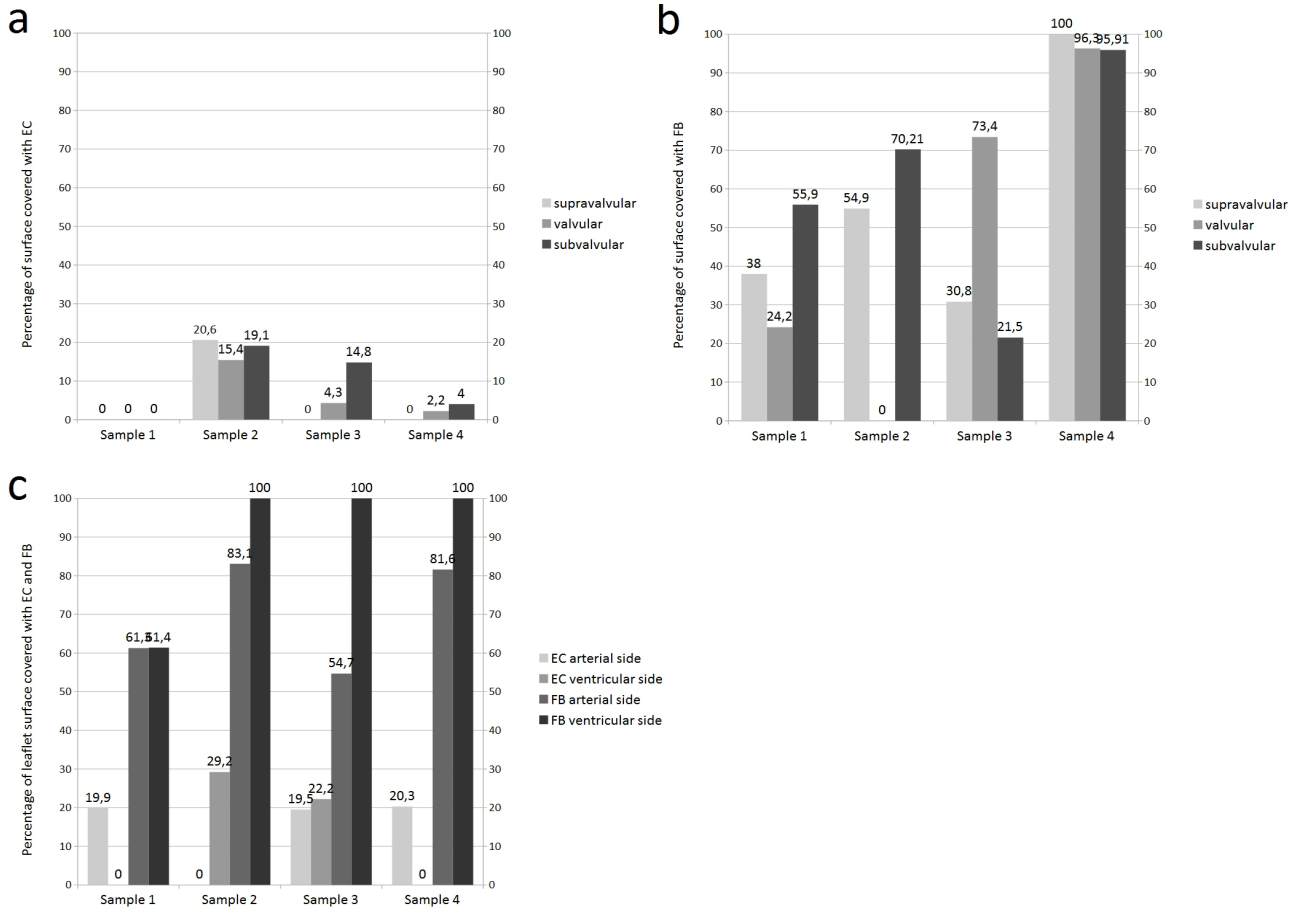

Fig 5-20 Percentage of the aortic wall and the leaflet covered by an EC and FB layer *(a) The percentage of EC covering on the aortic wall decreased distinctly after crimping and perfusion. Although, three of the samples retained part of the cells, the overall number of cell covered surface is low, at a maximum 20,6 %. (b) The distribution of FB is very inhomogeneous in between the different samples. While sample 4 retained nearly full FB coverage, the valvular wall section of sample 2 was devoid of any cells. (c) The results on the leaflet are similar to that on the aortic wall. However, the percentage of FB covering on the ventricular side was higher compared to the arterial side in three out of four samples.*

6. Discussion

At the beginning of this study, we hypothesized that the crimping and perfusion of a seeded aortic valve would not make a difference in the cell layer integrity. Based on the results of the study by Scheuer *et al.* (2013), who demonstrated an intact cellular coating on a polyurethane valve after crimping, we conducted our study on aortic valve homografts. Four homografts were thawed and decellularized to remove cell debris. Afterwards they were reseeded under dynamic conditions with allogenic FB and EC. To test the stability of the cell layer, the reseeded homografts were crimped and put under pulsatile perfusion for three days. While Scheuer *et al.* (2013) only crimped the polyurethane valve, we also put the valves under perfusion to further investigate the stability of the cell layer. However, the results demonstrated a damage to the EC as well as the FB layer.

One difference between the study conducted by Scheuer *et al.* (2013) and ours was the use of aortic valve homografts. Cryopreserved aortic valve homografts were used for the TAVI model. Although the supply of homografts is limited, they still present one of the best suited scaffolds for heart valve tissue engineering, as they preserve the complex valve structure, the optimal hemodynamic properties and are potentially less immunogenic than a xenogenic valve. (Jana et al. 2014) For the investigation of the stability of cell layers under simulated physiologic conditions, homografts are the optimal scaffold material. While the immunogenic potential of cryopreserved homografts is low, cryopreservation itself does not completely remove the cellular components. Yet, most of the cells become apoptotic due to the damage sustained during harvesting, processing and cryopreserving of the valve (Hopkins et al. 2009). Nevertheless, this cell debris still maintains its antigenic potential and can induce an inflammatory response in the host body (Hopkins et al. 2009; Meyer et al. 2005). Welters *et al*. (2002) described a strong human leukocyte antibodies (HLA) response to allografts, which were not HLA matched. Especially when a second homograft transplantation was necessary, HLA titers were high. Hopkins *et al.* (2009) showed that the decellularization of cryopreserved homografts in a sheep model reduced calcification and improved their durability. Meyer *et al*. (2005) reported a reduced cellular immune response to decellularized aortic homografts in a rat model. Furthermore, over a period of three months decellularized homograft elicited a decreased humoral immune response in humans compared to non decellularized homografts (Kneib et al. 2012). Calcification, stenosis and valve failure can result from an immune response (Hopkins 2006; Zehr et al. 2005). Especially in younger patients the early structural failure of the valve is a problem. It can be associated with an intense immune response (Lund et al. 1999). To minimize possible immune response *in vivo* and to enable recellularization on a donor-cell free homograft, we removed these cells and cell remnants. We used a mixture of the anionic detergents SDS and SD to achieve this result. SDS provides excellent cell removal capabilities (Gilbert et al. 2006). However, there are mixed reports about the integrity of the ECM after SDS treatment.

Whereas Kasimir *et al*. (2003) reported severe structural alteration of the ECM, Grauss *et al*. (2003) and Liao *et al*. (2008) demonstrated no loss or disruption of the elastic lamellae and a preserved collagen distribution. These contradictory findings may be contributed to the different concentration, duration times and combination with other decellularization agents. The reports for SD are similar to those of SDS. Zhou *et al*. (2010) described better ECM preservation for SD compared to SDS and trypsin . Contrary, Gilbert *et al*. (2006) reported greater tissue disruption after SD treatment than decellularization with SDS. In our decellularization process we used a solution of SDS 0.5 % and SD 0.5 %. The concentration of SD and SDS was between the concentration most studies used for their experiments (SDS between 0.1 % and 1 %, SD between 0.25 % and 1 %) (Dijkman et al. 2012; Zhou et al. 2010; Liao et al. 2008).

To evaluate ECM quality after decellularization, our immunohistochemial analysis included a Collagen IV staining. The staining showed collagen fibre distribution in the *tunica intima* and the aortic wall. Liao *et al.* (2008) obtained similar results after a decellularization protocol using SDS 0.1 %/RNAse 20 µg/ml/DNAse 0.2 mg/ml. The Movats Pentachrome staining performed by Liao *et al.* (2008) demonstrated a more intense staining of the *fibrosa* of the valve leaflet after decellularization with SDS compared to the decellularization with trypsin and Triton-X.

We achieved almost complete cell removal in all our samples. Albeit in one sample staining with hematoxylin colored cell nuclei in the deeper layers of the valve, the surface was cell and debris free. After the removal of the cells, we conducted a thorough washing process of the homografts to clear any potential remnants of the decellularization solution. Rieder *et al*. (2004) reported inefficient seeding attempts on SDS treated aortic homografts compared with SD. While they used a lower concentration of SDS (0.1 %) they did not perform an intense washing cycle after decellularization. This may contribute to the low seeding efficiency of SDS treated valves in this study. Cebotari *et al.* (2010) compared the cytotoxity of three different SDS/SD solutions, SDS 1 %, SD 1 % and SDS/SD 0.5/0.5 %. After the incubation of porcine pulmonary valves in each solution for 24 h under continuous shaking they performed altogether 10 washing cycles with PBS. Samples of the washing solution were taken after each washing cycle. Lactatdehydrogenase was used to test for cytotoxity. The cytotoxity of the SDS/SD solution decreased significantly after the fifth washing cycle. The solution was nontoxic after the seventh washing cycle. Furthermore, metabolic testing of the seeded cells demonstrated metabolic activity of the cells after the second washing cycle in the group using the SD/SDS solution. In our decellularization protocol the valve were rinsed with PBS over 7 days to remove cell remnants and potential toxic chemicals. Decellularization with a combination of SDS and SD is a well acknowledged technique in our work group. The decellularized homografts showed no cell remnants and excellent reseeding capabilities (Haller et al. 2013b; Haller et al. 2013a).

Decellularization of homografts increases their durability by decreasing their immunogenic potential.

However, the acellular ECM cannot regenerate or adapt to varying physiological conditions. Previous studies showed that an intact autologous EC layer reduced thrombogenicity and inflammation of the aortic valve leaflets (Lehner 1997). A cell coating can also contribute to ECM production and create a viable and growing valve with autologous cells. The samples of the heart valves taken after seeding demonstrated a confluent monolayer of EC, as well as an underlying multilayer of FB. The CD 31 staining showed a homologous, intact monolayer of EC visible on the aortic wall surface. Haller *et al*. (2013a) showed that the EC layer of a SDS/SD treated, reseeded aortic valve stayed intact after low-flow conditioning. These findings confirmed the effective seeding on SDS/SD treated valves. The possible seeding inhibition by residual SDS which was reported by Rieder *et al*. (2004) was neither observed in the study of Haller *et al*. (2013a) nor in this experiment. The EC were still adherent after conditioning. An influence of the decellularization with SDS/SD on the adherence of the cells is not very likely.

Previous studies showed that the preseeding with FB increased the adherence of EC on porcine valves (Schopka et al. 2009; Gulbins et al. 2003a). In our study, we seeded vascular FB on the decellularized homografts before we applied the EC. Collagen IV, which is produced by vascular FB, also supports EC adhesion (Schopka et al. 2009). The cells were harvested from the vena saphena magna. This vein is easy to access and the vascular cells display excellent quality for heart valve tissue engineering (Yang et al. 2012; Schnell et al. 2001; Gulbins et al. 2005). However, Butcher *et al*. (2004) reported differences between vascular and valvular cells, especially between vascular and valvular EC. While vascular EC align themselves parallel to the blood flow, valvular EC adjust perpendicular when put under shear stress. The comparison of gene transcription profiles of valvular and vascular EC under different hemodynamic conditions also suggests a distinct difference between the two cell types (Butcher et al. 2006). Vascular EC were used in this study. These cells proved to be shear stress resistant and able to build a homologous cell layer on the surface of an aortic valve (Haller et al. 2013a; Schopka et al. 2009). Nevertheless the differences between vascular and valvular EC may contribute to the adherence potential after crimping and perfusion. Further experiments with valvular EC ought to enable more insight in these properties and may produce better adherence after crimping.

A dynamic seeding procedure was performed to achieve homogeneously distributed cells. Nasseri *et al.* (2003) demonstrated that a dynamic seeding procedure provided better nutrient and cell distribution on a 3-D scaffold. Our results showed a multilayer of FB, as well as a cobblestone pattern of EC on the surface after dynamic recellularization. Early perfusion experiments demonstrated that EC statically seeded on vascular grafts showed poor attachment to the surface once exposed to arterial levels of shear stress (Inoguchi et al. 2007; Herring 1991; Shindo et al. 1987). This indicates that abrupt, high shear stress may damage the EC layer. EC under non flow conditions and EC under shear stress have a different morphology. While EC under static conditions display a cobblestone pattern in light microscopy, EC under flow elongate their shape and align themselves parallel to the flow (Butcher, Nerem 2007). The

elongated shape and the alignment with the blood flow decrease spatial fluctuation of the shear stress and reduce the maximum shear stress (Noria et al. 1999). Also, intercellular adhesion molecules reorganize when exposed to shear stress. A study from Noria *et al*. (1999) demonstrated that adherens junctions in EC changed their configuration from belt-like in static EC cultures to a localized plaque form. In addition, other adhesion molecules, including $\alpha_5\beta_1$ Fibronectin receptor and $\alpha_v\beta_3$ Vitronectin receptor integrins and the cytoskeletal-associated protein Vinculin and Talin, change their distribution pattern when submitted to shear stress (Girard, Nerem 1995). In our study the decellularized aortic valve showed an intact, confluent EC layer after dynamic seeding. The EC layer displayed a cobblestone morphology as well as high expression of VE-Cadherin. VE-Cadherin is an intercellular adhesion protein, which plays an important role in cell-cell interaction and in the maintenance of the EC barrier (Corada et al. 2001). Crosby *et al.* (2005), demonstrated in their experiment, that VE-Cadherin is critical for vasculogenesis and prevents the disassembly of nascent vessels. The staining against VE-Cadherin was deeply colored in our experiment. The recellularized wall as well as the residual cells on the aortic wall after crimping and perfusion exhibited a strong expression of VE-Cadherin. Knowing the importance of VE-Cadherin for vasculogenesis and accurate EC function, the high expression of this protein suggests a functioning EC layer.

After the crimping process we submitted the seeded homograft to shear stress. Although the flow was gradually increased, the EC layer did not adhere to the FB layer. EC layers which were preconditioned demonstrated an increased ability to withstand hemodynamic shear stress (Yazdani et al. 2010; Ott, Ballermann 1995). The lack of a conditioning phase before crimping may have contributed to the lacking ability of the EC layer to withstand the pulsatile flow. First crimping experiments did not show a significant damage to the cell layer after crimping. Furthermore, as slowly increasing shear stress improves the EC ability to cope with higher shear stress. Based on this data, it was reasonable to omit the precondition phase. Any handling of the aortic valve increases the risk for contamination as well as increasing the time, which a possible tissue engineered valve needs for completion. Omitting needless steps during the manufacturing process is mandatory. However, our results showed a considerable decrease of EC on the aortic wall and the leaflet. Further experiments with a precondition phase may improve the EC adherence.

Not only the EC layer, the FB layer as well was reduced on the aortic wall and the leaflet. After crimping and perfusion the FB covered roughly 55 % of the wall's surface and 80 % of both leaflet sides. A comparison between the FB layer on the ventricular and the arterial side of the aortic leaflet revealed a difference in cell distribution. While the FB layer on the ventricular side covered about 90 %, the FB layer on the arterial side coated only 70 %. When we look at the hemodynamics of the aortic valve leaflet there is a difference between the arterial and ventricular side. The arterial side is subjected to so called “vortices” or oscillatory shear stress while the ventricular side experiences primarily laminar shear stress

(Yap et al. 2012a; Balachandran et al. 2011). *In vitro* laminar shear stress is a protective factor for EC against inflammation and oxidative stress (Butcher et al. 2006; Cunningham, Gotlieb 2005). By contrast, a disturbed blood flow contributes to the formation of atherosclerosis (Cunningham, Gotlieb 2005). These different shear stress conditions may be an explanation for the calcification of the aortic valve leaflet, which predominantly occurs on the arterial side of the leaflet (Yap et al. 2012b). Our results could indicate that oscillatory shear stress damages the FB layer and decreases confluency. The parts of the aortic valve, which where subjected to laminar flow, retained most of the FB layer. An i*n vivo* experiment showed that vascular FB after vascular injury contribute to the formation of neointima and intimal hyperplasia (Shi, Tarbell 2011). Depending on whether the FB layer is confluent or subconfluent, they change their phenotype marker expression and migration potential according to the applied shear stress (Garanich et al. 2007). Moreover, Grabowski *et al*. (1993) showed that a FB monolayer increased the expression of tissue factor once submitted to shear stress. Considering the fact that FB produce tissue factor and may induce coagulation, the effect of laminar shear stress and oscillatory shear stress on the different valve sides should be further investigated.

Studies suggest a possible damage of the ECM and the cell layer by the crimping process. In our studies the valves were crimped for 10 min. Kiefer *et al*. (2011) showed that after the crimping process of a bovine pericardial valve major changes in the structural morphology of collagen fibres occurred. A transcatheter valve (Edwards Sapien bioprosthesis) was crimped for different periods of time ranging from 1 hour to 1 month. The fragmentation of the valve's leaflet was most prominent in the valve, which was crimped for 1 month. These significant results indicate that the crimping process of a valve should be as short as possible. In contrast, numerous studies report no damage to the structural integrity of tissue engineered heart valves (TEHV) after crimping. Moreira *et al*. (2014), Schmidt *et al*. (2010) and Dijkman *et al*. (2012) demonstrated an intact collagen distribution in the valve leaflets of TEHV. Moreira *et al.* (2014) crimped the valve for 20 min and received similar results. Although, longer crimping should be avoided as demonstrated by Kiefer *et al*. (2011) short crimping periods up to 20 min seem not to alter the valve's structural integrity. In our study the crimping process lasted up to 10 min. The valve was subjected in medium during this time. Considering the results from these previous studies, a severe damage to the ECM of the valve and the wall was not anticipated.

In our research group we demonstrated an intact cell layer after the crimping process (Scheuer et al. 2013). However, another experiment, which was conducted after this study, from our research group further investigated the crimping process. In this study performed by König *et al.* (2016) biohybrid valves (polyurethane walls, decellularized homograft leaflets) were seeded, then crimped and put under perfusion. Samples were taken after crimping and after perfusion. A live/dead assay was conducted. After the crimping process, an increase in dead cells was observed in the cell layer. However, after the perfusion procedure, these cells disappeared and the overall cell count decreased. Like this study already

anticipated, König *et al.* (2016) reasoned, that the crimping process damages especially the EC layer severely. Schmidt *et al.* (2010) found similar results. They crimped a TEHV which was seeded with myofibroblasts and EC. After seeding the valves were preconditioned with low flow. However, after the crimping procedure the EC layer showed incomplete endothelialization. This was contributed to the surface friction during crimping. Dijkman *et al.* (2012) demonstrated only a small and local damage on the layer of mesenchymal stem cells on a TEHV after crimping. Furthermore, Moreira *et al.* (2014) reported similar results about the effects of the crimping process on the EC layer on a tissue engineered valve.

In this study we did not take valve samples after the crimping process. Due to the fact, that pulsatile perfusion had to be performed on the valve after crimping, the leaflets could not be removed. Samples from the aortic wall may not represent significant samples. Their location at the end of the stent and the "crimping zone" may produce falsified results. However, the issue of the crimping damage on the cell layer has yet to be resolved and further investigation is clearly necessary.

We were first to examine the effect of perfusion after crimping on the EC layer. Although the limited number of valves restricts the validity of the results. Furthermore, other factors (different cells, low flow conditioning before crimping) have to be further investigated. However, first results indicate a heavier impact of the crimping process than previous studies suggest. Nevertheless, Schmidt *et al*. (2010) reported no thromboembolic event after crimping and delivering the valve *in vivo*. Still, the crimping process seems to disturb the cell-cell interaction of the first layer, the EC. Especially, when the use of other scaffold material is considered for an *in vivo* use a viable, intact EC layer is important to reduce thrombogenicity and calcification. Previous studies showed that an EC layer decreases calcification rate and degeneration of the BHV (Jansson et al. 2001; VeDepo et al. 2016). Furthermore, a cell coated homograft also enables growth and modification of the ECM. Seeded with the patient's own cells the thrombogenicity as well as inflammation will be reduced. The slow degradation of the scaffold over time and the production of new ECM from the autologous cells can create a durable heart valve, which is able to grow. Especially younger patients will benefit from this solution. In younger patients degradation rate of BHV is higher than in adult patients. Moreover, the gradual growth of the heart valve is not possible and this subjects young patients to subsequent vale replacement surgeries over time.

7. Summary

To date an ideal heart valve prosthesis does not exist. Tissue engineering may enable the creation of an optimal valve prosthesis. We evaluated the performance of such a tissue engineered valve and assessed the cell layer integrity. In our study we wanted to know if the crimping process during a TAVI damages the cell layer of a tissue engineered valve when put under perfusion. We used an aortic valve homograft whose ECM structure provides ideal qualities in terms of mechanical stability and cell adhesion. After the decellularization process, which decreases the immunogenic potential of the valve and facilitates cell adhesion, we seeded cells from a different donor on the scaffold. The crimping process was performed analogously to a TAVI procedure. The perfusion process was simulated using a bioreactor. After perfusion we took samples for evaluation with immunohistology and SEM.

After the recellularization 100 % of the wall was covered with FB as well as EC. After perfusion, samples showed a loss of cell coating. The EC layer was reduced to an average of 10 %, the FB layer decreased to 65 %. While there was no difference in the EC layer on the leaflet's arterial and ventricular side, the FB distribution was different. 70 % of the arterial side of the leaflet was covered with FB and 90 % of the ventricular side. This difference may be attributed to the different flow conditions on the different sides of the leaflet. The overall decrease in cell layer density implies a damage, which is done to the cell layer during the crimping process. König *et al.* (2016) conducted a study, which demonstrated the damage to the cells on a biohybrid valve after crimping. After perfusion, these dead cells disappeared from the leaflets. These results further support our findings.

A tissue engineered valve, which has to be implanted via the TAVI procedure, first has to withstand the crimping procedure. Different approaches have to be considered to enhance the adherence of the cells to the valve. A precondition phase may improve the attachment of the cells. Optimizing the crimping procedure may be another option. Another approach would be the *in vivo* endothelialization of the valve. Aubin *et al.* (2016) demonstrated in their study a successful *in vitro* endothelialization of decellularized ovine pulmonary heart valves and aortic grafts. However, they failed to prove a significant enhancement of *in vivo* endothelialization of the scaffolds. Further, platelet attachment, immune cell activation and an excessive proliferation of smooth muscle cells has to be avoided.

Tissue engineered valves are a promising approach to overcome the shortcomings of the currently available heart valve prostheses. Schmidt *et al.* (2010) demonstrated in their experiment a successful transapical implantation of a TEHV. They used a self-expandable nitinol stent to avoid the strain on the leaflets during reexpansion with a balloon. However, the leaflet surface showed only partial endothelialization and the pliability of the valve was reduced, most likely due to the absence of elastin.

The current shortcomings of TEHV point out the need for further studies to improve cell attachment to enable the implantation of a fully functional valve prosthesis.

Publication Bibliography

Abdel-Wahab, M.; Mehilli, J.; Frerker, C.; Neumann, F.-J.; Kurz, T.; Tölg, R. et al. (2014): Comparison of balloon-expandable vs self-expandable valves in patients undergoing transcatheter aortic valve replacement: the CHOICE randomized clinical trial. In *JAMA* 311 (15), pp. 1503–1514.

Alavi, S. H.; Groves, E. M.; Kheradvar, A. (2014): The effects of transcatheter valve crimping on pericardial leaflets. In *The Annals of Thoracic Surgery* 97 (4), pp. 1260–1266.

Atala, A.; Mooney, D. J. (Eds.) (1996): Synthetic Biodegradable Polymer Scaffolds. Boston, MA: Birkhäuser Boston.

Aubin, H.; Mas-Moruno, C.; Iijima, M.; Schütterle, N.; Steinbrink, M.; Assmann, A. et al. (2016): Customized Interface Biofunctionalization of Decellularized Extracellular Matrix: Toward Enhanced Endothelialization. In *Tissue Engineering Part C: Methods* 22 (5), pp. 496–508.

Aumüller, G. (2007): Anatomie. 208 Tabellen. Stuttgart: Thieme (Duale Reihe).

Bader, A.; Schilling, T.; Teebken, O. E.; Brandes, G.; Herden, T.; Steinhoff, G.; Haverich, A. (1998): Tissue engineering of heart valves--human endothelial cell seeding of detergent acellularized porcine valves. In *Eur J Cardiothorac Surg* 14 (3), pp. 279–284.

Badrossamay, M. R.; Balachandran, K.; Capulli, A. K.; Golecki, H. M.; Agarwal, A.; Goss, J. A. et al. (2014): Engineering hybrid polymer-protein super-aligned nanofibers via rotary jet spinning. In *Biomaterials* 35 (10), pp. 3188–3197.

Badylak, S. F. (2004): Xenogeneic extracellular matrix as a scaffold for tissue reconstruction. In *Transplant Immunology* 12 (3-4), pp. 367–377. DOI:

Badylak, S. F.; Gilbert, T. W. (2008): Immune response to biologic scaffold materials. In *Seminars in Immunology* 20 (2), pp. 109–116.

Balachandran, K.; Sucosky, P.; Yoganathan, A. P. (2011): Hemodynamics and Mechanobiology of Aortic Valve Inflammation and Calcification. In *International Journal of Inflammation* 2011 (4), pp. 1–15.

Bloomfield, . (2002): Choice of heart valve prosthesis. In *Heart (British Cardiac Society)* 87 (6), pp. 583–589.

Bonow, R. O.; Leon, M. B.; Doshi, D.; Moat, N. (2016): Management strategies and future challenges for aortic valve disease. In *The Lancet* 387 (10025), pp. 1312–1323.

Braghirolli, D. I.; Steffens, D.; Pranke, P. (2014): Electrospinning for regenerative medicine: a review of the main topics. In *Drug Discovery Today* 19 (6), pp. 743–753.

Brennan, J. M.; Edwards, F. H.; Zhao, Y.; O'Brien, S.; Booth, M. E.; Dokholyan, R. S. et al. (2013): Long-term safety and effectiveness of mechanical versus biologic aortic valve prostheses in older patients: results from the Society of Thoracic Surgeons Adult Cardiac Surgery National Database. In *Circulation* 127 (16), pp. 1647–1655.

Bryant, S. J.; Anseth, K. S. (2001): The effects of scaffold thickness on tissue engineered cartilage in photocrosslinked poly(ethylene oxide) hydrogels. In *Biomaterials* 22 (6), pp. 619–626.

Butany, J.; Ahluwalia, M. S.; Munroe, C.; Fayet, C.; Ahn, C.; Blit, P. et al. (2003): Mechanical heart valve prostheses. In *Cardiovascular Pathology* 12 (6), pp. 322–344.

Butcher, J. T.; Nerem, R. M. (2007): Valvular endothelial cells and the mechanoregulation of valvular pathology. In *Philosophical Transactions of the Royal Society B: Biological Sciences* 362 (1484), pp. 1445–1457.

Butcher, J. T.; Penrod, A. M.; García, A. J.; Nerem, R. M. (2004): Unique morphology and focal adhesion

development of valvular endothelial cells in static and fluid flow environments. In *Arteriosclerosis, Thrombosis, and Vascular Biology* 24 (8), pp. 1429–1434.

Butcher, J. T.; Tressel, S.; Johnson, T.; Turner, D.; Sorescu, G.; Jo, H.; Nerem, R. M. (2006): Transcriptional profiles of valvular and vascular endothelial cells reveal phenotypic differences: influence of shear stress. In *Arteriosclerosis, Thrombosis, and Vascular Biology* 26 (1), pp. 69–77.

Cahill, T. J.; Prendergast, B. D. (2016): Infective endocarditis. In *The Lancet* 387 (10021), pp. 882–893.

Capulli, A. K.; MacQueen, L. A.; Sheehy, Sean P.; Parker, K. K. (2016): Fibrous scaffolds for building hearts and heart parts. In *Advanced drug delivery reviews* 96, pp. 83–102.

Carabello, B. A. (2007): Aortic Valve Disease. In James T. Willerson, Hein J. J. Wellens, Jay N. Cohn, David R. Holmes (Eds.): Cardiovascular Medicine. London: Springer London, pp. 381–392.

Cebotari, S.; Tudorache, I.; Jaekel, T.; Hilfiker, A.; Dorfman, S.; Ternes, W. et al. (2010): Detergent Decellularization of Heart Valves for Tissue Engineering: Toxicological Effects of Residual Detergents on Human Endothelial Cells. In *Artificial Organs* 34 (3), pp. 206–210.

Charitos, E.s I.; Sievers, H.-H. (2013): Anatomy of the aortic root: implications for valve-sparing surgery. In *Annals of cardiothoracic surgery* 2 (1), pp. 53–56.

Coffey, S.; Cairns, B. J.; Iung, B. (2016): The modern epidemiology of heart valve disease. In *Heart (British Cardiac Society)* 102 (1), pp. 75–85.

Cohen, G.; Zagorski, B.; Christakis, G. T.; Joyner, C. D.; Vincent, J.; Sever, J. et al. (2010): Are stentless valves hemodynamically superior to stented valves? Long-term follow-up of a randomized trial comparing Carpentier-Edwards pericardial valve with the Toronto Stentless Porcine Valve. In *The Journal of Thoracic and Cardiovascular Surgery* 139 (4), pp. 848–859.

Corada, M.; Liao, F.; Lindgren, M.; Lampugnani, M. G.; Breviario, F.; Frank, R. et al. (2001): Monoclonal antibodies directed to different regions of vascular endothelial cadherin extracellular domain affect adhesion and clustering of the protein and modulate endothelial permeability. In *Blood* 97 (6), pp. 1679–1684.

Crapo, P. M.; Gilbert, T. W.; Badylak, S. F. (2011): An overview of tissue and whole organ decellularization processes. In *Biomaterials* 32 (12), pp. 3233–3243.

Crosby, C. V. (2005): VE-cadherin is not required for the formation of nascent blood vessels but acts to prevent their disassembly. In *Blood* 105 (7), pp. 2771–2776.

Cunningham, K. S.; Gotlieb, A. I. (2005): The role of shear stress in the pathogenesis of atherosclerosis. In *Laboratory investigation; a journal of technical methods and pathology* 85 (1), pp. 9–23.

Dasi, L. P.; Simon, H. A.; Sucosky, P.; Yoganathan, A. P. (2009): Fluid mechanics of artificial heart valves. In *Clinical and Experimental Pharmacology and Physiology* 2009 (36), pp 225-237

Deck, J. D. (1986): Endothelial cell orientation on aortic valve leaflets. In *Cardiovascular Research* 20 (10), pp. 760–767.

Delmo Walter, E. M.; de By, T. M. M. H.; Meyer, R.; Hetzer, R. (2012): The future of heart valve banking and of homografts: perspective from the Deutsches Herzzentrum Berlin. In *HSR proceedings in intensive care & cardiovascular anesthesia* 4 (2), pp. 97–108.

Dhandayuthapani, B.; Yoshida, Y.; Maekawa, T.; Kumar, D. S. (2011): Polymeric Scaffolds in Tissue Engineering Application: A Review. In *International Journal of Polymer Science* 2011 (5110), pp. 1–19.

Dijkman, P. E.; Driessen-Mol, A.; Frese, L.; Hoerstrup, S. P.; Baaijens, F. P. T. (2012): Decellularized homologous tissue-engineered heart valves as off-the-shelf alternatives to xeno- and homografts. In *Biomaterials* 33 (18), pp. 4545–4554.

Dohmen, P. M.; Konertz, W. (2009): Tissue-engineered heart valve scaffolds. In *Annals of thoracic and*

cardiovascular surgery : official journal of the Association of Thoracic and Cardiovascular Surgeons of Asia 15 (6), pp. 362–367.

Drury, J. L.; Mooney, D. J. (2003): Hydrogels for tissue engineering. Scaffold design variables and applications. In *Biomaterials* 24 (24), pp. 4337–4351.

Dumont, K.; Yperman, J.; Verbeken, E.; Segers, P.; Meuris, B.; Vandenberghe, S. et al. (2002): Design of a new pulsatile bioreactor for tissue engineered aortic heart valve formation. In *Artificial Organs* 26 (8), pp. 710–714.

Duran, C.; Kumar, N.; Gometza, B.; Halees, Z. A. (1991): Indications and limitations of aortic valve reconstruction☆☆☆. In *The Annals of Thoracic Surgery* 52 (3), pp. 447–454.

Durst, C. A.; Cuchiara, M. P.; Mansfield, E. G.; West, J. L.; Grande-Allen, K. J. (2011): Flexural characterization of cell encapsulated PEGDA hydrogels with applications for tissue engineered heart valves. In *Acta biomaterialia* 7 (6), pp. 2467–2476.

Eikelboom, J. W.; Connolly, S. J.; Brueckmann, M.; Granger, C. B.; Kappetein, A. P.; Mack, M. J. et al. (2013): Dabigatran versus warfarin in patients with mechanical heart valves. In *The New England journal of medicine* 369 (13), pp. 1206–1214.

Engelmayr, G. C., JR; Cheng, M.; Bettinger, C. J.; Borenstein, J. T.; Langer, R.; Freed, L. E. (2008): Accordion-like honeycombs for tissue engineering of cardiac anisotropy. In *Nature materials* 7 (12), pp. 1003–1010.

Engelmayr, G. C., JR; Hildebrand, D. K.; Sutherland, F. W. H.; Mayer, J. E., JR; Sacks, M. S. (2003): A novel bioreactor for the dynamic flexural stimulation of tissue engineered heart valve biomaterials. In *Biomaterials* 24 (14), pp. 2523–2532.

Engelmayr, G. C., JR; Sales, V. L.; Mayer, J. E., JR; Sacks, M. S. (2006): Cyclic flexure and laminar flow synergistically accelerate mesenchymal stem cell-mediated engineered tissue formation: Implications for engineered heart valve tissues. In *Biomaterials* 27 (36), pp. 6083–6095.

Fan, Y.-D.; van Hoeck, B.; Holovska, V.; Jashari, R. (2012): Evaluation of decontamination process of heart valve and artery tissues in European Homograft Bank (EHB): a retrospective study of 1,055 cases. In *Cell and tissue banking* 13 (2), pp. 297–304.

Fanning, J. P.; Platts, D. G.; Walters, D. L.; Fraser, J. F. (2013): Transcatheter aortic valve implantation (TAVI): valve design and evolution. In *International journal of cardiology* 168 (3), pp. 1822–1831.

Flanagan, T. C.; Wilkins, B.; Black, Al.; Jockenhoevel, S.; Smith, T. J.; Pandit, A. S. (2006): A collagen-glycosaminoglycan co-culture model for heart valve tissue engineering applications. In *Biomaterials* 27 (10), pp. 2233–2246.

Furukawa, H.; Tanemoto, K. (2015): Current topics on bicuspid aortic valve: clinical aspects and surgical management. In *Annals of thoracic and cardiovascular surgery : official journal of the Association of Thoracic and Cardiovascular Surgeons of Asia* 21 (4), pp. 314–321.

Garanich, J. S.; Mathura, R. A.; Shi, Z.-D.; Tarbell, J. M. (2007): Effects of fluid shear stress on adventitial fibroblast migration: implications for flow-mediated mechanisms of arterialization and intimal hyperplasia. In *American journal of physiology. Heart and circulatory physiology* 292 (6), pp. H3128-35.

Ghavidel Mehr, N.; Li, X.; Ariganello, M. B.; Hoemann, C. D.; Favis, B. D. (2014): Poly(epsilon-caprolactone) scaffolds of highly controlled porosity and interconnectivity derived from co-continuous polymer blends: model bead and cell infiltration behavior. In *Journal of materials science. Materials in medicine* 25 (9), pp. 2083–2093.

Gilbert, T. W.; Sellaro, T. L.; Badylak, S. F. (2006): Decellularization of tissues and organs. In *Biomaterials* 27 (19), pp. 3675–3683.

Girard, P. R.; Nerem, R. M. (1995): Shear stress modulates endothelial cell morphology and F-actin organization through the regulation of focal adhesion-associated proteins. In *Journal of cellular physiology* 163 (1), pp. 179–193.

Gott, V. L.; Alejo, D. E.; Cameron, D. E. (2003): Mechanical heart valves. 50 years of evolution. In *The Annals of Thoracic Surgery* 76 (6), pp. S2230-S2239.

Gould, R. A.; Chin, K.; Santisakultarm, T. P.; Dropkin, A.; Richards, J. M.; Schaffer, C. B.; Butcher, J. T. (2012): Cyclic strain anisotropy regulates valvular interstitial cell phenotype and tissue remodeling in three-dimensional culture. In *Acta biomaterialia* 8 (5), pp. 1710–1719.

Grabowski, E. F.; Zuckerman, D. B.; Nemerson, Y. (1993): The functional expression of tissue factor by fibroblasts and endothelial cells under flow conditions. In *Blood* 81 (12), pp. 3265–3270.

Grauss, R. W.; Hazekamp, M. G.; van Vliet, S.; Gittenberger-de Groot, A C; DeRuiter, M. C. (2003): Decellularization of rat aortic valve allografts reduces leaflet destruction and extracellular matrix remodeling. In *The Journal of Thoracic and Cardiovascular Surgery* 126 (6), pp. 2003–2010.

Grauss, R. W.; Hazekamp, M. G.; Oppenhuizen, F.; van Munsteren, C. J.; Gittenberger-de Groot, A. C.; DeRuiter, M. C. (2005): Histological evaluation of decellularised porcine aortic valves: matrix changes due to different decellularisation methods. In *European journal of cardio-thoracic surgery : official journal of the European Association for Cardio-thoracic Surgery* 27 (4), pp. 566–571.

Gulbins, H.; Pritisanac, A.; Dauner, M.; Petzold, R.; Goldemund, A.; Doser, M. et al. (2006): Seeding of human vascular cells onto small diameter polyurethane vascular grafts. In *Thorac Cardiovasc Surg* 54 (2), pp. 102–107.

Gulbins, H.; Goldemund, A.; Anderson, I.; Haas, U.; Uhlig, A.; Meiser, B.; Reichart, B. (2003a): Preseeding with autologous fibroblasts improves endothelialization of glutaraldehyde-fixed porcine aortic valves. In *The Journal of Thoracic and Cardiovascular Surgery* 125 (3), pp. 592–601.

Gulbins, H.; Kreuzer, E.; Reichart, B. (2003b): Homografts: a review. In *Expert review of cardiovascular therapy* 1 (4), pp. 533–539.

Gulbins, H.; Pritisanac, A.; Uhlig, A.; Goldemund, A.; Meiser, B. M.; Reichart, B.; Daebritz, S. (2005): Seeding of Human Endothelial Cells on Valve Containing Aortic Mini-Roots: Development of a Seeding Device and Procedure. In *The Annals of Thoracic Surgery* 79 (6), pp. 2119–2126.

Haller, N.; Hollweck, T.; König, F.; Thierfelder, N.; Wintermantel, E.; Hagl, C.; Akra, B. (2013a): Low-flow Conditioning of Decellularized and Re-seeded Homografts in a Novel Pulsatile Bioreactor. In *Advances in Biomedical Engineering Research* 1 (4).

Haller, N.; Hollweck, T.; Thierfelder, N.; Schulte, J.; Hausherr, J.-Ma.; Dauner, M.; Akra, B. (2013b): Noninvasive analysis of synthetic and decellularized scaffolds for heart valve tissue engineering. In *ASAIO journal (American Society for Artificial Internal Organs : 1992)* 59 (2), pp. 169–177.

Hasan, A.; Ragaert, K.; Swieszkowski, W.; Selimović, S.; Paul, A.; Camci-Unal, G. et al. (2013): Biomechanical properties of native and tissue engineered heart valve constructs. In *J Biomech.*

Herring, M. B. (1991): Endothelial cell seeding. In *Journal of Vascular Surgery* 13 (5), pp. 731–732.

Hildebrand, D. K.; Wu, Z. J.; Mayer, J. E., JR; Sacks, M. S. (2004): Design and hydrodynamic evaluation of a novel pulsatile bioreactor for biologically active heart valves. In *Annals of biomedical engineering* 32 (8), pp. 1039–1049.

Hjortnaes, J.; Shapero, K.; Goettsch, C.; Hutcheson, J. D.; Keegan, J.; Kluin, J. et al. (2015): Valvular interstitial cells suppress calcification of valvular endothelial cells. In *Atherosclerosis* 242 (1), pp. 251–260.

Hockaday, L. A.; Kang, K. H.; Colangelo, N. W.; Cheung, P. Y. C.; Duan, B.; Malone, E. et al. (2012): Rapid

3D printing of anatomically accurate and mechanically heterogeneous aortic valve hydrogel scaffolds. In *Biofabrication* 4 (3), p. 35005.

Hoerstrup, S. P.; Sodian, R.; Daebritz, S.; Wang, J.; Bacha, E. A.; Martin, D. P. et al. (2000): Functional living trileaflet heart valves grown in vitro. In *Circulation* 102 (19 Suppl 3), pp. III44-9.

Hoerstrup, S. P.; Sodian, R.; Sperling, J. S.; Vacanti, J. P.; Mayer, J. E., JR (2000b): New pulsatile bioreactor for in vitro formation of tissue engineered heart valves. In *Tissue Engineering* 6 (1), pp. 75–79.

Hoffman, J. I. E. (2009): The natural and unnatural history of congenital heart disease. Chichester, UK, Hoboken, NJ: Wiley-Blackwell.

Hopkins, R. A. (2006): Bioprosthetic valves and laudable inflammation? In *Circulation* 114 (4), pp. 261–264.

Hopkins, R. A.; Jones, A. L.; Wolfinbarger, L.; Moore, M. A.; Bert, A. A.; Lofland, G. K. (2009): Decellularization reduces calcification while improving both durability and 1-year functional results of pulmonary homograft valves in juvenile sheep. In *The Journal of Thoracic and Cardiovascular Surgery* 137 (4), pp. 907-13, 913e1-4.

Inoguchi, H.; Tanaka, T.; Maehara, Y.; Matsuda, T. (2007): The effect of gradually graded shear stress on the morphological integrity of a huvec-seeded compliant small-diameter vascular graft. In *Biomaterials* 28 (3), pp. 486–495.

Iop, L.; Renier, V.; Naso, F.; Piccoli, M.; Bonetti, A.; Gandaglia, A. et al. (2009): The influence of heart valve leaflet matrix characteristics on the interaction between human mesenchymal stem cells and decellularized scaffolds. In *Biomaterials* 30 (25), pp. 4104–4116.

Jana, S.; Tefft, B. J.; Spoon, D. B.; Simari, R. D. (2014): Scaffolds for tissue engineering of cardiac valves. In *Acta biomaterialia* 10 (7), pp. 2877–2893.

Jana, S.; Lerman, A.; Simari, R. D. (2015): In Vitro Model of a Fibrosa Layer of a Heart Valve. In *ACS applied materials & interfaces* 7 (36), pp. 20012–20020.

Jansson, K.; Bengtsson, L.; Swedenborg, J.; Haegerstrand, A. (2001): In vitro endothelialization of bioprosthetic heart valves provides a cell monolayer with proliferative capacities and resistance to pulsatile flow. In *The Journal of Thoracic and Cardiovascular Surgery* 121 (1), pp. 108–115.

Kasimir, M. T.; Rieder, E.; Seebacher, G.; Silberhumer, G.; Wolner, E.; Weigel, G.; Simon, P. (2003): Comparison of different decellularization procedures of porcine heart valves. In *The International journal of artificial organs* 26 (5), pp. 421–427.

Keane, T. J.; Swinehart, I. T.; Badylak, S. F. (2015): Methods of tissue decellularization used for preparation of biologic scaffolds and in vivo relevance. In *Methods (San Diego, Calif.)* 84, pp. 25–34.

Khorramirouz, R.; Sabetkish, S.; Akbarzadeh, A.; Muhammadnejad, A.; Heidari, R.; Kajbafzadeh, A.-M. (2014): Effect of three decellularisation protocols on the mechanical behaviour and structural properties of sheep aortic valve conduits. In *Advances in medical sciences* 59 (2), pp. 299–307.

Kiefer, P.; Gruenwald, F.; Kempfert, J.; Aupperle, H.; Seeburger, J.; Mohr, F. W.; Walther, T. (2011): Crimping may affect the durability of transcatheter valves: an experimental analysis. In *The Annals of Thoracic Surgery* 92 (1), pp. 155–160.

Kim, B.-S.; Mooney, D. J. (2000): Scaffolds for Engineering Smooth Muscle Under Cyclic Mechanical Strain Conditions. In *J. Biomech. Eng.* 122 (3), p. 210.

Kirsch, J.; May, A. M.; Lorke, D.; Winkelmann, A.; Schwab W. et al. (2010): Taschenlehrbuch Anatomie. 1st ed. Stuttgart: Thieme.

Kneib, C.; von Glehn, C Q C; Costa, F D A; Costa, M T B A; Susin, M. F. (2012): Evaluation of humoral immune response to donor HLA after implantation of cellularized versus decellularized human heart

valve allografts. In *Tissue antigens* 80 (2), pp. 165–174.

Kobayashi, J. (2011): Stentless aortic valve replacement: an update. In *Vascular health and risk management* 7, pp. 345–351.

Kolb, H. C.; Finn, M. G.; Sharpless, K. Barry (2001): Click Chemistry: Diverse Chemical Function from a Few Good Reactions. In *Angewandte Chemie (International ed. in English)* 40 (11), pp. 2004–2021.

König, F.; Lee, J.-S.; Akra, B.; Hollweck, T.; Wintermantel, E.; Hagl, C.; Thierfelder, N. (2016): Is Transcatheter Aortic Valve Implantation of Living Tissue-Engineered Valves Feasible? An In Vitro Evaluation Utilizing a Decellularized and Reseeded Biohybrid Valve. In *Artif Organs* 40 (8), pp. 727–737.

König, F.; Hollweck, T.; Pfeifer, S.; Reichart, B.; Wintermantel, E.; Hagl, C.; Akra, B. (2012): A Pulsatile Bioreactor for Conditioning of Tissue-Engineered Cardiovascular Constructs under Endoscopic Visualization. In *JFB* 3 (4), pp. 480–496.

Kortsmit, J.; Driessen, N. J. B.; Rutten, M. C. M.; Baaijens, F. P. T. (2009a): Real time, non-invasive assessment of leaflet deformation in heart valve tissue engineering. In *Annals of biomedical engineering* 37 (3), pp. 532–541.

Kortsmit, J.; Rutten, M. C. M.; Wijlaars, M. W.; Baaijens, F. P. T. (2009b): Deformation-controlled load application in heart valve tissue engineering. In *Tissue engineering. Part C, Methods* 15 (4), pp. 707–716.

Kuck, K.-H.; Eggebrecht, H.; Figulla, H. R.; Haude, M.; Katus, H.; Möllmann, H. et al. (2015): Qualitätskriterien zur Durchführung der transvaskulären Aortenklappenimplantation (TAVI). In *Kardiologe* 9 (1), pp. 11–26.

Lehner, G. (1997): Endothelialized biological heart valve prostheses in the non-human primate model. In *European Journal of Cardio-Thoracic Surgery* 11 (3), pp. 498–504.

Liao, J.; Joyce, E. M.; Sacks, M. S. (2008): Effects of decellularization on the mechanical and structural properties of the porcine aortic valve leaflet. In *Biomaterials* 29 (8), pp. 1065–1074.

Linnoila, I.; Petrusz, P. (1984): Immunohistochemical techniques and their applications in the histopathology of the respiratory system. In *Environmental health perspectives* 56, pp. 131–148.

Lund, O.; Chandrasekaran, V.; Grocott-Mason, R.; Elwidaa, H.; Mazhar, R.; Khaghani, A. et al. (1999): Primary aortic valve replacement with allografts over twenty-five years: Valve-related and procedure-related determinants of outcome. In *The Journal of Thoracic and Cardiovascular Surgery* 117 (1), pp. 77–91.

Mackie, B. D. (2013): Aortic Valve Anatomy. With assistance of Yasmine Subhi Ali. Edited by Medscape. Available online at http://emedicine.medscape.com/article/1922899-overview#a1, updated on 4/7/2016, checked on 5/5/2016.

Maganti, K.; Rigolin, V. H.; Sarano, M. E.; Bonow, R. O. (2010): Valvular heart disease: diagnosis and management. In *Mayo Clinic Proceedings* 85 (5), pp. 483–500.

Maurer, G. (2006): Aortic regurgitation. In *Heart* 92 (7), pp. 994–1000.

Mazine, A.; Badiwala, M.; Cohen, G. (2016): Year in review: complex valve reconstruction. In *Current opinion in cardiology* 31 (2), pp. 154–161.

McMullan, D. M.; Oppido, G.; Alphonso, N.; Cochrane, A. D.; d'Acoz, Y.; Brizard, C. P. (2006): Evaluation of downsized homograft conduits for right ventricle-to-pulmonary artery reconstruction. In *The Journal of Thoracic and Cardiovascular Surgery* 132 (1), pp. 66–71.

Meyer, S. R.; Nagendran, J.; Desai, L. S.; Rayat, G. R.; Churchill, T. A.; Anderson, C. C. et al. (2005): Decellularization reduces the immune response to aortic valve allografts in the rat. In *The Journal of Thoracic and Cardiovascular Surgery* 130 (2), pp. 469–476.

Michelena, H. I.; Desjardins, V. A.; Avierinos, J.-F.; Russo, A.; Nkomo, V. T.; Sundt, T. M. et al. (2008):

Natural history of asymptomatic patients with normally functioning or minimally dysfunctional bicuspid aortic valve in the community. In *Circulation* 117 (21), pp. 2776–2784.

Minakata, K.; Schaff, H. V.; Zehr, K. J.; Dearani, J. A.; Daly, R. C.; Orszulak, T. A. et al. (2004): Is repair of aortic valve regurgitation a safe alternative to valve replacement? In *The Journal of Thoracic and Cardiovascular Surgery* 127 (3), pp. 645–653.

Misfeld, M.; Sievers, H.-H (2007): Heart valve macro- and microstructure. In *Philosophical Transactions of the Royal Society B: Biological Sciences* 362 (1484), pp. 1421–1436.

Miyata, T.; Conte, M. S.; Trudell, L. A.; Mason, D.; Whittemore, A. D.; Birinyi, L. K. (1991): Delayed exposure to pulsatile shear stress improves retention of human saphenous vein endothelial cells on seeded ePTFE grafts. In *J. Surg. Res.* 50 (5), pp. 485–493.

Mol, A.; Driessen, N. J. B.; Rutten, M. C. M.; Hoerstrup, S. P.; Bouten, C. V. C.; Baaijens, F. P. T. (2005): Tissue engineering of human heart valve leaflets: a novel bioreactor for a strain-based conditioning approach. In *Annals of biomedical engineering* 33 (12), pp. 1778–1788.

Montoya, C. V.; McFetridge, P. S. (2009): Preparation of Ex Vivo –Based Biomaterials Using Convective Flow Decellularization. In *Tissue Engineering Part C: Methods* 15 (2), pp. 191–200.

Moreira, R.; Velz, T.; Alves, N.; Gesche, V. N.; Malischewski, A.; Schmitz-Rode, T. et al. (2014): Tissue-Engineered Heart Valve with a Tubular Leaflet Design for Minimally Invasive Transcatheter Implantation. In *Tissue engineering. Part C, Methods.*

Moroni, F.; Mirabella, T. (2014): Decellularized matrices for cardiovascular tissue engineering. In *American journal of stem cells* 3 (1), pp. 1–20.

Nasseri, B. A.; Pomerantseva, I.; Kaazempur-Mofrad, M. R.; Sutherland, F. W H; Perry, T.; Ochoa, E. et al. (2003): Dynamic rotational seeding and cell culture system for vascular tube formation. In *Tissue Engineering* 9 (2), pp. 291–299.

Niklason, L. E.; Abbott, W.; Gao, J.; Klagges, B.; Hirschi, K. K.; Ulubayram, K. et al. (2001): Morphologic and mechanical characteristics of engineered bovine arteries. In *Journal of Vascular Surgery* 33 (3), pp. 628–638.

Nishimura, R. A.; Otto, C. M.; Bonow, R. O.; Carabello, B. A.; Erwin, J. P.; Guyton, R. A. et al. (2014): 2014 AHA/ACC guideline for the management of patients with valvular heart disease: a report of the American College of Cardiology/American Heart Association Task Force on Practice Guidelines. In *Journal of the American College of Cardiology* 63 (22), pp. E57-185.

Noria, S.; Cowan, D. B.; Gotlieb, A. I.; Langille, B. L. (1999): Transient and steady-state effects of shear stress on endothelial cell adherens junctions. In *Circulation Research* 85 (6), pp. 504–514.

Ott, M. J.; Ballermann, B. J. (1995): Shear stress-conditioned, endothelial cell-seeded vascular grafts: improved cell adherence in response to in vitro shear stress. In *Surgery* 117 (3), pp. 334–339.

Otto, C. M.; Kuusisto, J.; Reichenbach, D. D.; Gown, A. M.; O'Brien, K. D. (1994): Characterization of the early lesion of 'degenerative' valvular aortic stenosis. Histological and immunohistochemical studies. In *Circulation* 90 (2), pp. 844–853.

Paruchuri, S.; Yang, J.-H.; Aikawa, E.; Melero-Martin, J. M.; Khan, Z. A.; Loukogeorgakis, S. et al. (2006): Human pulmonary valve progenitor cells exhibit endothelial/mesenchymal plasticity in response to vascular endothelial growth factor-A and transforming growth factor-beta2. In *Circulation Research* 99 (8), pp. 861–869.

Parvin N. S.; Blaser, M. C.; Santerre, J. P.; Caldarone, C. A.; Simmons, C. A. (2016): Biomechanical conditioning of tissue engineered heart valves: Too much of a good thing? In *Advanced drug delivery reviews* 96, pp. 161–175.

Patel, A.; Gaharwar, A. K.; Iviglia, G.; Zhang, H.; Mukundan, S.; Mihaila, S. M. et al. (2013): Highly elastomeric poly(glycerol sebacate)-co-poly(ethylene glycol) amphiphilic block copolymers. In *Biomaterials* 34 (16), pp. 3970–3983.

Patel, A. N.; Genovese, J. (2011): Potential clinical applications of adult human mesenchymal stem cell (Prochymal®) therapy. In *Stem cells and cloning : advances and applications* 4, pp. 61–72.

Patsalis, P. C.; Al-Rashid, F.; Neumann, T.; Plicht, B.; Hildebrandt, H. A.; Wendt, D. et al. (2013): Preparatory balloon aortic valvuloplasty during transcatheter aortic valve implantation for improved valve sizing. In *JACC. Cardiovascular interventions* 6 (9), pp. 965–971.

Pibarot, P.; Dumesnil, J. G. (2009): Prosthetic heart valves: selection of the optimal prosthesis and long-term management. In *Circulation* 119 (7), pp. 1034–1048.

Polchow, B.; Kebbel, K.; Schmiedeknecht, G.; Reichardt, A.; Henrich, W.; Hetzer, R.; Lueders, C. (2012): Cryopreservation of human vascular umbilical cord cells under good manufacturing practice conditions for future cell banks. In *J Transl Med* 10, p. 98.

Ramos-Vara, J. A.; Miller, M. A. (2014): When tissue antigens and antibodies get along: revisiting the technical aspects of immunohistochemistry--the red, brown, and blue technique. In *Veterinary pathology* 51 (1), pp. 42–87.

Remenyi, B.; ElGuindy, A.; Smith, S. C.; Yacoub, M.; Holmes, D. R. (2016): Valvular aspects of rheumatic heart disease. In *The Lancet* 387 (10025), pp. 1335–1346.

Rieder, E.; Kasimir, M.-T.; Silberhumer, G.; Seebacher, G.; Wolner, E.; Simon, P.; Weigel, G. (2004): Decellularization protocols of porcine heart valves differ importantly in efficiency of cell removal and susceptibility of the matrix to recellularization with human vascular cells. In *The Journal of Thoracic and Cardiovascular Surgery* 127 (2), pp. 399–405.

Ruel, J.; Lachance, Ge. (2010): Mathematical modeling and experimental testing of three bioreactor configurations based on windkessel models. In *Heart international* 5 (1), pp. e1.

Sacks, M. S.; David M., W.; Schmidt, D. E. (2009): On the biomechanics of heart valve function. In *Journal of Biomechanics* 42 (12), pp. 1804–1824.

Sacks, M. S.; Mirnajafi, A.; Sun, W.; Schmidt, P. (2006): Bioprosthetic heart valve heterograft biomaterials: structure, mechanical behavior and computational simulation. In *Expert Review of Medical Devices* 3 (6), pp 817-834.

Sales, V. L.; Engelmayr, G. C., JR; Johnson, J. A., JR; Gao, J.; Wang, Y.; Sacks, M. S.; Mayer, J. E., JR (2007): Protein precoating of elastomeric tissue-engineering scaffolds increased cellularity, enhanced extracellular matrix protein production, and differentially regulated the phenotypes of circulating endothelial progenitor cells. In *Circulation* 116 (11 Suppl), pp. I55-63.

Sanz-Garcia, A.; Oliver-de-la-Cruz, J.; Mirabet, V.; Gandia, C.; Villagrasa, A.; Sodupe, E.; Escobedo-Lucea, C. (2015): Heart valve tissue engineering: how far is the bedside from the bench? In *Expert reviews in molecular medicine* 17, pp. e16.

Schenke-Layland, K.; Vasilevski, O.; Opitz, F.; König, K.; Riemann, I.; Halbhuber, K. J. et al. (2003): Impact of decellularization of xenogeneic tissue on extracellular matrix integrity for tissue engineering of heart valves. In *Journal of Structural Biology* 143 (3), pp. 201–208.

Scheuer, M.; Hollweck, T.; Bombien, R.; Kozlik-Feldmann, R.; Haas, U.; Fano, C. et al. (2013): Mechanical Integrity of Tissue Engineered Stented Transapical Heart Valves after Crimping Procedure. In *EMR* 2 (2).

Schmid, C. (2014): Leitfaden Erwachsenen herzchirurgie. 3. Aufl., [aktualisiert]. Berlin: Springer Medizin.

Schmidt, D.; Mol, A.; Odermatt, B.; Neuenschwander, S.; Breymann, C.; Gossi, M. et al. (2006): Engineering of biologically active living heart valve leaflets using human umbilical cord-derived

progenitor cells. In *Tissue Engineering* 12 (11), pp. 3223–3232.

Schmidt, D.; Dijkman, P. E.; Driessen-Mol, A.; Stenger, R.; Mariani, C.; Puolakka, A. et al. (2010): Minimally-Invasive Implantation of Living Tissue Engineered Heart Valves. In *Journal of the American College of Cardiology* 56 (6), pp. 510–520.

Schmidt, R. F.; Thews, G. (1983): Human physiology. Berlin, New York: Springer-Verlag.

Schnell, A. M.; Hoerstrup, S. P.; Zund, G.; Kolb, S.; Sodian, R.; Visjager, J. F. et al. (2001): Optimal cell source for cardiovascular tissue engineering: venous vs. aortic human myofibroblasts. In *The Thoracic and cardiovascular surgeon* 49 (4), pp. 221–225.

Schoen, F. J. (2011): Heart valve tissue engineering: quo vadis? In *Current opinion in biotechnology* 22 (5), pp. 698–705.

Schopka, S.; Schmid, F.-X.; Hirt, S.; Birnbaum, D. E.; Schmid, C.; Lehle, K. (2009): Recellularization of biological heart valves with human vascular cells: in vitro hemocompatibility assessment. In *Journal of biomedical materials research. Part B, Applied biomaterials* 88 (1), pp. 130–138.

Seliktar, D.; Black, R. A.; Vito, R. P.; Nerem, R. M. (2000): Dynamic mechanical conditioning of collagen-gel blood vessel constructs induces remodeling in vitro. In *Annals of biomedical engineering* 28 (4), pp. 351–362.

Shi, Z.-D; Tarbell, J M. (2011): Fluid flow mechanotransduction in vascular smooth muscle cells and fibroblasts. In *Annals of biomedical engineering* 39 (6), pp. 1608–1619.

Shindo, S.; Takagi, A.; Whittemore, A. D. (1987): Improved patency of collagen-impregnated grafts after in vitro autogenous endothelial cell seeding. In *Journal of Vascular Surgery* 6 (4), pp. 325–332.

Simmons, C. A.; Grant, G. R.; Manduchi, E.; Davies, P. F. (2005): Spatial heterogeneity of endothelial phenotypes correlates with side-specific vulnerability to calcification in normal porcine aortic valves. In *Circulation Research* 96 (7), pp. 792–799.

Spoon, D. B.; Tefft, B. J.; Lerman, A.; Simari, R. D. (2013): Challenges of biological valve development. In *Interventional Cardiology* 5 (3), pp. 319–334.

Stock, U. A.; Nagashima, M.; Khalil, P. N.; Nollert, G. D.; Herdena, T.; Sperling, J. S. et al. (2000): Tissue-engineered valved conduits in the pulmonary circulation. In *The Journal of Thoracic and Cardiovascular Surgery* 119 (4), pp. 732–740.

Stortecky, S.; Buellesfeld, L.; Wenaweser, P.; Windecker, S. (2012): Transcatheter aortic valve implantation: the procedure. In *Heart (British Cardiac Society)* 98 Suppl 4, pp. iv44-51.

Strober, W. (2015): Trypan Blue Exclusion Test of Cell Viability. In *Current protocols in immunology* 111, pp. A3.B.1-3.

Syedain, Z. H.; Tranquillo, R. T. (2009): Controlled cyclic stretch bioreactor for tissue-engineered heart valves. In *Biomaterials* 30 (25), pp. 4078–4084.

Tandon, R.; Sharma, M.; Chandrashekhar, Y.; Kotb, M.; Yacoub, M. H.; Narula, J. (2013): Revisiting the pathogenesis of rheumatic fever and carditis. In *Nature reviews. Cardiology* 10 (3), pp. 171–177.

Ugurlucan, M.; Yerebakan, C.; Furlani, D.; Ma, N.; Steinhoff, G. (2009): Cell Sources for Cardiovascular Tissue Regeneration and Engineering. In *Thorac Cardiovasc Surg* 57 (02), pp. 63–73.

van Kooten, T. G.; Schakenraad, J. M.; van der Mei, H. C.; Dekker, A.; Kirkpatrick, C. J.; Busscher, H. J. (1994): Fluid shear induced endothelial cell detachment from glass--influence of adhesion time and shear stress. In *Med Eng Phys* 16 (6), pp. 506–512.

VeDepo, M. C.; Detamore, M. S.; Hopkins, R. A.; Converse, G. L. (2016): Recellularization of decellularized heart valves: Progress toward the tissue-engineered heart valve. In *Journal of tissue engineering* 8, pp. 204173141772632.

Vesely, I. (2003): The evolution of bioprosthetic heart valve design and its impact on durability. In *Cardiovascular pathology : the official journal of the Society for Cardiovascular Pathology* 12 (5), pp. 277–286.

Vismara, R.; Soncini, M.; Talo, G.; Dainese, L.; Guarino, A.; Redaelli, A.; Fiore, G. B. (2010): A bioreactor with compliance monitoring for heart valve grafts. In *Annals of biomedical engineering* 38 (1), pp. 100–108.

Voet, D. (2002): Fundamentals of Biochemistry 2002 Update: John Wiley & Sons.

Wan, W. K.; Campbell, G.; Zhang, Z. F.; Hui, A. J.; Boughner, D. R. (2002): Optimizing the tensile properties of polyvinyl alcohol hydrogel for the construction of a bioprosthetic heart valve stent. In *Journal of biomedical materials research* 63 (6), pp. 854–861.

Wassenaar, C.; Wijsmuller, E. G.; van Herwerden, L. A.; Aghai, Z.; van Trieht, C. L.J.; Bos, E. (1995): Cracks in cryopreserved aortic allografts and rapid thawing. In *The Annals of Thoracic Surgery* 60, pp. S165-S167.

Weber, B.; Emmert, M. Y.; Hoerstrup, S. P. (2012): Stem cells for heart valve regeneration. In *Swiss medical weekly* 142, pp. W13622.

Weber, B.; Scherman, J.; Emmert, M. Y.; Gruenenfelder, J.; Verbeek, R.; Bracher, M. et al. (2011): Injectable living marrow stromal cell-based autologous tissue engineered heart valves: first experiences with a one-step intervention in primates. In *European heart journal* 32 (22), pp. 2830–2840.

Wei, G.; Ma, P. X. (2004): Structure and properties of nano-hydroxyapatite/polymer composite scaffolds for bone tissue engineering. In *Biomaterials* 25 (19), pp. 4749–4757.

Welters, M. J.P; Oei, F. B.S; Witvliet, M. D.; Vaessen, L. M.B; Cromme-Dijkhuis, A. H.; Bogers, A. d. J.J.C et al. (2002): A broad and strong humoral immune response to donor HLA after implantation of cryopreserved human heart valve allografts. In *Human Immunology* 63 (11), pp. 1019–1025.

Wu, Z.; Zhou, Y.; Li, N.; Huang, M.; Duan, H.; Ge, J. et al. (2009): The use of phospholipase A(2) to prepare acellular porcine corneal stroma as a tissue engineering scaffold. In *Biomaterials* 30 (21), pp. 3513–3522.

Yang, M.; Chen, C.-Z.; Shu, Y.-S.; Shi, W.-P.; Cheng, S.-F.; Gu, Y. J. (2012): Preseeding of human vascular cells in decellularized bovine pericardium scaffold for tissue-engineered heart valve: an in vitro and in vivo feasibility study. In *Journal of biomedical materials research. Part B, Applied biomaterials* 100 (6), pp. 1654–1661.

Yap, C. H.; Saikrishnan, N.; Tamilselvan, G.; Yoganathan, A. P. (2012a): Experimental measurement of dynamic fluid shear stress on the aortic surface of the aortic valve leaflet. In *Biomechanics and modeling in mechanobiology* 11 (1-2), pp. 171–182.

Yap, C. H.; Saikrishnan, N.; Yoganathan, A. P. (2012b): Experimental measurement of dynamic fluid shear stress on the ventricular surface of the aortic valve leaflet. In *Biomech Model Mechanobiol* 11 (1-2), pp. 231–244.

Yazdani, S. K.; Tillman, B. W.; Berry, J. L.; Soker, S.; Geary, R. L. (2010): The fate of an endothelium layer after preconditioning. In *Journal of Vascular Surgery* 51 (1), pp. 174–183.

Ye, X.; Shao, Y.-l.; Zhou, M.; Li, J.; Cai, L. (2009): Research on micro-structure and hemo-compatibility of the artificial heart valve surface. In *Applied Surface Science* 255 (13-14), pp. 6686–6690.

Yoganathan, A. P.; He, Z.; Casey Jones, S. (2004): Fluid mechanics of heart valves. In *Annual review of biomedical engineering* 6 (1), pp. 331-362

Yoganathan, A. P.; Chandran, K. B.; Sotiropoulos, F. (2005): Flow in prosthetic heart valves: state-of-the-art and future directions. In *Annals of biomedical engineering* 33 (12), pp. 1689–1694.

Zehr, K. J.; Yagubyan, M.; Connolly, H. M.; Nelson, S. M.; Schaff, H. V. (2005): Aortic root replacement

with a novel decellularized cryopreserved aortic homograft: postoperative immunoreactivity and early results. In *The Journal of Thoracic and Cardiovascular Surgery* 130 (4), pp. 1010–1015.

Zeng, Y. I.; Sun, R.; Li, X.; Liu, M.; Chen, S.; Zhang, P. (2016): Pathophysiology of valvular heart disease. In *Experimental and therapeutic medicine* 11 (4), pp. 1184–1188.

Zernike, F. (1942): Phase contrast, a new method for the microscopic observation of transparent objects. In *Physica* 9 (7), pp. 686–698.

Zhang, X.; Xu, B.; Puperi, D. S.; Wu, Y.; West, J. L.; Grande-Allen, K. J. (2015): Application of hydrogels in heart valve tissue engineering. In *Journal of long-term effects of medical implants* 25 (1-2), pp. 105–134.

Zhou, J.; Fritze, O.; Schleicher, M.; Wendel, H.-P.; Schenke-Layland, K.; Harasztosi, C. et al. (2010): Impact of heart valve decellularization on 3-D ultrastructure, immunogenicity and thrombogenicity. In *Biomaterials* 31 (9), pp. 2549–2554.

Ziegelmueller, J. A.; Lange, R.; Bleiziffer, S. (2015): Access and closure of the left ventricular apex: state of play. In *Journal of Thoracic Disease* 7 (9), pp. 1548-1555.

Zund, G.; Hoerstrup, S. P.; Schoeberlein, A.; Lachat, M.; Uhlschmid, G.; Vogt, P. R.; Turina, M. (1998): Tissue engineering: a new approach in cardiovascular surgery: Seeding of human fibroblasts followed by human endothelial cells on resorbable mesh. In *European journal of cardio-thoracic surgery : official journal of the European Association for Cardio-thoracic Surgery* 13 (2), pp. 160–164.

Appendices

1. Informed consent

LMU KLINIKUM DER UNIVERSITÄT MÜNCHEN
CAMPUS GROSSHADERN
HERZCHIRURGISCHE KLINIK UND POLIKLINIK

Patienteneinverständniserklärung zur Spende von Biomaterial für die herzchirurgische Forschung

Dr. med. Nikolaus Thierfelder
Leiter medizinische Forschung der
AG „Kardiovaskuläres Tissue Engineering"

Telefon +49 (0)89 4400-74791
Telefax +49 (0)89 4400-78671
Email: Nikolaus.Thierfelder@med.uni-muenchen.de
http://hch.klinikum.uni-muenchen.de

Postanschrift:
Marchioninistr. 15
81377 München

Sehr geehrter Patient,

die Forschungsgruppe „Kardiovaskuläres Tissue Engineering" der herzchirurgischen Klinik versucht neuartige, individualisierte Therapiekonzepte für die Zukunft zu entwickeln und zu etablieren. Hierfür sind wir auf die Verwendung von gespendetem Gewebe, insbesondere Zellen, angewiesen. Es ist möglich, dass im Rahmen ihrer Bypass-Operation nicht verwertbare Reststücke von Gefäßen anfallen. Wir würden sie bitten, dieses Gewebe für Forschungszwecke freizugeben.

Ich, ... , geboren am, ... , wurde von meinem Arzt um die Spende von Biomaterial gebeten. Ich hatte die Möglichkeit Fragen zu stellen und habe die Antworten verstanden.

Ich hatte ausreichend Zeit, mich für die Spende der übrig bleibenden/gebliebenen Gefäßstücke aus meiner Operation frei zu entscheiden und weiß, dass die Verwendung nur zu medizinischen Forschungszwecken dient.
Darüber hinaus bin ich darüber informiert worden, dass mir aus einer Verweigerung meines Einverständnisses keinerlei Nachteile erwachsen. Ich bin darüber informiert worden, dass mein Gewebe nur in vollständig anonymisierter Form verwendet wird. Im Falle eines Widerrufs dieser Einwilligung ist eine Vernichtung der Proben deshalb nicht möglich.

Ich erkläre hiermit mein freiwilliges Einverständnis zur Verwendung der übrig bleibenden/gebliebenen Gefäßstücke aus meiner Operation.

Eine Kopie der Einverständniserklärung habe ich erhalten.

München, den .....

Unterschrift des Patienten

Unterschrift des aufklärenden Arztes

Für ihre Unterstützung der Wissenschaft möchten wir uns im Namen unserer Forschungsabteilung bei Ihnen bedanken!

Dr. med. Nikolaus Thierfelder

Prof. Dr. med. Christian Hagl (Klinikdirektor)

2. Presentations

S. Eilenberger, T. Hollweck, U. Haas, A. Uhlig, C. Hagl, B. Akra

Mechanical Integrity of colonized Homografts after Stenting, Crimping and Perfusion

Presentation – 43. Jahrestagung der Deutschen Gesellschaft für Thorax-, Herz- & Gefäßchirurgie 2014

S. Eilenberger, Munich

Mechanical integrity of decellularised, stented and re-seeded human aortic valves after crimping and perfusion

Presentation – Baltic Summer Academy 2013 Regenerative Medicine in Cardiac Surgery

3. Material

Cell isolation, Culturing and Perfusion

Materials	Company	REF-Number
6-Well plates	TPP, Traisdingen, Switzerland	92412
BD Perfusion, Syringe with needle, 50 ml	Becton Dickinson GmbH, Heidelberg, Germany	30038
Bottle Top Filters 0,2 µm	Nalgene Labware, Thermo Fisher Scientific, Roskilde, Denmark	595-4520
Bottle Top Filters 0,45 µm	Nalgene Labware, Thermo Fisher Scientific, Roskilde, Denmark	295-4545
Calcein AM – LIVE/DEAD Viability/Cytotoxicity Kit	Invitrogen GmbH, Karlsruhe, Germany	L3224
Cell culture flask 75 cm^2, 162 cm^2	Costar, Corning Incoporated, Corning, USA	3290,32
Cell culture flask, 12.5 cm^2	Becton Dickinson GmbH, Heidleberg, Germany	353107
Collagenase Typ 2 CLS-2 (240 U/mg)	Worthington Biochemical Corporation/CellSystems GmbH, St. Katharinen, Germany	1476
Cryo Tube vials	Nunc GmbH & Co. KG, Langenselbold, Germany	375418
Dimethyl Sulfoxide	Sigma Aldrich Chemie GmbH, Taufkirchen, Germany	D5879
Disposable Scalpel, 20	Feather Safety Razor Co., LTD, Medical Division, Japan	02.001.30.020
Endothelial Cell Growth Medium + Supplement Mix	Promocell GmbH, Heidelberg, Germany	C-22010
Fetal Calf Serum (FCS)	Lonza Group AG, Basel, Switzerland	
Fibroblast Cell Growth Medium + Supplement Mix	Promocell GmbH, Heidelberg, Germany	C-23010
Gentamycin 10mg/ml	Invitrogen GmbH, Karlsruhe, Germany	15750-037
Glutaraldehyd	Sigma Aldrich Chemie GmbH, Taufkirchen, Germany	49630
HCl (1N)	Pharmacy, University of Munich Hospital, Germany	L0306
Heparin 25.000 I.E./5 ml	B. Braun Melsungen AG, Melsungen, Germany	126/317126/0403
Human serum albumin 20%	ZLB Behring, Bern, Switzerland	300296
Medium 199 Earle	Biochrom AG, Berlin, Germany	F0665
Millex-GS filter unit (0,22 µm)	Millipore Corporation, MA, USA	SLGSO33SS
Mulitdirectional stopcock	B. Braun Melsungen AG, Melsungen, Germany	16494C
Na-CaCO	Sigma Aldrich Chemie GmbH, Taufkirchen, Germany	20838
Neolus Luer Needle (0,9x70mm)	Terumo Europe N.V., Leuven, Belgium	74203-02
PBS Dulbecco	Biochrom AG, Berlin, Germany	L1825
Penicillin 10 000 U/ml-Streptomycin 10 mg/ml solution	Sigma Aldrich Chemie GmbH, Taufkirchen, Germany	P4458
Perfusion Tube Set, Custom Product	Medos Medizintechnik AG, Stolberg, Germany	MEH82396
Culture Dishes, 35 mm diameter	Nunc GmbH & Co. KG, Langenselbold, Germany	4021
PKH26GL	Sigma Aldrich Chemie GmbH, Taufkirchen, Germany	PKH26GL-1KT

Plain Drape, Secu-Drape	Sengewald, clinic innovations, Rohrdorf-Thansau, Germany	504572
Plastic Jars	R.E. Boll OHG, Munich, Germany	3500129
Plastic Screw Cup Storage Bottle, 500ml	Costar, Corning Incorporated, Corning, USA	8393
PP Tube with screw cap, sterile, 50ml	Greiner Bio-One GmbH, Frickenhausen, Germany	210261
PS Multipurpose Container, sterile, 30ml	Greiner Bio-One GmbH, Frickenhausen, Germany	201170
Serological Pipettes 1, 2, 5, 10, 25ml	Costar, Corning Incorporated, Corning, USA	4485, 4486, 4487, 4488, 4489
Surgical Gloves sterile	Semperit GmbH, Vienna, Austria	822751805
Suture (3/0)	Resorba, Nuernberg, Germany	91513
Syringe Filter (0,2µm)	Nalgene, Rochester, NY, USA	19-2520
Transfer pipette 3,5ml	Sarstedt AG & Co, Nuembrecht, Germany	86.1171.001
Trypan Blue Solution 0,4%	Sigma Aldrich Chemi GmbH, Taufkirchen, Germany	T8154
Trypsin – EDTA solution (10x)	Sigma Aldrich Chemie GmbH, Taufkirchen, Germany	T4174
Vessel cannules	Medtronic GmbH, Meerbusch, Germany	30004
Water for Injection Ph. Eur. Sterile and pyrogene-free	Fresenius Kabi AG, Bad Homburg, Germany	1080181
Wide Mouth jars 250ml	Nalgene Labware, Thermo Fisher Scientific, Roskilde, Denmark	2118-0008
Wide Mouth jars 950ml	Nalgene Labware, Thermo Fisher Scientific, Roskilde, Denmark	2118-0032

Solutions

Name	Composition	Quantitiy
Storage Solution	M199 Penicillin-Streptomycin	20 ml 1 ml
Rinsing solution	M199 Heparin Gentamycin	194 ml 1 ml 5 ml
Collagenase Solution EC	Collagenase 240U Human serum albumine	10 mg 8 ml
Collagenase Solution FB	Collagenase 240U Human serum albumine	20 ml 8 ml
Stopp solution	M199 FCS 20%	500 ml 125 ml
Cryomedium (1,5 ml per vial)	Cell growth medium FCS 11 % DMSO	1.05 ml 0.3 ml 0.45 ml
Endothelial cell growth medium	Growth medium Endothelial cell supplement Fetal calf serum 6 % Penicillin-Streptomycin	500 ml 10 ml 30 ml 1 ml
Fibroblast cell growth medium	Growth medium Fibroblast supplement Fetal calf serum Penicillin-Streptomycin	500 ml 10 ml 55 ml (11 %) 1 ml

Aortic Valve Storage, Decellularization and Recellularization

Materials	Company	REF-Number
2-Propanol >99%	Sigma Aldrich Chemie GmbH, Taufkirchen, Germany	085K3463
Amikacin	Bristol GmbH, Munich, Germany	
Amphotericin B	Squibb – von Heyden GmbH, Munich, Germany	
Ciprofloxacin	Bayer AG, Leverkusen, Germany	
Chloroform 99%	Sigma Aldrich Chemie GmbH, Taufkirchen, Germany	96596KS
Metronidazol	Bayer AG, Leverkusen, Germany	
Freezing bags	Dr. Marx Medizintechnik GmbH, Gauting, Munich	
Sodiumdeoxycholate (SD)	Sigma Aldrich Chemie GmbH, Taufkirchen, Germany	031M0192V
Sodiumdodecylsulfate (SDS)	Sigma Aldrich Chemie GmbH, Taufkirchen, Germany	031M0028V
Vankomycin	Lilly GmbH, Gießen, Germany	

Solutions

Name	Composition	Quantity
Cryopreservation solution	M 199 DMSO	200 ml 22.6 ml
Decellularisation Solution	PBS Sodiumdeoxycholate Sodiumdodecylsulfat	500ml 0.5 % (2.5 g) 0.5 % (2.5 g)
Storage Solution AV	M199 Penicillin-Streptomycin	249 ml 1 ml
FIX II	Aqua bidest Glutaraldehyd HCl (1N) Na-CaCO	456 ml 43.5 ml 0.75 ml 5.65 g
Thawing solution	M199 Penicillin-Streptomycin	500 ml 1 ml
Storage Soluation Decell	M199 Penicillin/Streptomycin	500 ml 1 ml

Scanning Electron Microscopy

Materials	Company	REF-Number
Acetone for analysis	Merck KgaA, Darmstadt, Germany	1.00014.5000
Ethanol 30, 50, 70 and 96 %	Pharmacy, University of Munich Hospital, Germany	
Ethanol 99.9 %	Pharmacy, University of Munich Hospital, Germany	
Specimen stubs, 12.5 mm	Bal-Tec GmbH, Schalksmuehle, Germany	G301Z
Carbon Adhesive Leit-Tabs	Bal-Tec GmbH, Schalksmuehle, Germany	G3347
Thermal Paper For Mitsubishi Video Copy Processor	Mitsubishi Electric Corporation, Tokyo, Japan	K65HM-CE

Immunohistochemistry

Materials	Company	REF-Number
AEC Peroxidase Substrate Kit	Vector Laboratories INC., California, USA	SK-4200

Anti Prolyl-4-Hydroxylase beta Mouse IgG1	Acris Antibodies GmbH, Herford, Germany	AF 0910-1
Anti Fibroblast, clone TE-7 0.1 mg/ml	Millipore GmbH, Schwalbach/Ts., Germany	CBL271
Anti-Fibronectin, rabbit polycolonal serum 0.6 mg/ml	Sigma Aldrich Chemie GmbH, Taufkirchen, Germany	F3648
Brij 35-Lösung	Merck KgaA, Darmstadt, Germany	1.01894.0100
Buffer solution pH 10,00	Mettler Toledo GmbH, Giessen, Germany	513 340 056
Buffer solution pH 4,01	Mettler Toledo GmbH, Giessen, Germany	513 340 059
Cover glass, round, 20mm	Zefa-Laborservice GmbH, Harthausen, Germany	Z0121405
Culture slides 4-well	Becton Dickinson GmbH, Heidelberg, Germany	354104
Culture slides 8-well	Becton Dickinson GmbH, Heidelberg, Germany	354108
EDTA	Sigma Aldrich Chemie GmbH, Taufkirchen, Germany	E6635
EnVision rb/m	Dako Deutschland GmbH, Hamburg, Germany	K4061
Formalin 4%	Microcos GmbH, Garching, Germany	29188
Hemalaun	Merck KgaA, Darmstadt, Germany	1.09249
Hydrogen peroxide	Sigma Aldrich Chemie GmbH, Taufkirchen, Germany	21676-3
Monoclonal Antibody VE-Cadherin CD 144 0.2 mg/ml	Beckmann Coulter Inc., Marseille, France	PN IM1597
Monoclonal Antibody, MS X, Connexin 43 1 mg/ml	Millipore GmbH, Schwalbach/Ts., Germany	MAB3067
Monoclonal Mouse Anti-Collagen, Typ IV 5.4 mg/ml	Sigma Aldrich Chemie GmbH, Taufkirchen, Germany	C1926
Monoclonal Mouse Anti-Human Clone CD31 Endothelial Cell 1:30	Dako Deutschland GmbH, Hamburg, Germany	M0823
Monoclonal Mouse Anti-Human Smooth Muscle Actin 44 mg/ml	Dako Deutschland GmbH, Hamburg, Germany	M0851
Monoclonal Mouse Anti-Human Smooth Muscle Myosin 954 mg/l	Dako Deutschland GmbH, Hamburg, Germany	M3558
Slide Superfrost-OT Plus	Schubert & Weiss-OMNILAB GmbH & Co. KG, Munich, Germany	9161155
Swine Immunoglobulin	Dako Deutschland GmbH, Hamburg, Germany	X0906
Target Retrieval Solution 10x concentrate	Dako Deutschland GmbH, Hamburg, Germany	S1699
Tris-Base	Merck KgaA, Darmstadt, Germany	1.08382
Tris-Borate-EDTA, Buffer, 10x concentrate	Sigma Aldrich Chemie GmbH, Taufkirchen, Germany	T4415-4L
Ultramount Aqueous Permanent Mouting Medium	Dako Deutschland GmbH, Hamburg, Germany	S1964
Xylol	Carl Roth GmbH + Co. KG, Karlsruhe, Germany	9713.3
Lab CD106/VCAM-1 AB-3 Mouse 200 µg/ml	ThermoFischer Scientific, Waltham, USA	MS-1101-P
Anti-ICAM-1, clone W-CAM-1 1:20	Millipore GmbH, Schwalbach/Ts., Germany	MAB2130

Equipments

3-D-Adjustable Table	University of Applied Sciences, Munich, Germany
Air oxygen proportioner	Tescan Corporation Minneapolis, Minnesota, USA
Analytical Balance, ABS 770	Gottl. Kern & Sohn GmbH, Balingen-Frommern, Germany
Transcatheter Balloon 2,0cm	Edwards Lifesciences Corporation, Irvine, USA
Berlin Heart EXCOR® Adult	Berlin Heart GmbH, Berlin, Germany
Bio Photometer	Eppendorf AG, Hamburg, Germany
Cell Seeding Device	University of Munich Hospital, Munich, Germany
Centrifuge, 5804R	Eppendorf AG, Hamburg, Germany
Centrifuge, Mikro 22R	Hettich, Tuttlingen, Germany
Centrifuge, Rotina 46R	Hettich, Tuttlingen, Germany
Clamp Forceps	University of Munich Hospital, Munich, Germany
Cobalt-chromium stent (CoCr, NP35N)	Curtsey of
Crimper	University of Munich Hospital, Munich, Germany
Critical Point Dryer, CPD 30	Bal-Tec GmbH, Schalksmuehle, Germany
Digital Camera, EOS 300 D	Canon Inc., Japan
Dissecting Scissors	University of Munich Hospital, Munich, Germany
Dressing Forceps	University of Munich Hospital, Munich, Germany
Dry spinning equipment in clean room	iTV-Denkendorf, Germany
Electrophoresis Power Supply, EPS 300	Pharmacia Biotech, Cambridge, England
Endoscope, Borescope BS-10	Voltcraft, Hirschau, Germany
Flow meter, HT311	Transonic Systems Inc., Stuttgart, Germany
Freezer -20°C, Comfort Plus	Siemens, Munich, Germany
Frigocut 2700	Leica, Brensheim, Germany
Gel Electrophoresis Apparatus, Horizon 58	Life Technologies™, California, USA
Glass jar with 3 luer connection	Custom Product, Gaßner Glastechnik GmbH, Munich, Germany
Hegar Dilatator	University of Munich Hospital, Munich, Germany
High speed CCD Camera	PCO AG, Kelheim, Germany
Incubator, APT line TM CB	Binder GmbH, Tuttlingen, Germany
Incubator, Hera Cell, Heraeus	Kendro Laboratory Products, Hanau, Germany
Kidney Bowls	University of Munich Hospital, Munich, Germany
Kryo 10	Planer PLC, Middlesex, United Kingdom
Lab Digital Water Bath, Julabo SW23	Kendro Laboratory Products, Hanau, Germany
Laboratory air pump, Laboport	KNF Neuberger GmbH, Freiburg, Germany
Lamina Airflow, Hera Safe	Kendro Laboratory Products, Hanau, Germany
Light microscope, Axiovert 35	Carl Zeiss MicroImaging GmbH, Göttingen, Germany
Low Shear Rheometer	Rotovisco RV 100, Thermo Haake GmbH, Karlsruhe, Germany
Magnetic stirrers and hot plate	IKA Works, Staufen, Germany
MicroAmp 96-Well Tray/Retainer Set	Applied Biosystems Inc., California, USA
Microwave	Siemens, Munich, Germany
Nalgene Nunc Cryo 1°C Freezing container	Nalgene Labware, Thermo Fisher Scientific, Roskilde, Denmark
Neubauer improved counting chamber	Brand GmbH + Co. KG, Wertheim, Germany
Paraffin Tissue Floating Bath, Round Model	Medax GmbH & Co. KG, Rendsburg, Germany
Perfusor, Secura RS232	B. Braun Melsungen AG, Melsungen, Germany
pH-meter, inoLab	WTW GmbH, Weilheim, Germany

Pipetboy	Eppendorf AG, Hamburg, Germany
Plastic bag sealer Polystar	Rische + Herfurth GmbH, Hamburg, Germany
Pressure Amplifier, HBM Typ 3962	Hottinger Baldwin Messtechnik, Darmstadt, Germany
Pressure monitor, Sirecust 304 D	Siemens, Munich, Germany
Pressure sensors, HBM 12926 Typ P11	Hottinger Baldwin Messtechnik, Darmstadt, Germany
Pressure transducer	GOULD Statham, CA, USA
Pulsatile roller pump	Stoeckert, Munich, Germany
Scanning electron microscope, Evo LS10	Zeiss, Oberkochen, Germany
Sequence detection system for Real-Time PCR, ABI PRISM 7700	Applied Biosystems Inc., California, USA
Signal connection box	Data Translation GmbH, Bietigh, Germany
Single channel pipettes (10, 100, 200, 1000 µl)	Eppendorf AG, Hamburg, Germany
Sputter Coater, SCD 50	Bal-Tec GmbH, Schalksmuehle, Germany
Tecplot software, Version 10	Amtec Engineering Inc., Houston-Texas, USA
Temperature sensor, ETS-D4	IKA Works, Staufen, Germany
UV-Transilluminator, Rainbow CCTV RMB92	Vilber Lourmat GmbH, Eberhardzell, Germany
Ventricle Assist Device	MEDOS Medizintechnik AG, Stolberg, Germany
Video Copy Processor, P66DE	Mitsubishi, Tokyo, Japan
Vortex-Mixer, MS1 Mini shaker	IKA Works, Staufen, Germany

Acknowledgment

This thesis was a long and rocky road. And it would not have been possible without the help and support of many people.

I would like to extend my gratitude to Prof. Dr. Hagl, who offered me the possibility to conduct this study at the tissue engineering laboratory at the department of heart-thoracic surgery at the Universitätsklinikum Großhadern.

I also thank Dipl.-Ing. Dr. Bassil Akra for his constant input and criticism.
I will always be thankful to Dipl.-Ing Fabian König and Dr. Nikolaus Thierfelder for their continuous support when the completion of this thesis seemed far away. They took it upon themselves to pull it all together. Without their constructive criticism and the time they invested I would be still at square one.
Special thanks to Fr. Ulrike Haas. The warm ray of hope in the midst of chaos.
Dr. Ing. Trixi Hollweck for her support. Moreover she was always ready to give advice and showed me the ropes in the lab.
Thanks to Fr. Antje Uhlig, who taught me the handling of the homografts.
Florian Herrmann for a snickers at the right time.
Further thanks to Fr. Henn, who supported the preparation of the specimen for IHC.
And a big thanks to all other students at the lab. A sorrow shared is a sorrow halved.

Last but not least I want to express my greatest gratitude to my family. They pulled it through with me, even when I was insufferable and did not believe in it myself.

Eidesstattliche Versicherung

Eilenberger Stefanie
Name, Vorname

Ich erkläre hiermit an Eides statt, dass ich die vorliegende Dissertation mit dem Thema

“The Effect of TAVI-Simulation and Perfusion on the Cell Layer of decellularized and re-seeded Homografts”

selbständig verfasst, mich außer der angegebenen keiner weiteren Hilfsmittel bedient und alle Erkenntnisse, die aus dem Schrifttum ganz oder annähernd übernommen sind, als solche kenntlich gemacht und nach ihrer Herkunft unter Bezeichnung der Fundstelle einzeln nachgewiesen habe.

Ich erkläre des Weiteren, dass die hier vorgelegte Dissertation nicht in gleicher oder in ähnlicher Form bei einer anderen Stelle zur Erlangung eines akademischen Grades eingereicht wurde.

Augsburg, 05.03.2019	Stefanie Eilenberger
Ort, Datum	Unterschrift Doktorandin/Doktorand